The Distribution of $\delta^{18}O$ in the Arctic Ocean: Implications for the Freshwater Balance of the Halocline and the Sources of Deep and Bottom Waters

Die Verteilung von $\delta^{18}O$ im Arktischen Ozean: Implikationen für die Süßwasserbilanz der Halokline und die Quellen des Tiefen- und Bodenwassers

---

Dorothea Bauch

Ber. Polarforsch. 159 (1995)
ISSN 0176 - 5027

Dorothea Bauch
Lamont-Doherty Earth Observatory
Palisades NY 10964, USA

Die vorliegende Arbeit ist die leicht veränderte Fassung einer Dissertation, die im Februar 1994 an der Naturwissenschaftlich-Mathematischen Gesamtfakultät der Universität Heidelberg eingereicht worden ist. Die Veränderungen betreffen einen Teilabschnitt der Diskussion.

Contents

Abstract

Data from sections across the Eurasian Basin of the Arctic Ocean occupied by the German Research Vessel *Polarstern* in 1987 and by the Swedish icebreaker *Oden* in 1991 are used to derive information on the freshwater balance of the Arctic Ocean halocline and on the sources of the deep waters of the Nansen, Amundsen and Makarov basins.

Salinity, $\delta^{18}O$ and mass balances allow separation of the river–runoff and the sea–ice meltwater fractions contained in the Arctic halocline. This provides the basis for tracking the river–runoff signal from the shelf seas across the central Arctic Ocean to Fram Strait. The halocline has to be divided into at least three lateral regimes: the southern Nansen Basin with net sea–ice melting, the northern Nansen Basin and Amundsen Basin with net sea–ice formation and increasing river–runoff fractions, and the Canadian Basin with minimum sea–ice meltwater and maximum river–runoff fractions and water of Pacific origin. In the Canadian Basin, silicate is used as a tracer to identify Pacific water entering through Bering Strait and an attempt is made to quantify its influence on the halocline waters of the Canadian Basin. For this purpose literature data from the CESAR and LOREX ice camps are used.

Based on mass balances and depending on the value of precipitation over the area of the Arctic Ocean the *average* mean residence time of the river–runoff fraction contained in the Arctic Ocean halocline is determined to be about 14 or 11 years. Water column inventories of river–runoff and sea–ice meltwater are calculated for a section just north of Fram Strait and implications for the ice export rate through Fram Strait are discussed.

Salinity, tritium, ^{3}He and the $\delta^{18}O$ ratio of halocline waters sampled during the 1987 *Polarstern* cruise to the Nansen Basin are used to estimate the mean residence time of the river–runoff component in the halocline and on the shelves of the Arctic

Ocean. These estimates are done by comparing ages of the halocline waters based on a combination of tracers yielding different time information: the tritium 'vintage' age which records the time that has passed since the river–runoff entered the shelf and the tritium/^{3}He age which reflects the time since the shelf waters left the shelf. The difference between the ages determined by these two methods is about 3 to 6 years. Correction for the initial tritium/^{3}He age of the shelf waters (about 0.5 to 1.5 years) yields a mean residence time of the river–runoff on the shelves of about 3.5 ± 2 years.

Comparison of the $^{18}O/^{16}O$ ratios of shelf water, Atlantic water and the deep waters of the Arctic Ocean indicate that the sources of the deep and bottom waters of the Eurasian Basin are located in the Barents and Kara seas.

Zusammenfassung

In der vorliegenden Arbeit wurden ozeanographische Profile aus dem Eurasischen Becken des Arktischen Ozeans in Kombination mit δ^{18}O–Werten bearbeitet, um sowohl Informationen über die Süßwasserbilanz der arktischen Halokline abzuleiten, als auch Aussagen über die Quellen des Tiefenwassers des Nansen, Amundsen und Makarov Beckens zu treffen. Die verwendeten Proben wurden auf Expeditionen des deutschen Forschungsschiffes *Polarstern* (ARK IV/3, 1987) und des schwedischen Eisbrechers *Oden* (ARCTIC'91) genommen.

Es wurden Massenbilanzen für die Salinität und den δ^{18}O Gehalt des Wassers aufgestellt, um die Fraktionen von Flußwasser und Meereisschmelzwasser am Wasser der Halokline zu errechnen. Diese Methode ermöglichte es, das Flußwassersignal von den Schelfgebieten über den zentralen Arktischen Ozean bis hin zur Framstraße zu verfolgen. Darüberhinaus konnte die Halokline in mindestens drei laterale Gebiete unterteilt werden: 1. Das südliche Nansen Becken mit einem Nettoschmelzen von Meereis; 2. das nördliche Nansen Becken und das Amundsen Becken mit Nettobildung von Meereis und nach Norden zunehmenden Flußwasserfraktionen; 3. das kanadische Becken mit maximaler Bildung von Meereis und maximalen Flußwasserfraktionen sowie Wasser pazifischen Ursprungs. Das durch die Beringstraße in den Arktischen Ozean fließende pazifische Wasser konnte anhand seiner Silikatkonzentrationen identifiziert werden und somit die pazifische Komponente in der Halokline quantifiziert werden. Zusätzliche Daten der CESAR und LOREX Eisstationen aus Literaturangaben ermöglichten die Überprüfung dieser Berechnungen auch für Stationen aus dem kanadischen Becken.

Basierend auf einer Massenbilanz des in der Halokline enthaltenen Flußwassers wurde seine *durchschnittliche* mittlere Aufenthaltsdauer im Arktischen Ozean auf etwa 11 bis 14 Jahre geschätzt. Es wurden Wassersäuleninventare für Flußwasser und Meereisschmelzwasser entlang eines von Westen nach Osten verlaufenden

Schnittes nördlich der Framstraße berechnet und die Implikationen für eine Meereisexportrate durch die Framstraße dargelegt.

Für Proben aus der Halokline des Nansen Beckens wurden unterschiedliche Altersinformationen des Wassers berechnet, die eine Abschätzung der mittleren Aufenthaltsdauer der Flußwasserfraktion in der Halokline und auf den Schelfgebieten ermöglichte. Hierbei wurde zum einen das Tritium–'vintage'–Alter mit Hilfe von Salinität, Tritium und $\delta^{18}O$ ermittelt. Dieses spiegelt die Zeit wider, die vergangen ist, seitdem das Flußwasser auf den Schelf geflossen ist. Zum anderen wurde das Tritium/^{3}He–Alter verwendet, das die Zeit reflektiert, die vergangen ist, seitdem das Wasser den Schelf verlassen hat. Die Differenz, der mit diesen Methoden ermittelten Alter, beträgt etwa 3 bis 6 Jahre. Nach der Korrektur um das ursprüngliche Tritium/^{3}He–Alter des Schelfwassers ergibt sich eine mittlere Aufenthaltsdauer des Flußwassers auf dem Schelf von 3.5 ± 2 Jahren.

Der Vergleich der $^{18}O/^{16}O$ Verhältnisse von Schelfwasser verschiedener Gebiete, atlantischem Wasser und dem Tiefen– und Bodenwasser des Arktischen Ozeans läßt erkennen, daß die Bildungsgebiete des Bodenwassers des Eurasischen Beckens in der Barents und Kara See liegen.

1 Introduction

Two thirds of the Earth surface is covered by oceans which influence many aspects of our environment including climate. Although the global importance of the oceans has been recognized, there are still regions that are only poorly understood. This is the case for the polar regions, which are difficult to access by research vessels. On the other hand, they are playing a major role in the global oceanic circulation and in global climate, since only in these regions deep waters are in direct contact with the atmosphere. For a general understanding of the global circulation it is therefore necessary to obtain knowledge about deep water formation and its mechanisms within the polar oceans.

Deep water formation is difficult to observe directly. Mostly, the source water masses and the processes involved in deep water formation have to be investigated indirectly. Classical oceanography provides a general picture of water mass distribution in the polar oceans from temperature and salinity data. From these data it is possible to derive potential deep water formation processes and rates. Mostly, such studies have large uncertainties and in many cases the parameters are not sensitive to distinguish between possible source waters. Measurements of trace substances of natural and anthoprogenic origin often can help to improve understanding of deep water formation by adding 'orthogonal' information to the parameter space.

The most important density structure of the Arctic Ocean is a cold halocline: while the temperatures are close to the freezing point of sea water, salinities show strong gradients. The halocline prevents deep convection within the Arctic Ocean and in this way helps to protect the permanent sea–ice cover. This density structure is thought to be maintained by advection of water from the broad shelf areas into the interior of the Arctic Ocean. On the shelves large amounts of freshwater are released as river–runoff and sea–ice is meltwater. Also large amounts of sea–ice are produced and brine is released into the water column during this process.

Present day deep water formation within the Greenland and Iceland seas have been found to be rather delicately balanced with respect to maintaining deep convection. It has been suggested that small variations of fresh water supplied to the convective gyres from the Arctic Ocean via the East Greeland Current may alter or stop convection [*Aagaard and Carmack,* 1989]. It has been concluded from temperature and salinity analysis that deep water must be formed within the Arctic Ocean. Because of the permanent sea–ice cover and the strong surface density structure deep convection is not possible in the central Arctic Ocean. Therefore, convection and brine release during sea–ice formation on the shelves is thought to be part of the mechanisms, which lead to Arctic Ocean deep water formation [*Aagaard et al.,* 1985]. ¿From this aspects it is important to better understand the pathways and transport rates of shelf waters across the Arctic Ocean into the East Greeland Current.

The $^{18}O/^{16}O$ ratios of Arctic river–runoff are strongly depleted relative to sea water, while sea–ice is only slightly fractionated relative to the water from which it was formed. These facts provide excellent potential for oxygen isotope measurements within the Arctic Ocean. The $^{18}O/^{16}O$ ratios in combination with oceanographic parameters allow to distinguish different freshwater sources and to trace their pathways from the shelf areas within the halocline. With the help of oxygen isotope measurements it is possible to study the influence of the different freshwater sources on the deep and bottom water masses of the Arctic Ocean. The investigation of the structure and circulation of the halocline has also an important application in the prediction of pathways of pollutions, since large amounts of pollutants are released from rivers and nuclear dumpsites on the Siberian shelves.

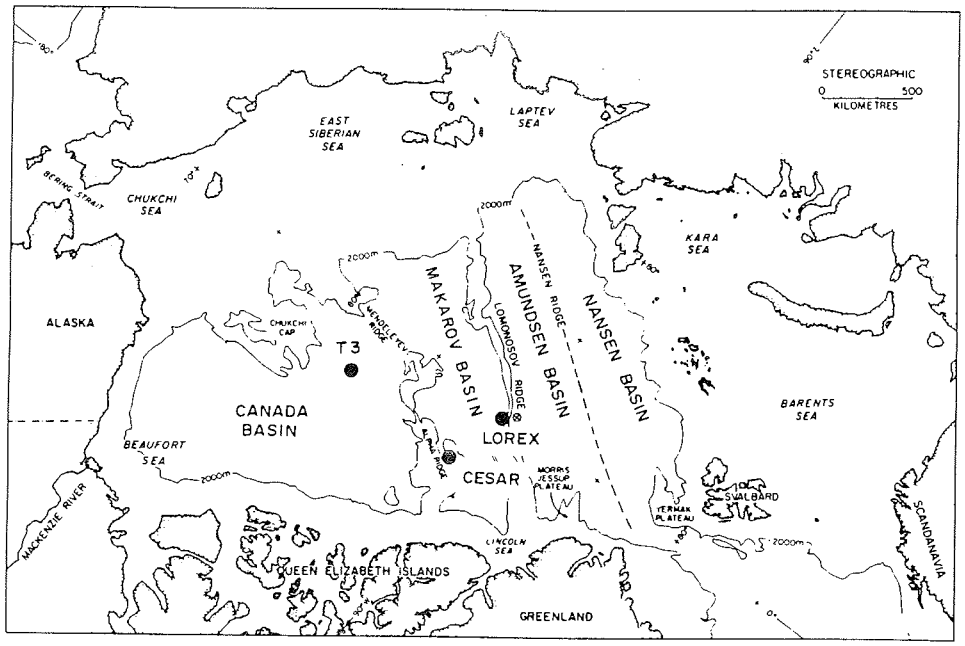

Figure 1: Geographic map of the Arcic Ocean, showing the locations of icecamps from which hydrographic data is available (taken from *Wallace et al.* [1987]).

2 General description of the Arctic Ocean

Scientific investigation of the Arctic Ocean began in the past century. In 1893 Fridtjof Nansen led an expedition in the Arctic Ocean, during which their ship drifted for three years in the Arctic ice. After this voyage several investigations have been carried out from drifting ice camps. Only recently research icebreakers have been able to carry out extensive oceanographic programs (e.g. ArkIV/3 [*PSSP*, 1988] and ARCTIC 91 [*Anderson and Carlson*, 1991]). These investigations were mostly focused on the Eurasian Basin (Nansen and Amundsen basins). In the Canadian Basin (Makarov and Canada basins), oceanographic data are only available from a few ice camps (e.g. LOREX, CESAR, AIWEX and T3). Figure 1 shows the bathymetry of the Arctic Ocean. The 2000 m isobath gives an indication for the major bathymetrical regimes.

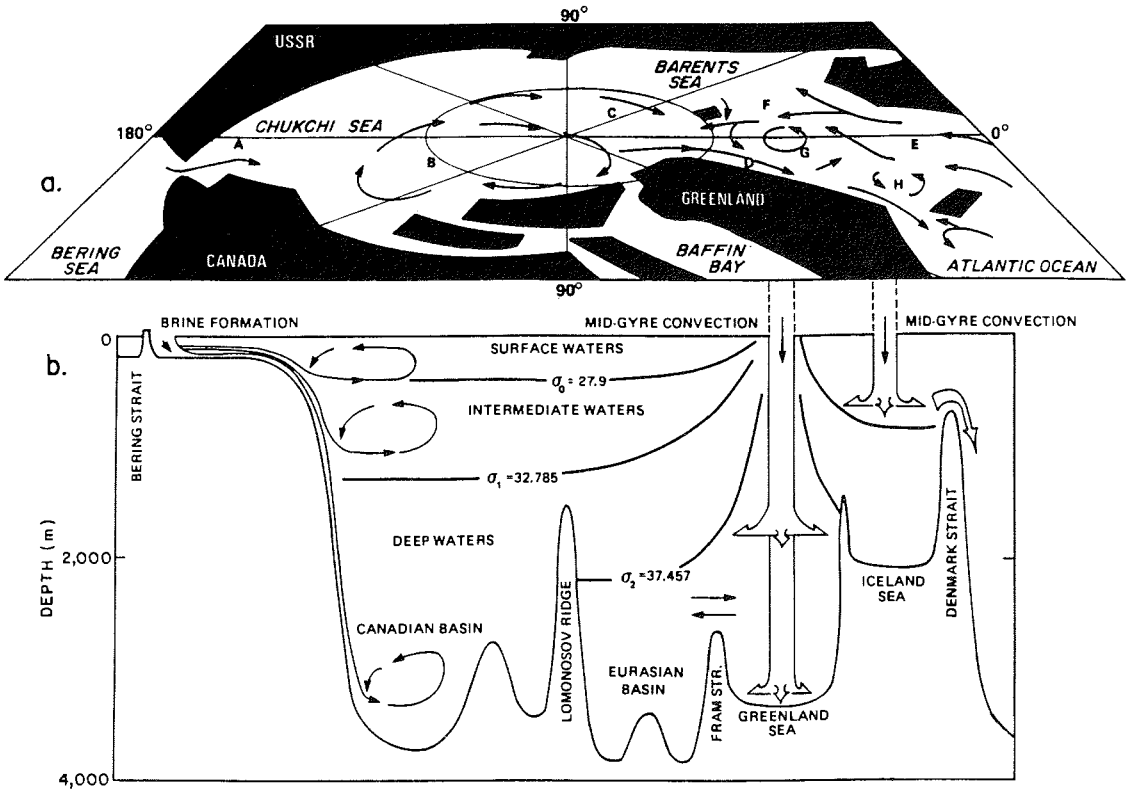

Figure 2: Schematic drawing of the circulation and water mass structure in the Arctic Ocean after *Aagaard et al.* [1985]. (a) Upper ocean circulation: Bering Strait inflow (A), Beaufort Gyre (B), Transpolar Drift (C), East Greenland Current (D), Norwegian Atlantic Current (E) West Spitzbergen Current (F), Greenland Gyre (G) and the Iceland Gyre (H). (b) Schematic vertical section along the 180°– 0°meridians. The selected isopycnals (σ_0, σ_1, σ_2) separate surface, intermediate and deep waters.

2.1 Hydrographic structure and circulation in the Arctic Ocean

For an overview of the circulation and processes within the Arctic Ocean Figure 2 (taken from *Aagaard et al.* [1985]) shows a schematic view of the surface circulation (Fig. 2 a), the deep circulation and processes (Fig. 2 b).

The wide shelf areas are an important feature of the Arctic Ocean. They cover about 1/3 of the Arctic Ocean area (see Fig. 1) while they represent only about 2 % of its volume. The Arctic Ocean interior is permanently covered by sea–ice, whereas the shelves are partly ice free during Arctic summer. The Arctic shelves receive about 0.1 Sv (1 Sv = $10^6 m^3/s$) river–runoff [*Aagaard and Carmack,* 1989; *Treshnikov,* 1985] which is about 1/10 of the global river discharge. The major part of the Arctic Ocean sea–ice is produced here and waters of high density are the result of this process. During sea–ice formation most of the salt is expelled from the crystal structure and brines are released from newly formed sea–ice. The movement of sea–ice within the Arctic Ocean is well known from drifting ice stations and buoy measurments [*Gordienko and Laktionov,* 1958; *Colony and Thorndike,* 1984]) (see Fig. 3). The main features are the anticyclonic Beaufort Gyre over the Canadian Basin and the Transpolar Drift. It can be assumed that the upper layer of the Arctic Ocean follows the sea–ice movement. This layer is probably equivalent to the mixed layer, which is about 20 to 50 m thick.

The cold halocline is the most dominant density structure within the Arctic Ocean. It is about 200 m thick and has temperatures close to the freezing point of sea water. The halocline prevents thermal convection within the Arctic Ocean interior and protects the permanent sea–ice cover from melting. The mean residence time of the halocline has been estimated to have minimum ages of about 3 to 15 years within the Eurasian Basin [*Schlosser et al.,* 1990; *Schlosser et al.,* 1994]. The halocline is assumed to be maintained by waters from the shelves which have a wide range

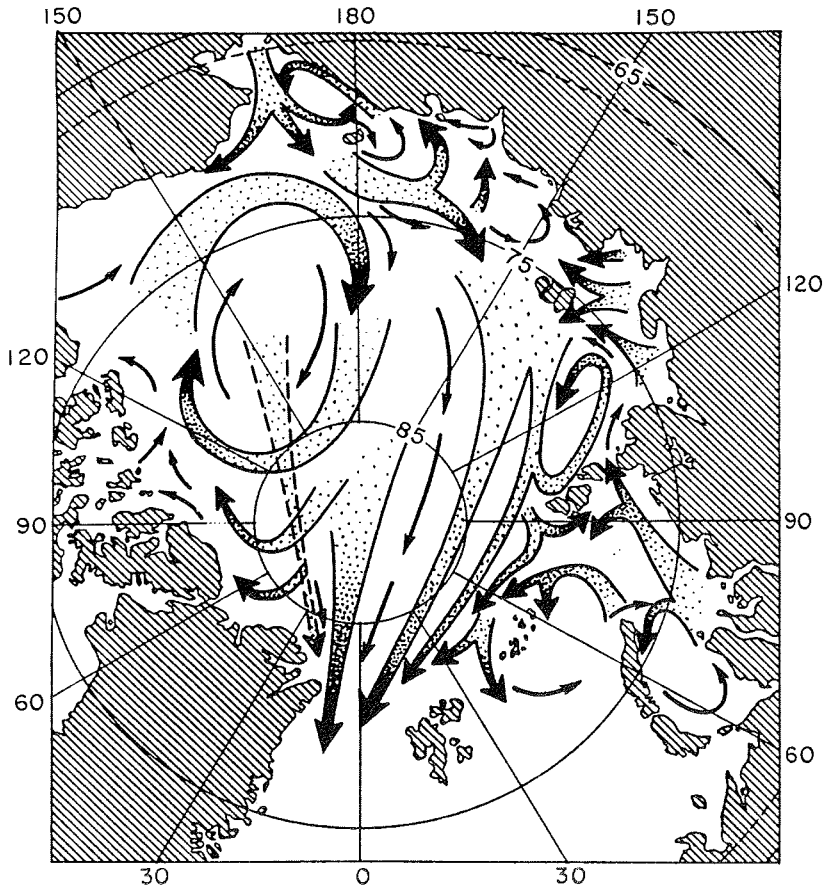

Figure 3: Mean sea–ice drift within the Arctic Ocean after *Gordienko and Laktionov* [1958].

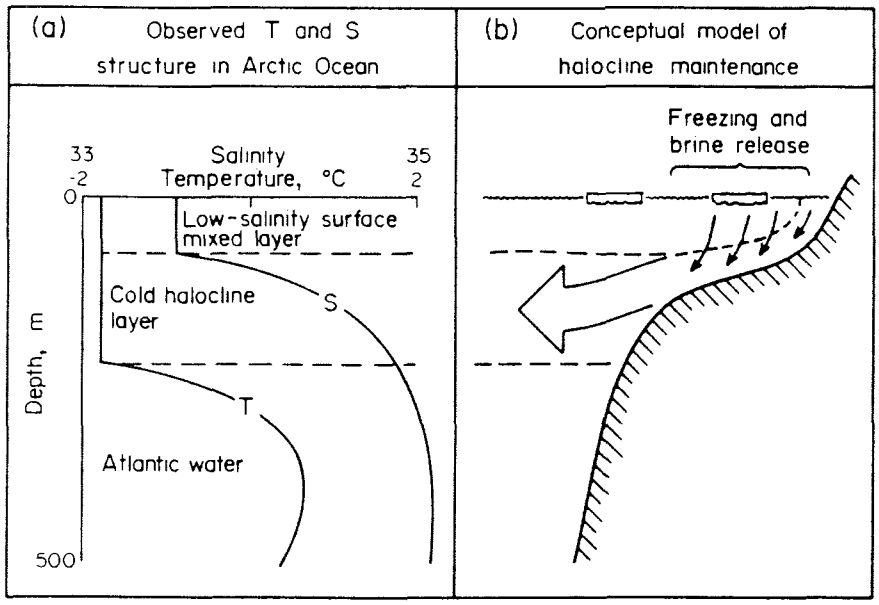

Figure 4: Schematic drawing to illustrate the maintnance of the Arctic Ocean halocline from the shelves after *Aagaard et al.* [1981].

of salinities due to river–runoff, sea–ice meltwater and brine release during sea–ice formation and usually are quite cold. Figure 4 shows a schematic view of the process as well as the temperature and salinity structure of the upper layers [*Aagaard et al.*, 1981]. Little is known about the structure and the flow patterns within the halocline. Chemical properties can be used to distinguish between lower and upper halocline waters. Lower Halocline Water (LHW) has a salinity of about 34.25, potential temperatures close to the freezing point of seawater and a pronounced NO minimum ($NO = [O_2] + 9 \cdot [NO_3]$ [*Broecker*, 1974]). Upper Halocline Water (UHW) is found throughout the Canadian Basin; it is associated with a salinity of 33.1 and a nutrient maximum which at least in part originates in the Pacific [*Kinney*

et al., 1970; *Moore et al.*, 1983; *Jones and Anderson*, 1986; *Wilson and Wallace*, 1990; *Jones et al.*, 1991*a*]. There are indications that the Upper Halocline Water originates in the Chukchi Sea while the Lower Halocline Water is formed in the Barents and Kara seas [*Jones and Anderson*, 1986; *Jones et al.*, 1991*a*].

At about 300 to 500 m depth a temperature maximum is observed. This water has its origin in the Atlantic Ocean from where water entering the Arctic Ocean via the West Spitzbergen Current through Fram Strait. This water mass is called the Atlantic layer and its lower boundary is located at about 800 m water depth. The circulation pattern of the Atlantic layer within the Arctic Ocean has been roughly described based on temperature and salinity core analysis [*Coachman and Barnes*, 1963]. Its circulation is assumed to be cyclonic over the whole Arctic Ocean, with several branches turning towards Fram Strait along the Nansen Gakkel Ridge and the Lomonosov Ridge. Estimates from transient tracer measurements suggest, that the Atlantic layer has a residence time between a few years north of the Barents Sea up to about 15 years in the southwestern Eurasian Basin [*Schlosser et al.*, 1990; *Schlosser et al.*, 1994; *Wallace et al.*, 1992]. This means that at some locations the waters of the Atlantic layer are younger than the overlaying upper halocline waters. There are no estimates for the residence time of the Atlantic layer within the Canadian Basin.

Below the Atlantic layer the temperatures are below 0°C and a slight salinity minimum is found. This layer is called Arctic Intermediate Water (AIW) and its lower boundary is located between about 1000 m and 1500 m water depth. The origin of AIW is relatively unclear. It is assumed to originate from Atlantic–derived water, which is strongly modified over the shelves. A branch of Atlantic–derived water is also entering the Arctic Ocean over the Barents and Kara seas [*Midttun*, 1985; *Pfirman et al.*, 1993*a*; *Aagaard et al.*, 1985; *Swift et al.*, 1983]. Part of it might form AIW while other parts are thought to feed the halocline. Atlantic–derived water plays an important role for the formation of the halocline in the Eurasian Basin.

In the Canadian Basin, nutrient–rich UHW is overlying the Atlantic core and is separating it from the surface water. In these regions, Atlantic–derived water might be less important for the formation of halocline waters [*Macdonald et al.*, 1989].

The waters below the Atlantic–derived layer show comparably small variations in their properties. The temperature and salinity structure shows a break near the isohaline 34.92 [*Aagaard et al.*, 1981; *Smethie et al.*, 1988]. Above the break the water in the Eurasian Basin is called Eurasian Basin Deep Water (EBDW) and below Eurasian Basin Bottom Water (EBBW). EBDW is defined by *Smethie et al.* [1988] as water with temperatures ranging between -0.7 to $-0.97°C$ and a quite narrow salinity range of 34.921 to 34.927. EBBW is defined to have a temperature range between -0.95 to $-0.94°C$ and increasing salinities between 34.930 and 34.940. The depth of the interface is close to the sill depth of Fram Strait of about 2600 m. The residence time of EBDW is estimated from transient tracers to be about 20 to 80 years [*Smethie et al.*, 1988; *Östlund et al.*, 1982; *Bönisch and Schlosser*, 1994], and the residence time for EBBW is estimated to be about 250 to 300 years [*Schlosser et al.*, 1990; *Anderson et al.*, 1989; *Bönisch and Schlosser*, 1994]. The mean age of the water in the Canadian Basin below about 1500 m, which is about the depth of the Lomonosov ridge (1600 m), has been estimated to be 500 to 800 years on the basis of ^{14}C data [*Östlund et al.*, 1987].

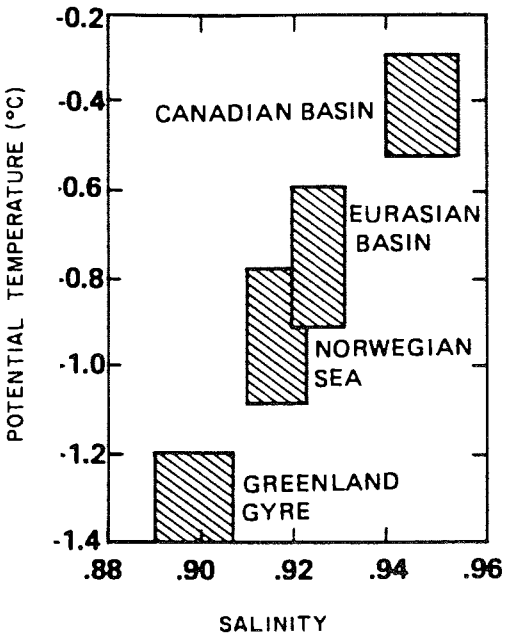

Figure 5: Schematic temperature versus salinity plot for the deep water of the Canadian and Eurasian basins and the Norwegian and Greenland seas (taken from *Aagaard et al.* [1985]).

The deep waters of the Arctic Ocean are known to exchange with each other and the waters of the adjacent seas. The temperature and salinity properties of the deep waters of the Eurasian Basin, the Canadian Basin, the Norwegian Sea and the Greenland Sea are falling on a straight mixing line (see Fig. 5 after *Aagaard et al.* [1985]). Canadian Basin deep water is the warmest and most saline and Greenland Sea deep water is the freshest and coldest. Saline water from the Arctic Ocean has been found to be flowing at mid-depth along the Greenland slope in the western part of the Greenland Sea. It mixes with newly formed deep water from the Greenland Sea to form Norwegian Sea deep water in the Jan Mayen Fracture

Zone [*Aagaard et al.*, 1985; *Smethie et al.*, 1988]. In the Greenland Sea, the density structure is very weak over the entire water column and open ocean convection is one of the possible mechanisms of deep water formation.

The sources of the deep and bottom waters within the Arctic Ocean are not known. The explanation of the origin of the high salinities is particulary difficult. The sources have been argued to be brines from the shelves, but the details and the responsible processes remain speculative [*Aagaard et al.*, 1985; *Jones and Anderson*, 1986; *Wallace et al.*, 1987; *Smethie et al.*, 1988; *Swift et al.*, 1983]. The idea of entrainment of brines from the shelves into the deep and bottom water is thought to be similar to the concept of the maintenance of the halocline. Dense brines which form as a result of sea–ice formation have been observed on the shelves (e.g. *Midttun* [1985]; *Pfirman et al.* [1993*a*]; *Melling and Lewis* [1982]). This water might flow off the shelves and sink down the continental slope as gravitational plumes [*Aagaard et al.*, 1985]. Current measurements made within the Arctic Ocean indicate narrow boundary currents parallel to the shelf edge [*Aagaard*, 1989] and no exchange across the shelf edge has been observed. Therefore it is generally proposed that submarine canyons might play an important role in the interaction between shelves and the deep basins. With the help of oxygen isotope ratios it should be possible to clarify this question with respect to rates of fresh water content of the deep and bottom waters and the origin of those fresh water sourses.

The contrast between the strong thermohaline forcing on the shelves and the strongly stratified structure of the Arctic Ocean interior has led to the conclusion, that the Arctic Ocean circulation is primarily forced from its boundaries. The hydrographic and chemical parameters from both the shelves and the interior basin have given evidence for the importance of the shelf regions as well as indications for differences between the waters of the different shelves [*Kinney et al.*, 1970; *Moore et al.*, 1983; *Jones and Anderson*, 1986; *Östlund et al.*, 1987; *Anderson et al.*, 1989]. In this respect the potential of tracers is considerable. Oxygen isotope ratios

can be used to distinguish the different freshwater sources due to an input of a distinctly depleted $\delta^{18}O$ signal of the river–runoff compared to a $\delta^{18}O$ signal of sea–ice meltwater close to the $\delta^{18}O$ signal of sea water. Additionally, chemical tracers as nitrate, phosphate, oxygen and silicate can be used to distinguish the contribution of Pacific water versus the contribution of Atlantic water.

2.2 Exchange with adjacent seas

The Arctic Ocean is strongly influenced by water from the Atlantic and Pacific oceans. High–salinity water enters through Fram Strait via the West Spitzbergen Current and over the Barents and Kara seas, while low–salinity water enters through Bering Strait from the Pacific. The outflowing water from the Arctic Ocean in turn is influencing the Atlantic and its northern extensions. Water is flowing south through Fram Strait and through the Canadian Archipelango.

Fram Strait is the 450 km wide and 2600 m deep gap between the northeast cape of Greenland and Spitzbergen. At a water depth of 2000 m it is still 100 km wide. Estimates of the transport through Fram Strait vary conciderably (between 2 Sv [*Mosby,* 1962] and 8 Sv [*Coachman and Aagaard,* 1974]). Most recent estimates range from about 5 to 6 Sv for the warm salty water flowing into the Arctic Ocean with the West Spritzbergen Current [*Hanzlick,* 1983]. About two thirds of this transport occurs above 600 m depth. A branch of Atlantic water is flowing into the Arctic Ocean over the Barents and Kara seas. Based on two months of current measurements between Norway and Bear Island, *Blindheim* [1989] calculated the water transport in and out of the southwestern Barents Sea to be about 3 Sv and 1 Sv, respectively. On the basis of a one year current meter record between Novaya Zemlya and Frans Josef Land, *Loeng et al.* [1993] obtained an outflow from the Barents Sea of 0.7 to 3.2 Sv (average: about 2 Sv). An estimate of about 1.2 Sv of water entering the Arctic Ocean either at the Barents or the Kara shelf break was

obtained by *Rudels* [1987] on the basis of mass balance and continuity consideration. In the East Greenland Current, 3 Sv are assumed to leave the Arctic Ocean above 700 m depth [*Foldvik et al.,* 1988]. A large amount of sea ice is transported south with the East Greenland Current and a big part of it is melting between 82 and 80 °N [*Vinje and Finnekasa,* 1986]. The estimates range between 0.10 Sv [*Hibler,* 1979] and 0.18 Sv [*Koerner,* 1983]. The freshwater transported with the East Greenland Current both in the water column and as sea–ice are of major importance for the thermohaline balance of the Greenland and Iceland seas.

At mid depth EBDW flows in a boundary current along the Greenland slope and eastwards through the Jan Mayen Fracture Zone where it mixes with GSDW to form new NSDW. Part of NSDW is feeding back into EBDW within the Arctic Ocean [*Smethie et al.,* 1988]. The deep exchange through Fram Strait has been estimated from tracer balances to be about 0.6 Sv in and about 0.9 Sv out of the Arctic Ocean; also the rates of deep water formation have been estimated to be about 0.3 Sv for EBDW and 0.04 Sv for EBBW [*Bönisch and Schlosser,* 1994].

The outflow of surface water from the Canadian Basin through the Canadian Archipelago was estimated from current meter data to be about 1.7 Sv [*Fissel et al.,* 1988].

Bering Strait is about 85 km wide and only about 50 m deep. Transport estimates based on current meter measurments give a flow rate of about 0.8 Sv with an anual amplitude of about 0.6 Sv and a considerable interannual variation [*Coachman and Aagaard,* 1988]. The flow is driven by a persistent pressure gradient between the Bering Sea and the Arctic Ocean. Little is known about the flow and modification of the water after it passes through the strait.

3 Determination of oxygen isotope ratios in natural waters

Oxygen is the most abundant element on Earth. It has three stable isotopes with the masses 16, 17 and 18 with relative abundances of 99.76% 0.04% and 0.20%, respectively [*Garlick,* 1969]. For studies of water movements in natural systems the $^{18}O/^{16}O$ ratio is a powerful tracer due to the fact that fractionation of oxygen isotopes labels water reservoirs with distinct $^{18}O/^{16}O$ ratios. Fractionation of the isotopic composition in the global water cycle occurs mainly during phase transitions (evaporation and condensation). As a result, freshwater derived from precipitation has a relatively wide range of $^{18}O/^{16}O$ ratios (more precisely: $H_2{}^{18}O/H_2{}^{16}O$ ratios), while ocean water shows a relatively small variation in its $^{18}O/^{16}O$ ratio and its isotopic composition is mainly determined by mixing between water masses and addition of freshwater in shelf regions.

3.1 Water–CO_2 equilibration method

In order to determine the $^{18}O/^{16}O$ ratio in water, CO_2 gas is equilibrated with the water sample and the CO_2 is analysed mass spectrometrically [*Epstein and Mayeda,* 1953]. For this method, the fractionation factor for isotopic equilibrium between CO_2 and H_2O as function of temperature has to be known.

The fractionation factor α is defined as the ratio of the number of any two isotopes in a chemical compound A devided by the corresponding ratio in another compound B: $\alpha_{A-B} = \frac{R_A}{R_B}$. The isotopic ratio of two compounds A and B actually measured in a laboratory are expressed in the δ–notation, i.e. the permille deviation of the $^{18}O/^{16}O$ ratio of the sample to that of a standard: $\delta_A(‰) = (\frac{R_A - R_B}{R_B}) \cdot 10^3$. The δ–value and the fractionation factor are approximately related by $\delta_A - \delta_B \cong 10^3 \cdot ln\ \alpha_{A-B}$. This approximation is excellent for differences in δ–values of less than

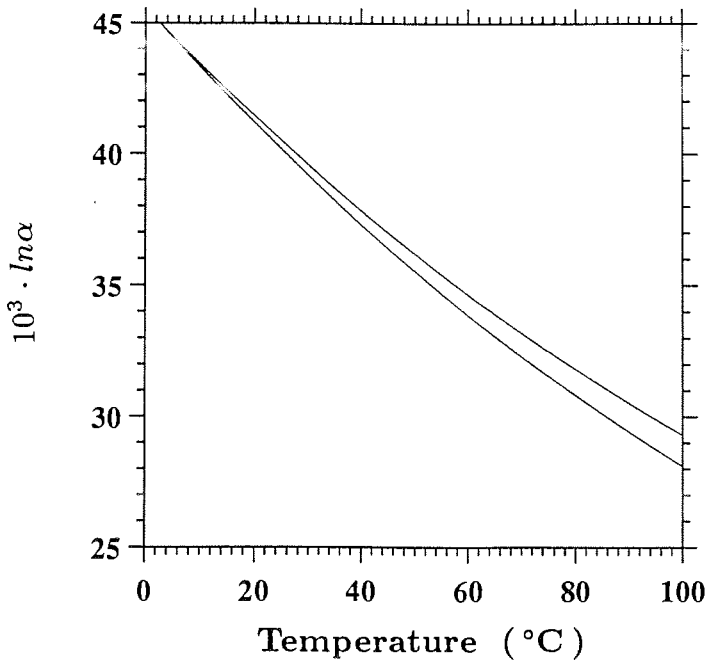

Figure 6: Fractionation of the $^{18}O/^{16}O$ ratios between water and CO_2 expressed as $10^3 ln\alpha$ versus temperature. The lower curve is from *Bottinga* [1973] and the upper curve from *O'Neil and Adami* [1969] (see text).

about $10‰$.

The fractionation factor between water vapor and CO_2 gas was determined experimentally at different temperatures and the results have been described by the formulas:

$10^3 \cdot ln\alpha = -0.0206 \cdot 10^6 \cdot T^{-2} + 17.99 \cdot 10^3 \cdot T^{-1} - 19.97$ [*Bottinga*, 1973]

$10^3 \cdot ln\alpha = 16.60 \cdot 10^3 \cdot T^{-1} - 15.19$ [*O'Neil and Adami*, 1969]

(see also Fig. 6)

$H_2{}^{18}O/H_2{}^{16}O$ measurements of water samples are usually given in the δ–notation

and calibrated using standard mean ocean water (SMOW) [*Craig,* 1961]:

$$\delta\,^{18}\mathrm{O}(‰) = \frac{^{18}\mathrm{O}/^{16}\mathrm{O}_{sample} - ^{18}\mathrm{O}/^{16}\mathrm{O}_{SMOW}}{^{18}\mathrm{O}/^{16}\mathrm{O}_{SMOW}} \cdot 1000$$

The $^{18}O/^{16}O$ ratio is determined by direct comparative measurements of a SMOW standard.

3.1.1 Routine operation of the water–CO_2 equilibration system

In this study, a system was used for equilibration of CO_2 with H_2O which allows simultaneous processing of 6 samples (Fig. 7, modified after *Fairbanks* [1982] and *Roether* [1970]). 5 ml of the water samples were pipetted into the 50 ml equilibration flasks. The vessels were attached to the system using 9 mm O-ring joints. The equilibration flasks were submerged into a temperature bath and the water temperature was controlled at about 18.0 °C by a regulator immersed in the bath. The equilibration flasks were opened simultaneously to a rotary pump ($50\,l \cdot min^{-1}$) to remove the atmospheric air. The flow was reduced by capillaries, consisting of precision bore glass capillaries (5 cm long, 0.65 cm O.D. and 500 μm I.D.) through which a 200μm diameter filament was inserted to adjust the leak rate and to reduce turbulence [*Roether,* 1970]. The system pressure was monitored on a thermocouple gauge and the samples were isolated after 5 minutes. The water samples were charged simultaneously with 400 mm Hg CO_2 gas. The CO_2 was taken from a tank of commercially purchased gas (Matheson Gas Product, scientific grade; purity better than 99.999%). After isolating the samples, the temperature of the bath was raised to 35 °C and the samples were equilibrated over night.

An aliquot of the CO_2 gas was taken from the equilibration flasks by expanding the gas into the volume of the capillary between the two stopcocks. The equilibration flask was isolated from the aliquot volume after 10 seconds to insure that no dissolved CO_2 was sampled, which would kinetically fractionate during transition from the

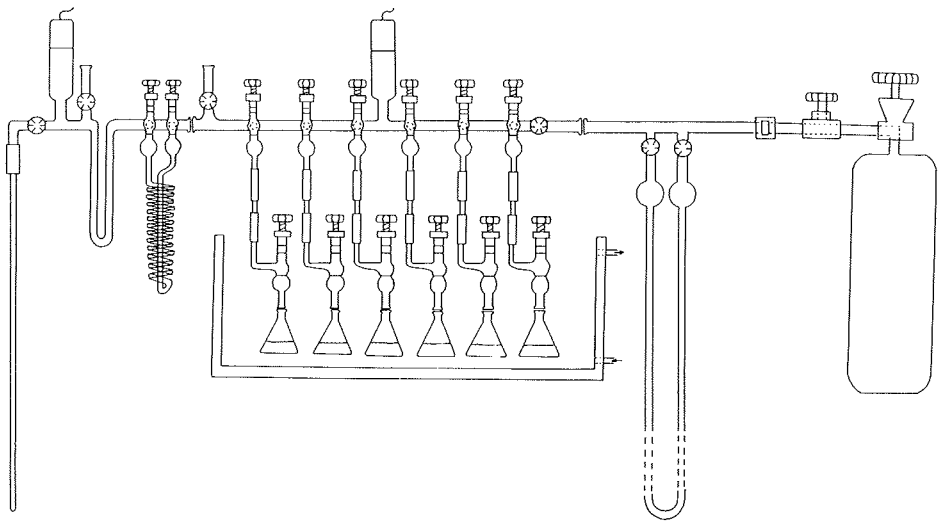

Figure 7: Schematic drawing of the apparatus used for equilibration of water samples and CO_2 gas.

Table 1: Water loss during sample preparation

stand	before pumping weight [g]	after 30 min pumping weight [g]	H_2O loss [mg/30 min]	H_2O loss / 5 min [mg]	[%]
1	43.7765	43.7345	42.0	7.0	0.14
2	43.6216	43.5775	44.1	7.4	0.15
3	44.4919	44.4481	43.8	7.3	0.15
4	44.0654	44.0215	43.9	7.3	0.15
5	39.3795	39.3363	43.2	7.2	0.14
6	40.9523	40.9100	42.3	7.1	0.14

water to the gas phase. The CO_2 aliquot was immediately passed through a coil cooled by a dry–ice/isopropanol alcohol bath to remove the water vapor and trapped in an U–tube colled to liquid N_2 temperature. After 5 minutes, non–condensables were removed and the U–tube was isolated. The temperature was raised to the temperature of a dry–ice/isopropanol alcohol bath and the CO_2 was trapped in a 1/4" O.D. glass tube cooled by liquid N_2. After a 5 minutes waiting period, the CO_2 sample was flame–sealed in the tube.

In the process of removing the atmospheric air, a small amount of the sample water is lost. The water will be fractionated during evaporation of water vapor. About 7 mg of water were lost after a pumping time of 5 minutes (see Tab. 1).

Assuming a fractionation of -10‰ in the lost water vapor relative to the remaining H_2O, and 0.2% of the original sample being lost, the remaining H_2O sample will have a $\delta^{18}O$ value which is about 0.020‰ higher than that of the original water sample. All samples and the water standard used for calibration are corrected for this isotopic change.

Usually, water–CO_2 equilibration is performed at room temperature and the

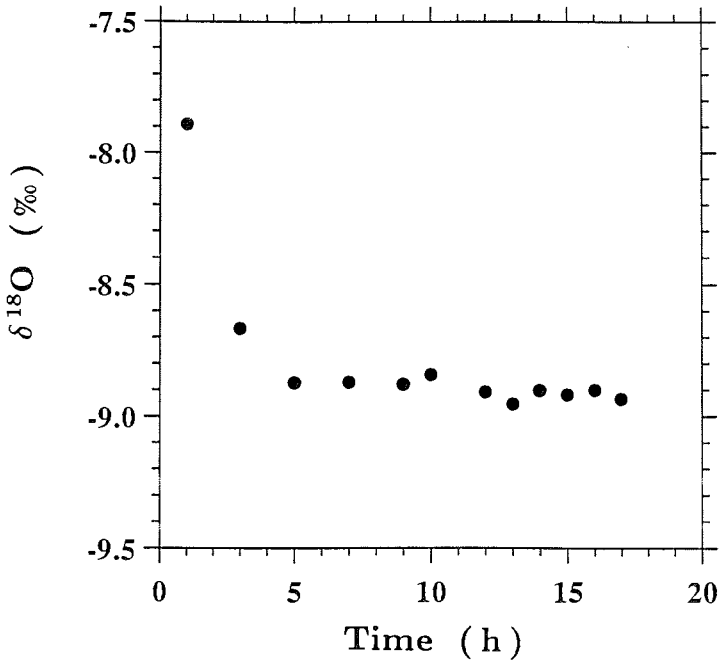

Figure 8: $\delta^{18}O$ results of replicate samples versus equilibration time.

samples are shaken or stirred to accelerate the gas exchange rate [*Roether*, 1970; *Fairbanks*, 1982]. The system used in this study had no mechanism to shake or stir the water samples. In order to achieve a reasonably short equilibration time, the equilibration temperature was raised above room temperature. At an equilibration temperature of 35 °C, the $\delta^{18}O$ values of a replicate sample become stable after about 6 hours (Fig. 8). For routine processing, the samples were kept at a constant temperature of 35 °C over night so that complete equilibration of the isotopic composition between the CO_2 gas and the water sample was guaranteed.

The temperature controller was able to hold a stable temperature at around 35 °C with maximum variations of about ± 0.05 °C over a time period of about 20 hours (checked externally with a mercury thermometer from Brooklyn Thermome-

ter; calibrated at 35 °C to ±0.01 °*C*). It was not possible to adjust the temperature setting to the exact same temperature between runs. Therefore a temperature within ± 0.2 °*C* of 35 °C was accepted and the δ^{18}O results were corrected to 35 °C by using the slope of the curves given by *Bottinga* [1973] and *O'Neil and Adami* [1969] (about 0.185 ‰/°C at 35°C).

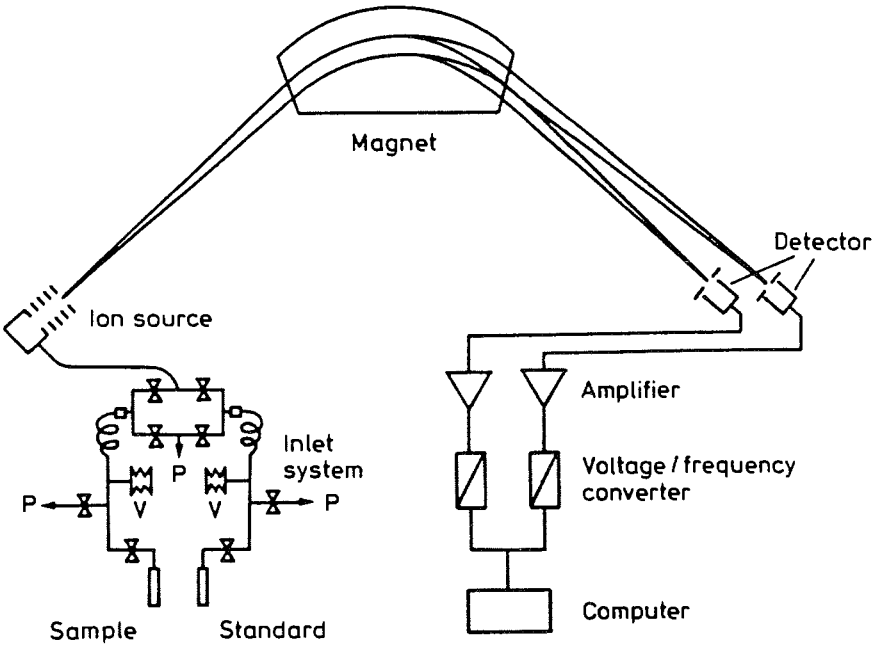

Figure 9: Schematic drawing of a mass spectrometer with double inlet system and double collector (taken from [*Hoefs*, 1987]). The mass spectrometer used for this study was equipped with a triple collector (see text).

3.2 Mass spectrometric measurement and calibration

For this study, a commercial mass spectrometer from Finnigan MAT (MAT 251) with a double inlet system and a triple collector was used (see Fig. 9 for a schematic view of a similar mass spectometer with double collector [*Hoefs*, 1987]). During an oxygen isotope measurement, the collectors were adjusted to count the isotopic compounds $^{12}C^{16}O^{16}O$ (mass 44), $^{12}C^{18}O^{16}O$, $^{13}C^{17}O^{16}O$ and $^{12}C^{17}O^{17}O$ (mass 46), and $^{13}C^{16}O^{16}O$ and $^{12}C^{17}O^{16}O$ (mass 45). About 99.8 % of the ion current of mass 46 is caused by $^{12}C^{18}O^{16}O$. Determination of mass 45 allows for correction of the

interference of different isotopic species with the molecular weight 46. This is done via the statistical distribution of ^{18}O, ^{17}O and ^{13}C and under the assumption that the isotopic fractionation of ^{17}O is half that of ^{18}O [*Gat and Gonfiantini,* 1981].

The inlet system has two reservoirs for CO_2 gas: one for the sample and one for the standard. From each reservoir, a capillary leads the gas in viscous flow to a change–over valve, and either sample or standard gas are released into the ion source of the mass spectrometer. The change–over valve allows to switch conveniently between standard and sample during a measurement. In the ion source, the CO_2 molecules form ions as a result of collisions between electrons and gas molecules. The electrons are emitted from a heated filament and have an energy of about 59 eV, which provides maximum efficiency for single ionisation of CO_2 molecules and a low probability for production of multiply charged ions. Therefore, the positive ions entering the magnetic field are essentially monoenergetic according to $1/2\,mv^2 = eV$, where eV is the electric field used for acceleration of the ions. In the magnetic field, the ions are deflected onto a circular path with radii proportional to the square root of m/e. After passing through the magnetic field, the separated ions are collected in an ion detector and converted into an electrical signal. The overall instrumental error of the mass spectrometer was between $\pm 0.010‰$ and $\pm 0.025‰$, determined from the standard deviations of 8 standard/sample ratio comparisons.

3.2.1 Routine operation of a mass spectrometric δ^{18}O measurement

In the beginning of each measurement day, the standard reservoir of the inlet system was filled with the laboratory CO_2 reference gas "BO5", which had been produced by dissolving $CaCO_3$ in acid. The reference gas aliquot was chosen large enough to give an initial reading of 6 V on the main collector (mass 44). The CO_2 sample enclosed in the flame sealed glass tube was placed in a tube cracker, consisting of stainless steel Ultratorr connectors with a flexible bellow part and a glass fritte facing the

inlet system to prevent glass parts from entering the system. After evacuating the system, the glass tube was broken and the gas was allowed to expand for 2 minutes into the sample reservoir of the inlet system. The initial voltage on the main collector was recorded and served as a measure for the sample size. The bellows of both the sample and the standard side were compressed, so that a reading of 6 V on the main collector was observed. After this step the computer–controlled measurement program of the mass spectrometer was started. The computer switches 8 times between sample and standard and determines 44/46 and 44/45 mass ratios. The measurement program calculates the average 44/46 and 44/45 ratios and applies an ion correction for $^{13}C^{17}O^{16}O$ and $^{12}C^{17}O^{17}O$ proportional to the 44/45 ratio and the 44/46 ratio assuming that the ^{17}O fractionation is half that of ^{18}O. This value is converted to a $\delta\,^{18}$O value of the sample relative to the reference gas BO5. For further details, see the operating manual and measurement program supplied by *Finnigan MAT* [1985].

3.2.2 Calibration of the mass spectrometric measurements

All $\delta\,^{18}$O measurement results are initially calibrated against the laboratory CO_2 reference gas BO5. The $\delta\,^{18}$O value of the water standard NADW (North Atlantic Deep Water, taken at 3000m depth in the North Atlantic during an expedition on RV Knorr in 1971) is known to be $0.22‰$ relative to SMOW from direct comparative measurements (*Fairbanks*, personal communication). For calibration of the sample measurements the ratios of $\delta\,^{18}$O values of NADW to BO5 was determined. With each set of 6 samples, one sample of NADW was equilibrated and measured. In this way, a significant number of NADW samples were analysed during each measurement period and a quality control was ensured for each equilibrated sample set. Each sample result was corrected from the equilibration temperature to 35.0 °C using the relationship $0.185‰$/°C (taken from *Bottinga* [1973]; *O'Neil and*

Table 2: Average $\delta^{18}O$ values of NADW versus BO5

time period	$\delta^{18}O$ [‰] NADW versus BO5	stand. dev. (σ)	number
Oct. 91	−1.014	±0.029	15
Nov. 91	−1.072	±0.021	38
Jan. 92	−1.075	±0.028	50
Feb. 92	−1.095	±0.023	24
Jun. 92	−1.111	±0.032	43
Sep. 92	−1.117	±0.030	38
Nov. 92	−1.070	±0.033	37
all	−1.085	±0.038	245

Adami [1969]). The average $\delta^{18}O$ value versus BO5 for all NADW samples measured in the measurement period was determined and this value was used for calculation of the $\delta^{18}O_{SMOW}$ value of each sample. The calibration is in first order a shift by the difference between the average $\delta^{18}O_{BO5}$ value of NADW and the $\delta^{18}O_{SMOW}$ value of NADW, but the δ–function is not simply additive: If δ' is the sample composition relative to a secondary standard, which deviates δ_{ST} from SMOW, then the sample composition relative to SMOW is: $\delta = \delta' + \delta_{ST} + \delta' \cdot \delta_{ST}$. Table 2 lists the average $\delta^{18}O$ results of NADW versus BO5 obtained during each measurement period (named after month and year of the measurement period).

A correction was applied for the initial $\delta^{18}O$ composition of the CO_2 gas used for equilibration. The ratio of oxygen atoms contained in 5 ml of liquid H_2O and in $45\,cm^3$ CO_2 at a pressure of 40 cm Hg is about 140:1. The tank CO_2 gas has a $\delta^{18}O$ value of -6.460 ± 0.010 with respect to BO5 and is about 5.5‰ lighter than SMOW and most of the processed ocean water samples. For a sample with the isotopic composition of 0‰ relative to SMOW, the necessary correction due to the initial $\delta^{18}O$ composition of the CO_2 gas used for equilibration is about +0.035‰,

while for a sample with an isotopic composition of $-3\,‰$ the correction is about $+0.014\,‰$.

The overall error of the $\delta^{18}O$ measurement, including the sample preparation was determined from the standard deviation (σ) of replicate samples of NADW. For the different measurement periods, the overall error ranged from $\pm 0.02\,‰$ to $\pm 0.03\,‰$ (see Tab. 2). For comparative reasons, the overall error was also estimated by calculation according to a Gaussian error progression from the estimated errors due to temperature stability ($\pm 0.05\,°C$), temperature correction ($\pm 0.050\,‰/°C$), knowledge of the shift between $\delta^{18}O$ values of SMOW and NADW ($\pm 0.010\,‰$), the $\delta^{18}O$ value of tank CO_2 ($\pm 0.010\,‰$) and the statistical error of the mass spectrometer measurement (± 0.010 to $\pm 0.025‰$). The results are dominated by the statistical error of the mass spectrometric measurement and range frm ± 0.015 to $\pm 0.030\,‰$.

Over the period of about one year, the isotopic composition of NADW compared to BO5 changed slightly (Fig. 10). Between October 1991 to September 1992 the average $\delta^{18}O$ value of NADW compared to BO5 decreased by about $0.1\,‰$. The $\delta^{18}O$ value of NADW for the last measurement period (November 92) is about $0.05\,‰$ heavier compared to the value obtained in the preceeding measurement period (September 1992). There are three possibile explanations for this shift: an isotopic change of the NADW water standard and of the BO5 reference gas and variations due to changes in the linearity of the mass spectrometer. The NADW water standard was kept in a 20 l glass bulb, sealed with a hard–rubber stopper and a layer of paraffin wax. About 10 l of the original 20 l H_2O were left. If the standard water was lost by evaporation or if it equilibrated with the enclosed atmospheric air, the remaining water would become isotopically heavier. This is the opposite effect than the one observed. Salinity was determined at two times and no significant difference was found. Three batches of NADW were taken from the bulb and no differences were observed between the batches (samples of NADW from different

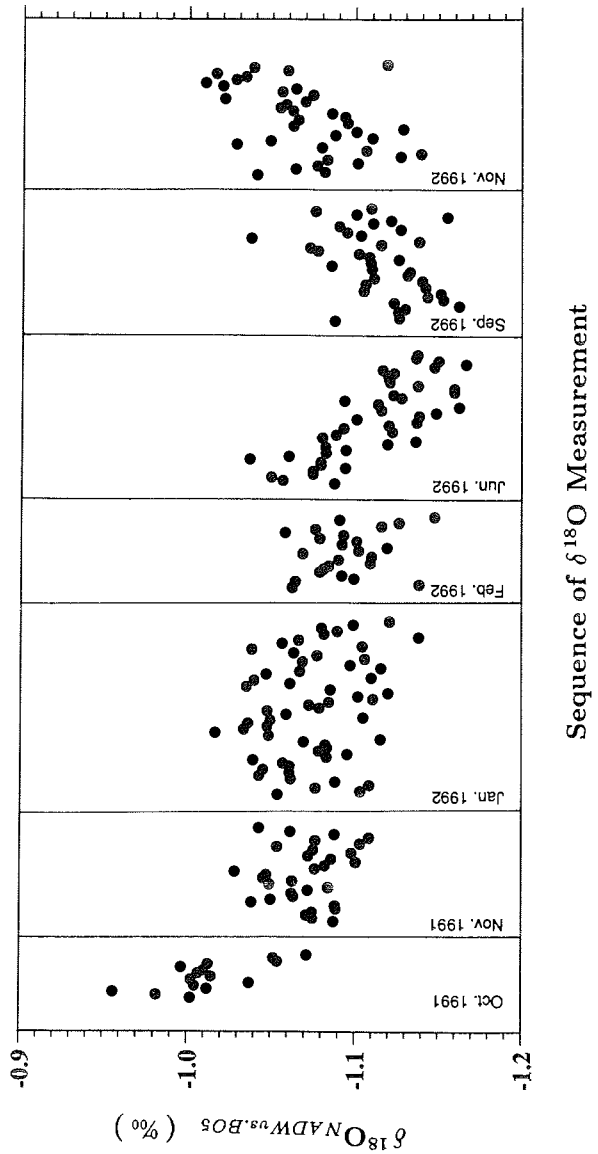

Figure 10: $\delta^{18}O$ versus BO5 results of NADW samples listed in the sequence of measurement. The measurement period is indicated.

batches were prepared in one set and measured during one day). The laboratory reference gas BO5 was kept in a stainless steel tank of about 21 volume, connected through a 60 cm long and 0.01 mm I.D. capillary to the inlet system of the mass spectrometer. Aliquots were taken by expansion into the capillary volume using an equilibration time of 2 minutes. A slight fractionation may occur during this process which would prefer the heavier molecules to stay in the tank. A small effect might be adding up over a long period of time. This scenario seems possible, since between October 91 and September 92 the pressure in the storage container dropped considerably (for the same amount of gas 2 aliquots were needed at the beginning and 5 aliquots at the end). This scenario cannot be an explanation for the isotopic change of NADW compared to BO5 between September 92 and November 92. For this effect, only the third possibility might be responsible: Internal changes in the mass–spectrometer might influence the electronics and the linearity of the mass spectrometer. The last possibility or a combination of the last two possibilities might serve as a possible explanation.

The size of the CO_2 samples varied depending on the stand number. Figure 11 shows the initial voltage versus the $\delta^{18}O$ of NADW samples obtained during the September 92 measurement period. The initial voltages read on the main collector can be used as an indication for the amount of CO_2 gas expanded into the sample reservoir. It seems that the volume between the stopcocks of the CO_2 equilibration apparatus differ from stand to stand.

Figure 12 shows the results of NADW versus the stand number on which the samples had been prepared during equilibration of water and CO_2 gas. The pattern in the plot is noisy and the differences are not significant and no correction was applied.

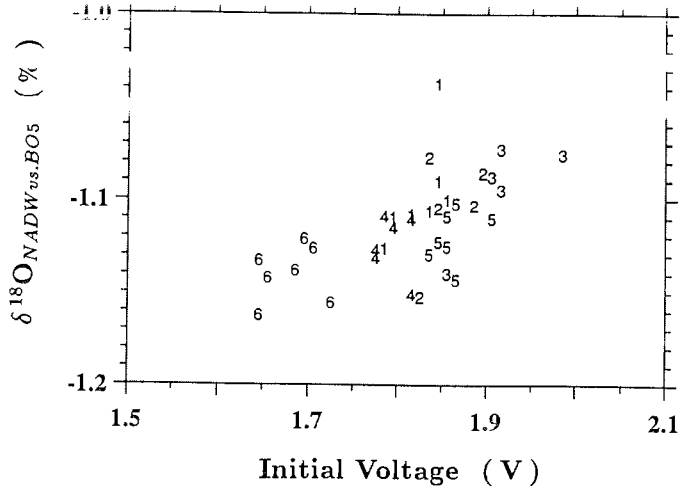

Figure 11: δ^{18}O versus BO5 results of NADW samples versus initial voltage for samples measured during September 1992 period. The numbers represent the stand on which the samples were prepared.

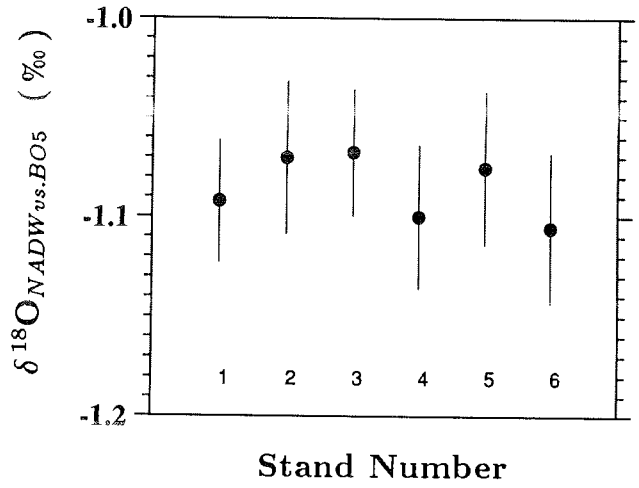

Figure 12: δ^{18}O versus BO5 results of NADW samples sorted by stand number, as indicated at the bottom. The errors are represented by the length of the bars.

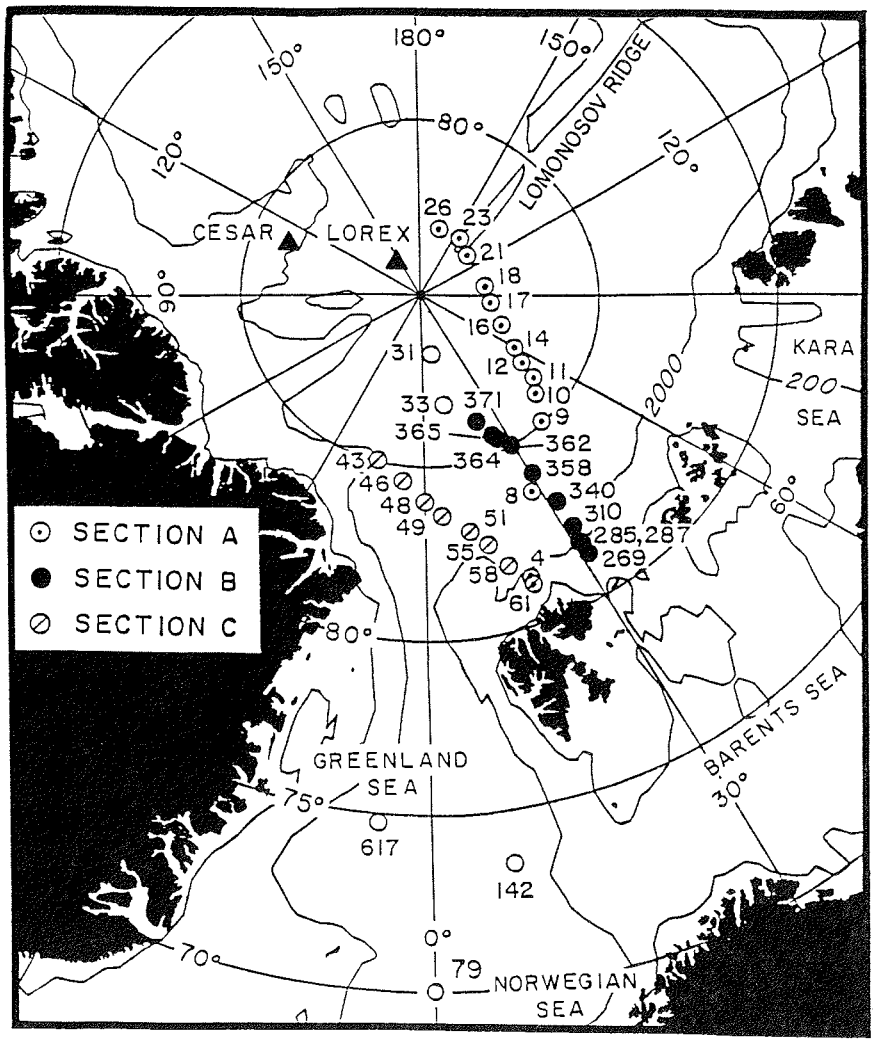

Figure 13: Geographic positions of the stations located in the central Arctic Ocean and the Norwegian and Greenland seas analysed for this study (ArkIV/3, ARCTIC 91, M71, M8). The positions of the CESAR and LOREX ice camps are also included.

4 Sample collection and measurement

4.1 Arctic Ocean and Norwegian and Greenland seas datasets

The Arctic Ocean data used in this study were collected along the 1987 Nansen Basin section occupied by the German research icebreaker *Polarstern* during the ArkIV/3 expedition [*PSSP*, 1988] and on sections covering the Nansen, Amundsen and Makarov basins occupied by the Swedish icebreaker *Oden* in the framework of the ARCTIC 91 expedition [*Anderson and Carlson*, 1991] (for geographic position of the stations, see Fig. 13).

Samples from two stations located in the Norwegian and Greenland seas (stations 617 and 79, respectively) were measured. These stations were occupied by the German research vessel *Meteor* in 1985 (M 71, sta. 79) and 1988 (M 8, sta. 617).

During each cruise hydrographic data and a variety of tracer data were collected (e.g. *PSSP* [1988]; *Anderson et al.* [1989]; *Anderson and Carlson* [1991]). Here ^{18}O and salinity data from the upper water column are discussed, obtained on sections occupied in 1987 (Barents Shelf to the Gakkel Ridge, section B in Fig. 13) and in 1991 (Barents Shelf to the Makarov Basin, section A in Fig. 13 and Yermak Plateau to Morris Jessup Plateau, section C in Fig. 13). Additionally ^{18}O data is evaluated, collected on stations in the central basins of the Arctic Ocean and the central Greenland and Norwegian seas covering the entire water column (stations 358, 16, 26, 33, 617 and 79 in Fig. 13).

A small fraction of the ^{18}O halocline samples collected in 1987 were measured at the Institute for Environmental Physics at the University of Heidelberg [*Schlosser et al.*, 1993]. Precision of these $^{18}O/^{16}O$ ratios was typically $\pm 0.07\,‰$. The major part of the ^{18}O samples were measured at the Lamont–Doherty Earth Observatory using a commercial mass spectrometer (MAT 251) after equilibration of the water samples with CO_2 (see Chap. 3). ^{18}O results are reported in the δ notation where

$\delta\,^{18}O$ is the permille deviation of the $^{18}O/^{16}O$ ratio of the sample from that of SMOW (Standard Mean Ocean Water). Precision of the L–DEO $\delta\,^{18}O$ data is about ± 0.02 to $0.03\,{}^{o}/_{oo}$.

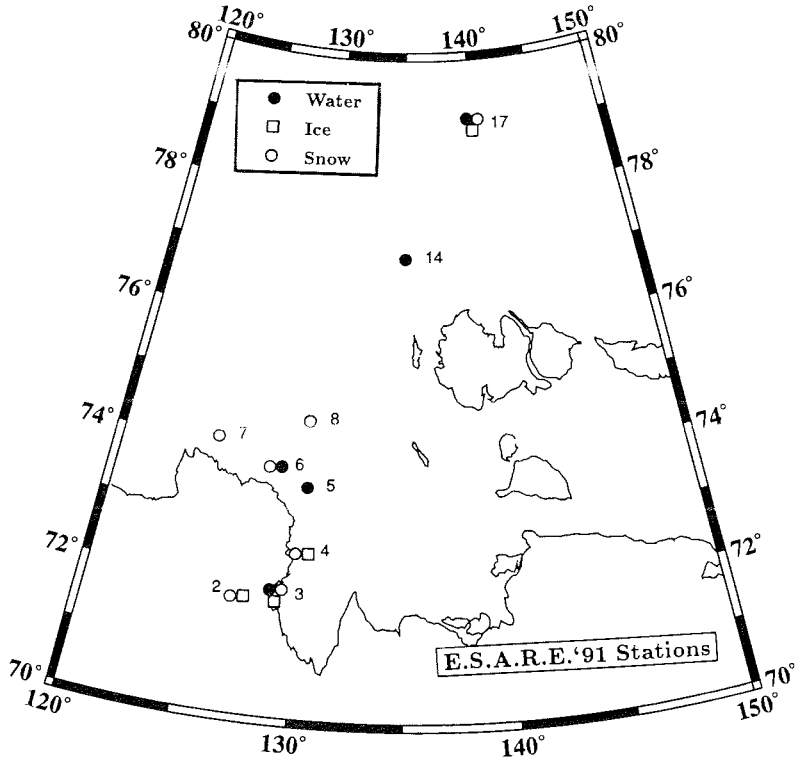

Figure 14: Geographic positions of the stations located in the Laptev Sea.

4.2 Laptev Sea dataset

Surface water samples and snow and ice samples were taken during the E.S.A.R.E.'92 expedition [*Dethleff et al.*, 1993] in the Laptev Sea and in the Lena River delta in April 1992 (for geographic position of the stations, see Fig. 14). The $\delta^{18}O$ measurements of this data set have an overall precision of about $\pm 0.03\,‰$. Salinity measurements were made in August 1992 after the samples arrived at L–DEO at a minisal instrument with an uncertainty smaller than ± 0.01 (AGE 2100 instrument specification: ± 0.003).

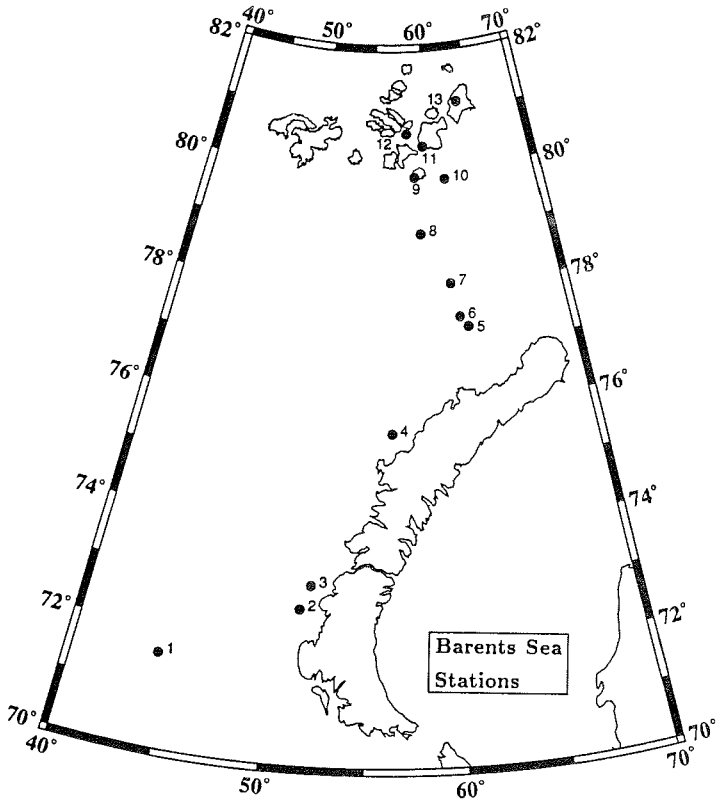

Figure 15: Geographic positions of the stations located in the Barents Sea.

4.3 Barents Sea dataset

Water samples were taken during the expedition with RV *Dalnie Zelentsy* [*Nürnberg and Groth,* 1993] in the Novaya Zemlya and Franz–Josef–Land area in the Barents Sea in August 1992 (for geographic position of the stations, see Fig. 15). The $\delta^{18}O$ measurements of this data set have an overall precision of about $\pm 0.03\,‰$. Salinity measurements were made in December 1992 after the samples arrived at L–DEO at a minisal instrument with an uncertainty smaller than ± 0.01 (AGE 2100 instrument specification: ± 0.003).

5 Results

5.1 Shallow Arctic Ocean

A general feature of the $\delta^{18}O$ distribution in the Eurasian Basin halocline (Fig. 16 a) are low values in the surface waters which increase with depth to reach a maximum of about 0.25 ‰ to 0.3 ‰ at about 300 to 500 m, i.e. in the core of the Atlantic water. The surface values are relatively high on the Barents Shelf (about 0.25 ‰ at station 269; and 0.03 ‰ at station 61; Fig. 2 a) and decrease with latitude to reach minimum values of about −2.54 ‰ at station 26 in the Makarov Basin. In section C north of Fram Strait, the minimum $\delta^{18}O$ value is −2.87 ‰ at station 43 at the western end of the section. This trend in the $\delta^{18}O$ pattern reflects the higher river–runoff fraction in the surface waters of the central Eurasian Basin and in the Canadian Basin.

The salinity distribution (Fig. 16 b) is similar to the $\delta^{18}O$ distribution with low values at the surface which increase to about 34.9 at 300 m depth. The surface values are relatively high on the Barents Shelf and decrease toward the north. The surface salinities on the Barents Shelf do not reach the values of the Atlantic core as is the case of $\delta^{18}O$. They stay at about 34.0 or lower. The surface salinity distribution shows a relative smooth south/north decrease, while the $\delta^{18}O$ distribution is characterized by a strong gradient in the central Nansen Basin with lower values found in the northern part of the section.

The temperature distribution shows values close to the freezing point of sea water near the surface (Fig. 16 c). At about 300 to 500 m the temperature distribution shows a local maximum reflecting the Atlantic core. The highest values are found near the shelf break of the Barents Sea.

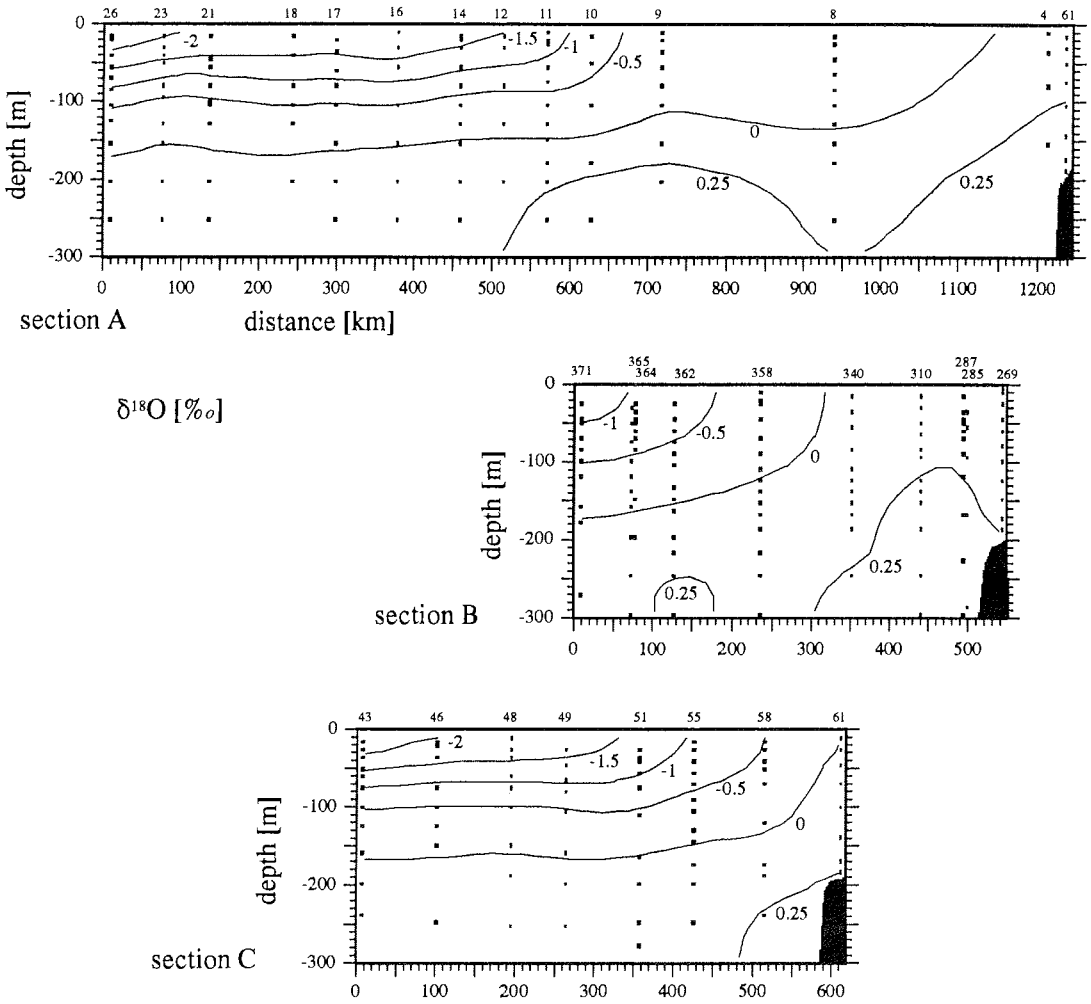

Figure 16: (a) $\delta^{18}O$ section of the upper 300 meters of the water column for three sections across the Eurasian Basin (for geographical position of the stations, see Fig. 13). (b) Same as in a) for salinity. (c) Same as in a) for potential temperature.

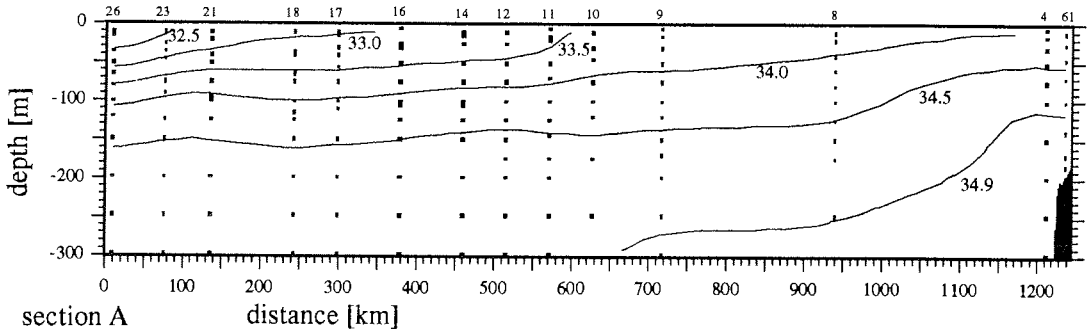
26 23 21 18 17 16 14 12 11 10 9 8 4 61
32.5
33.0
33.5
34.0
34.5
34.9
depth [m]
0
-100
-200
-300
0 100 200 300 400 500 600 700 800 900 1000 1100 1200
section A
distance [km]

salinity

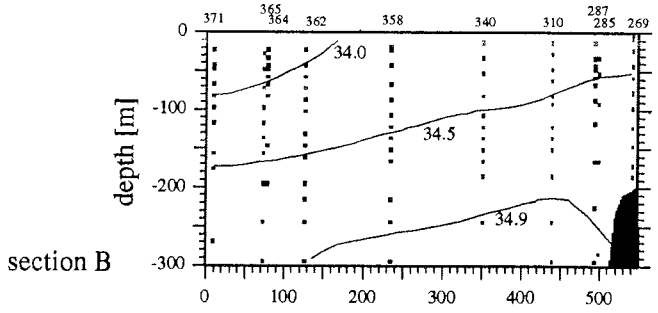
371 365 364 362 358 340 310 287 285 269
34.0
34.5
34.9
depth [m]
0
-100
-200
-300
0 100 200 300 400 500
section B

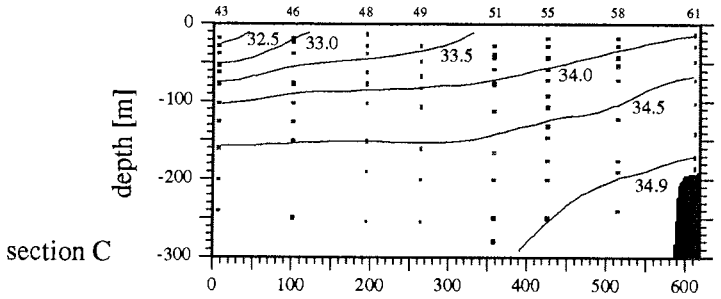
43 46 48 49 51 55 58 61
32.5
33.0
33.5
34.0
34.5
34.9
depth [m]
0
-100
-200
-300
0 100 200 300 400 500 600
section C

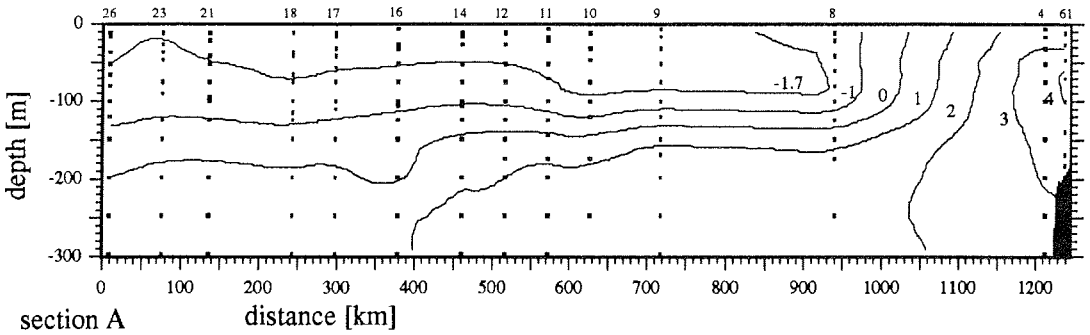
depth [m]
distance [km]
section A
pot.temperature [°C]
-1.7
-1
0
1
2
3
4

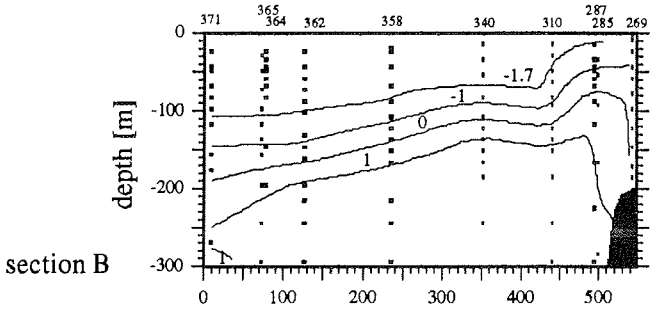
depth [m]
section B
-1.7
-1
0
1

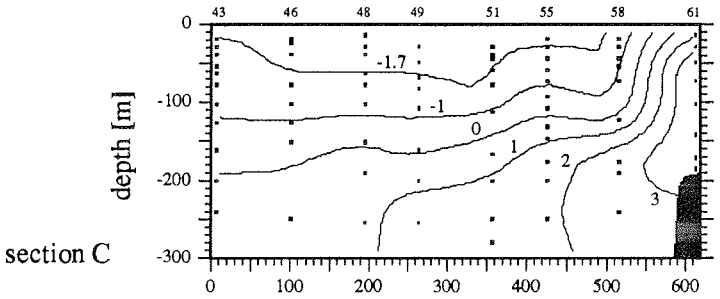
depth [m]
section C
-1.7
-1
0
1
2
3

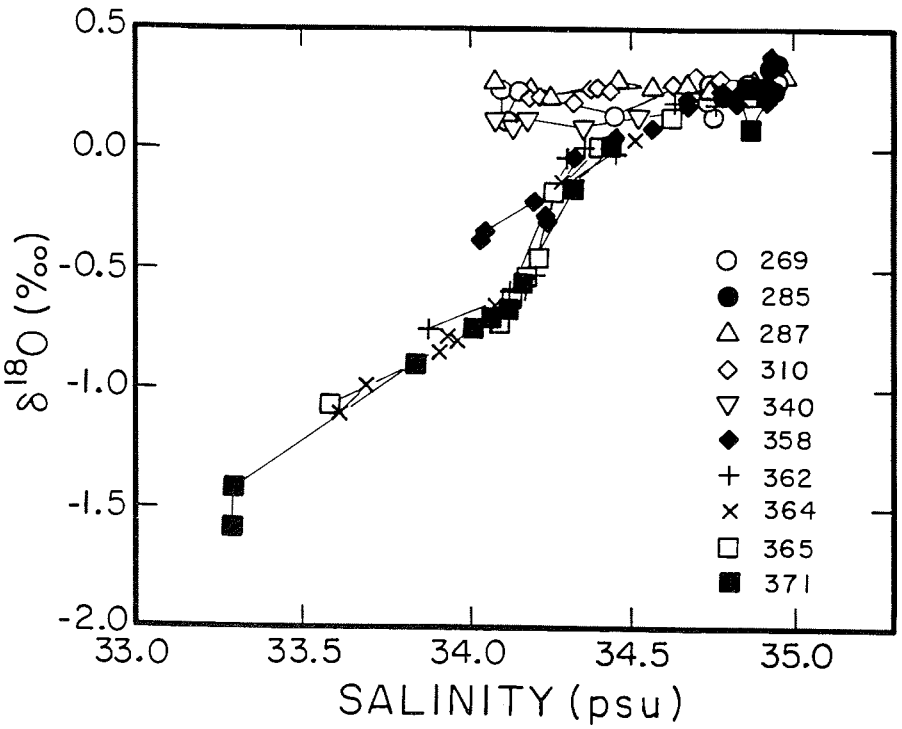

Figure 17: $\delta^{18}O$ versus salinity plot of stations located in the central Arctic Ocean (Ark IV/3 stations). (for geographical position of the stations see Fig. 13).

The $\delta^{18}O$ versus salinity plot for halocline waters (Fig. 17) is strongly non-linear. As the sea ice formation adds significant amounts of salt but influences the ^{18}O balance only slightly due to the small fractionation factor, the $\delta^{18}O$ versus salinity plot for halocline waters is basically meaningless with respect to mixing considerations without additional information.

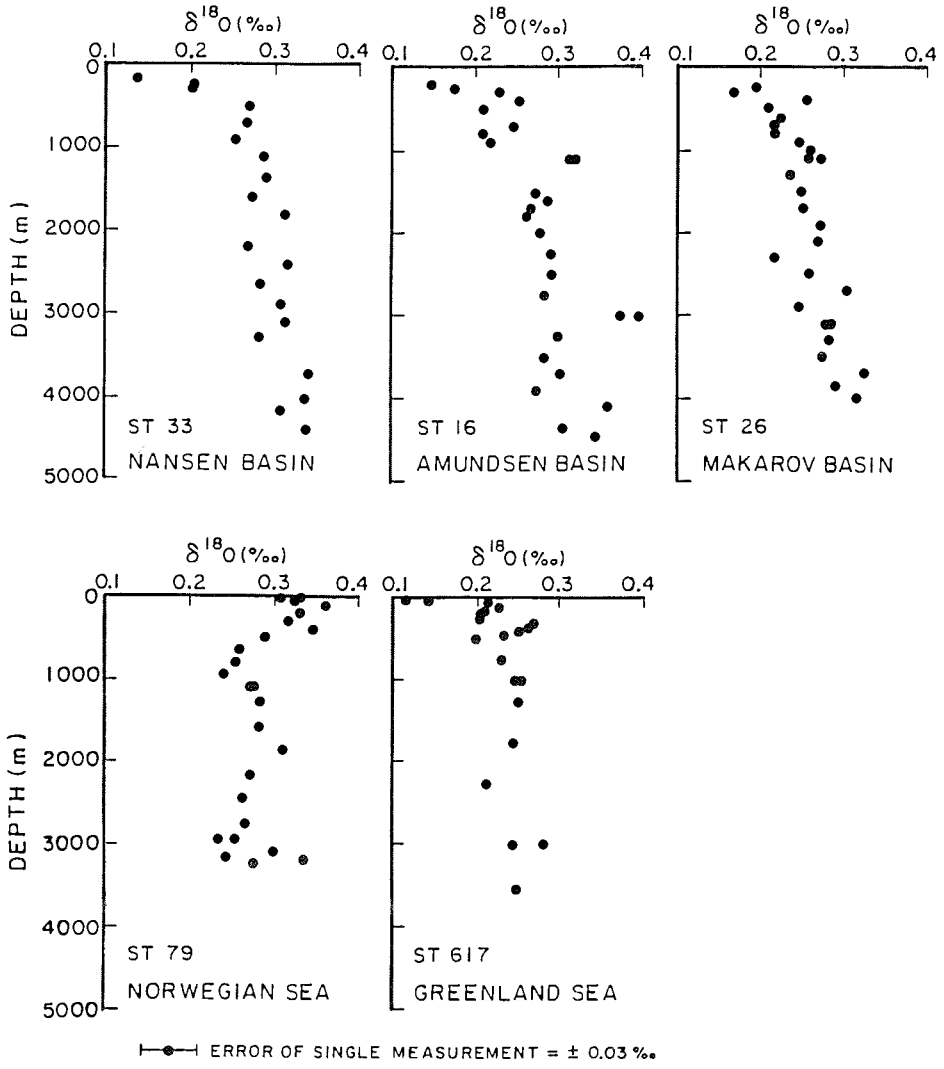

Figure 18: $\delta^{18}O$ versus depth plot of stations located in the central Arctic Ocean and the Norwegian and Greenland seas (for geographical position of the stations, see Fig. 13).

5.2 Deep Arctic Ocean and Norwegian and Greenland seas

Below the Atlantic water, $\delta^{18}O$ values are more or less constant to a depth of about 2600 m. Below this depth there is a slight increase in $\delta^{18}O$ of about 0.04 ‰ (Fig. 18). The deep profiles in the Greenland and Norwegian seas do not show this trend.

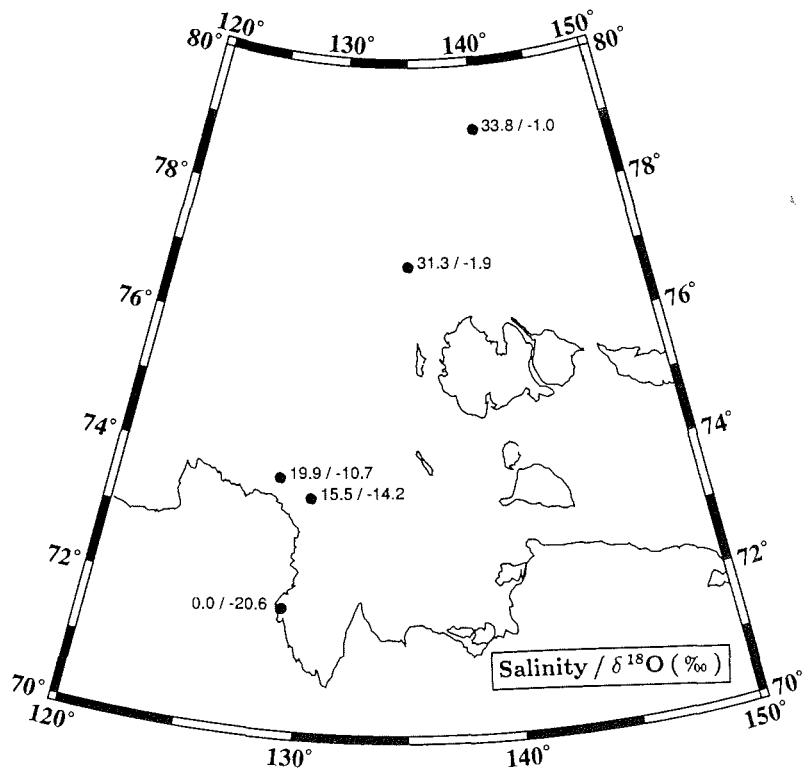

Figure 19: Salinity and $\delta^{18}O$ values of surface water samples in the Laptev Sea. The results are indicated next to the location of each sample.

5.3 Laptev Sea

The $\delta^{18}O$ values of the surface water samples increase from $-20.6\,‰$ found in the river delta to about $-1\,‰$ at 70°N latitude, while their salinity increases from 0 to about 34 (see Fig. 19). The ice samples show the same trend as the surface water samples: progressing northwards salinity increases (from 0 to 6) and $\delta^{18}O$ values increase from -16.8 to $-1.8\,‰$. The $\delta^{18}O$ values of the snow samples ranges from about $-28\,‰$ to about $-6\,‰$; but also their salinities ranges from 0 to about 29!

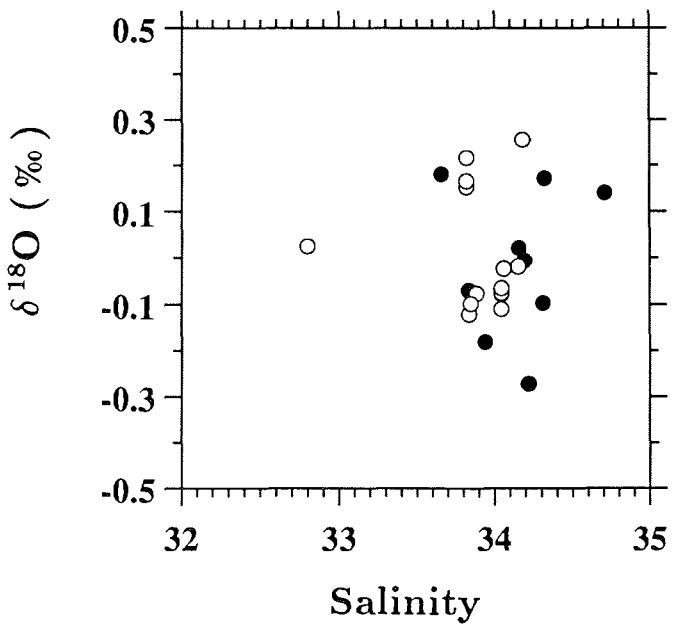

Figure 20: Salinity versus $\delta^{18}O$ of samples in the Barents Sea. The open dots are samples collected at a water depth of 5 m and the full dots are samples collected at a water water of 50 m or bottom depth.

5.4 Barents Sea

The water samples show relative little varition in $\delta^{18}O$ as well as in salinity (see Fig. 20). The samples taken near shore at Novaya Zemlya and Franz–Josef–Land show slightly lower $\delta^{18}O$ values than the samples taken in the passage between Novaya Zemlya and Franz–Josef–Land (see Tab. A.4 in the appendix). There is no systematic difference in $\delta^{18}O$ and salinity values between samples taken at 5 m depth and 50 m or bottom depth (see open and full dots in Fig. 20, respectively).

6 Discussion

6.1 Separation of river–runoff and sea–ice meltwater in the Arctic Ocean halocline

A combined salinity and ^{18}O mass balance can be used to distinguish between river–runoff and sea–ice meltwater in the freshwater component of the halocline [*Östlund and Hut,* 1984; *Schlosser et al.,* 1993]. The balance is governed by the following equations:

$$f_a + f_r + f_i = 1 \tag{1}$$

$$f_a \cdot S_a + f_r \cdot S_r + f_i \cdot S_i = S_m \tag{2}$$

$$f_a \cdot O_a + f_r \cdot O_r + f_i \cdot O_i = O_m \tag{3}$$

where f_a, f_r and f_i are the fractions of Atlantic water, river–runoff and sea–ice meltwater in a halocline water parcel, and S_a, S_r, S_i, O_a, O_r and O_i are the corresponding salinities and $\delta^{18}O$ values. S_m and O_m are the measured salinity and $\delta^{18}O$ of the halocline water. The parameters of this 3–component mass balance were chosen as follows (see also Tab. 3):

Atlantic water: In the calculation of the river–runoff and sea–ice meltwater fractions, Atlantic Water is refered to as the water of the Atlantic core observed in the interior of the Arctic Ocean. It has been shown before, that the Atlantic core is slightly modified along its flow path in the Arctic Ocean [*Coachman and Barnes,* 1963]. In the data from ArkIV/3 and ARCTIC 91 a systematic change can be seen in the temperature versus salinity and $\delta^{18}O$ versus salinity correlations of the Atlantic core (Figs. 21, a, b). The highest $\delta^{18}O$, salinity and temperature values are found in the southern part of the Eurasian Basin near Spitzbergen. The values

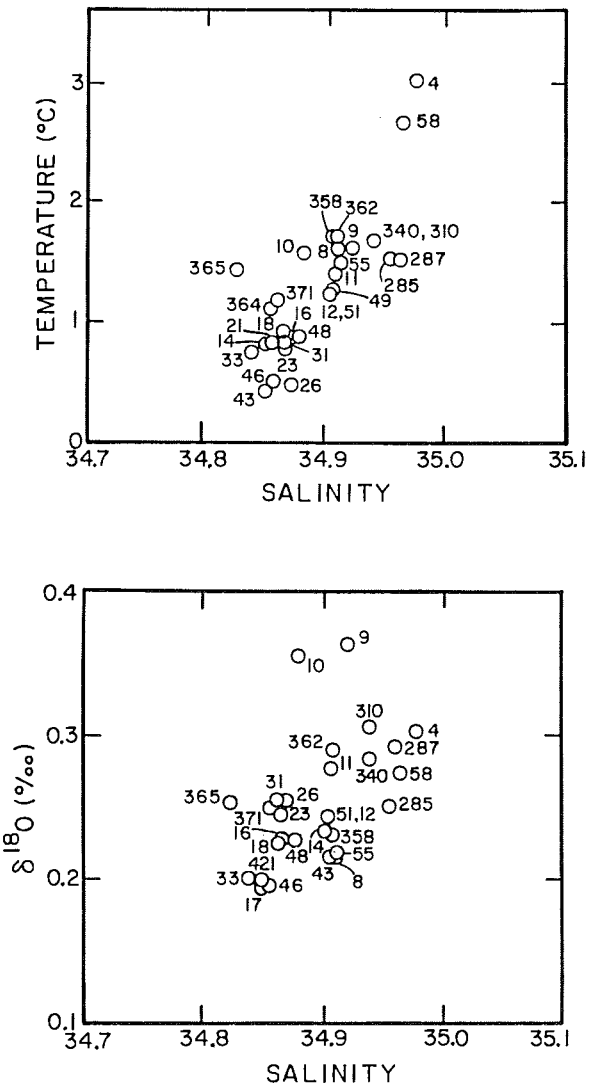

Figure 21: (a) Potential temperature versus salinity for the Atlantic core (identified by the temperature maximum); station numbers are indicated (b) same as in a) for $\delta^{18}O$ versus salinity.

Table 3: Parameters used in the 3–component mass balance

	salinity	$\delta^{18}O$ [‰]
Sea–ice meltwater	3	*surface**
River–runoff	0	-21
Atlantic water	34.92	0.3

* use $\delta^{18}O$ value of surface sample plus 2.1‰ for fractionation during sea–ice formation [*Melling and Moore*, 1994].

decrease towards the east and the north. The data support the flow pattern of Atlantic Water suggested by *Coachman and Barnes* [1963] and *Gordienko and Laktionov* [1958]: one branch of Atlantic Water is flowing eastward along the Siberian shelf break while a modified branch of Atlantic–derived water is flowing towards Fram Strait in the northern part of the sections. For the mass balance calculation therefore a salinity of 34.92 and a $\delta^{18}O$ value of 0.3 ‰ was assumed, representing the least modified Atlantic water inside the Arctic Ocean.

River–runoff: The few available $\delta^{18}O$ measurements from rivers flowing into the Arctic Ocean are close to the value of −21 ‰ suggested by Östlund and Hut [1984] as the best average for Arctic river–runoff. In the Lena delta a $\delta^{18}O$ value of −20.6‰ was measured (see Chap. 5.3). Measurements from the Lena river and smaller side streams near Yakutsk yield $\delta^{18}O$ values of about −19.6 ‰ (John Edmond; pers. comm.). For the Mackenzie river *Macdonald and Carmack* [1991] measured $\delta^{18}O$ values of about −20.1 ‰ near the river mouth in summer. *Krouse and Mackay* [1971] find $\delta^{18}O$ values of −20.3(7) ‰ about 400 km downstream the Mackenzie–Liard river confluence. For the Yukon river, which contributes indirectly to the Arctic Ocean via the Alaskan Coastal Current *Cooper and DeNiro* [1990] give $\delta^{18}O$ values of −22.4 and −21.7 ‰. These measurements show little variation in the isotopic composition of the Arctic Ocean rivers. Table

Table 4: Direct $\delta^{18}O$ measurements of Arctic Ocean rivers

River	Location	$\delta^{18}O$ [‰]	Authors
Lena	delta	−20.6	this study
Lena	near Yarkutsk	−19.9	J. Edmond pers. comm.
Mackenzie	delta	−20.1	*Macdonald and Carmack* [1991]
Mackenzie	upstream	−20.3	*Krouse and Mackay* [1971]
Yukon	upstream	−22.1	*Cooper and DeNiro* [1990]
Ob	bay	−16.3*	*Brezgunov et al.* [1983]
Yenisey	bay	−17.5*	*Brezgunov et al.* [1983]

* no information on data quality and measurement procedure is available

4 summarizes the available direct measurements.

Russian data indicate that the discharge of the Ob and Yenisey rivers is isotopically significantly heavier than -21‰ [*Brezgunov et al.*, 1983]. Since no information on the data quality is available these measurements were omitted. However, the possible systematic errors introduced by this omission will be discussed in Chap. 6.3.

Sea–ice meltwater: As we do not know where the sea ice which is contributing to the freshwater component of a specific water parcel is formed and the $\delta^{18}O$ value of the water from which it is formed is usually unknown, it is assumed that the sea–ice meltwater has the same $\delta^{18}O$ value as the surface water of the station for which the freshwater balance is estimated multiplied by a fractionation factor (about 1.0021 *Melling and Moore* [1994]). ^{18}O fractionation during sea–ice formation leads to enrichment of the heavier oxygen isotope in the ice. This approach is only a first order approximation of the true $\delta^{18}O$ value of sea–ice because sea–ice can move independently from surface water. It might therefore be formed from water with a $\delta^{18}O$ value which differs from that observed at the

sampling site. Variations in the assumptions made for both the $\delta^{18}O$ values of the sea–ice meltwater and the fractionation factor for sea ice formation within reasonable limits do not significantly effect the estimations. The salinity of sea ice is set to a value of 3 according to data from the literature (e.g. [*Pfirman et al.*, 1989]).

Using equations (1) to (3) and the salinity and oxygen isotope values for the individual water masses, the fractions of Atlantic water, sea–ice meltwater and river–runoff can be calculated. There is a trend of increasing river–runoff in the freshwater component with increasing distance from the Barents Shelf where the freshwater component is dominated by sea–ice meltwater (Fig. 22, a, b). In the northern part of sections A and B and in the western part of section C, the freshwater component consists practically exclusively of river–runoff and part of the freshwater has been used to form sea ice. The boundary between net sea–ice formation and net sea–ice melting is located in the central Eurasian Basin. This boundary coincides with the transition to a significant influence of river–runoff. The fraction of river–runoff is small in the southern part of the sections; north of the sea–ice meltwater boundary (i.e., the 0% sea–ice meltwater fraction isopleth), the river–runoff fractions in the surface water increase from about 2 % to about 12 %. In contrast to the sea–ice meltwater fractions, the river–runoff fractions do not level off, but increase monotonically towards the northern end of the sections.

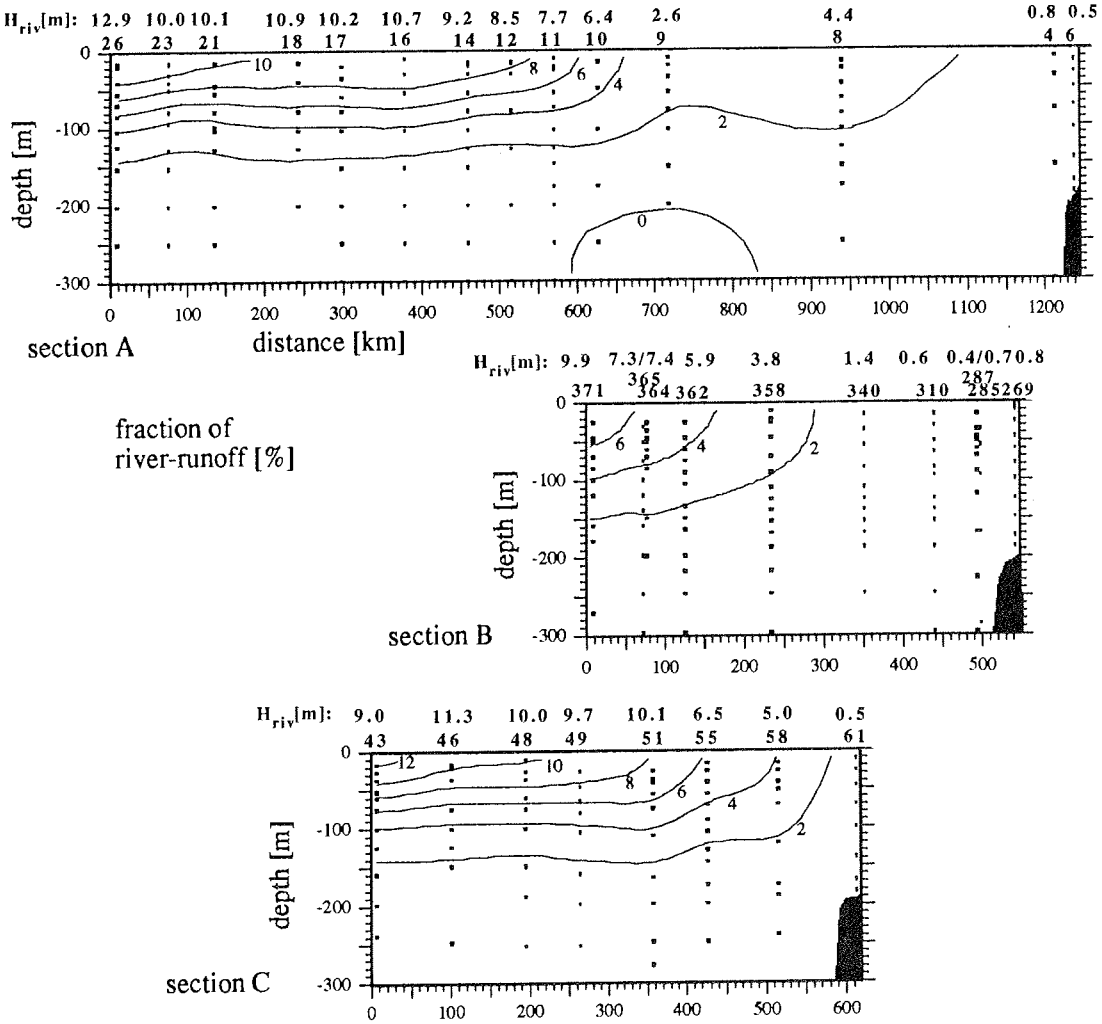

Figure 22: (a) Fraction of river–runoff contained in the halocline water for the upper 300 meters of the water column for three sections across the Eurasian Basin (for geographical position of the stations, see Fig. 13). (b) same as a) for the fraction of sea–ice meltwater contained in the halocline water. Positive numbers mean addition of freshwater by melting of sea ice; negative numbers indicate formation of sea ice (removal of freshwater).

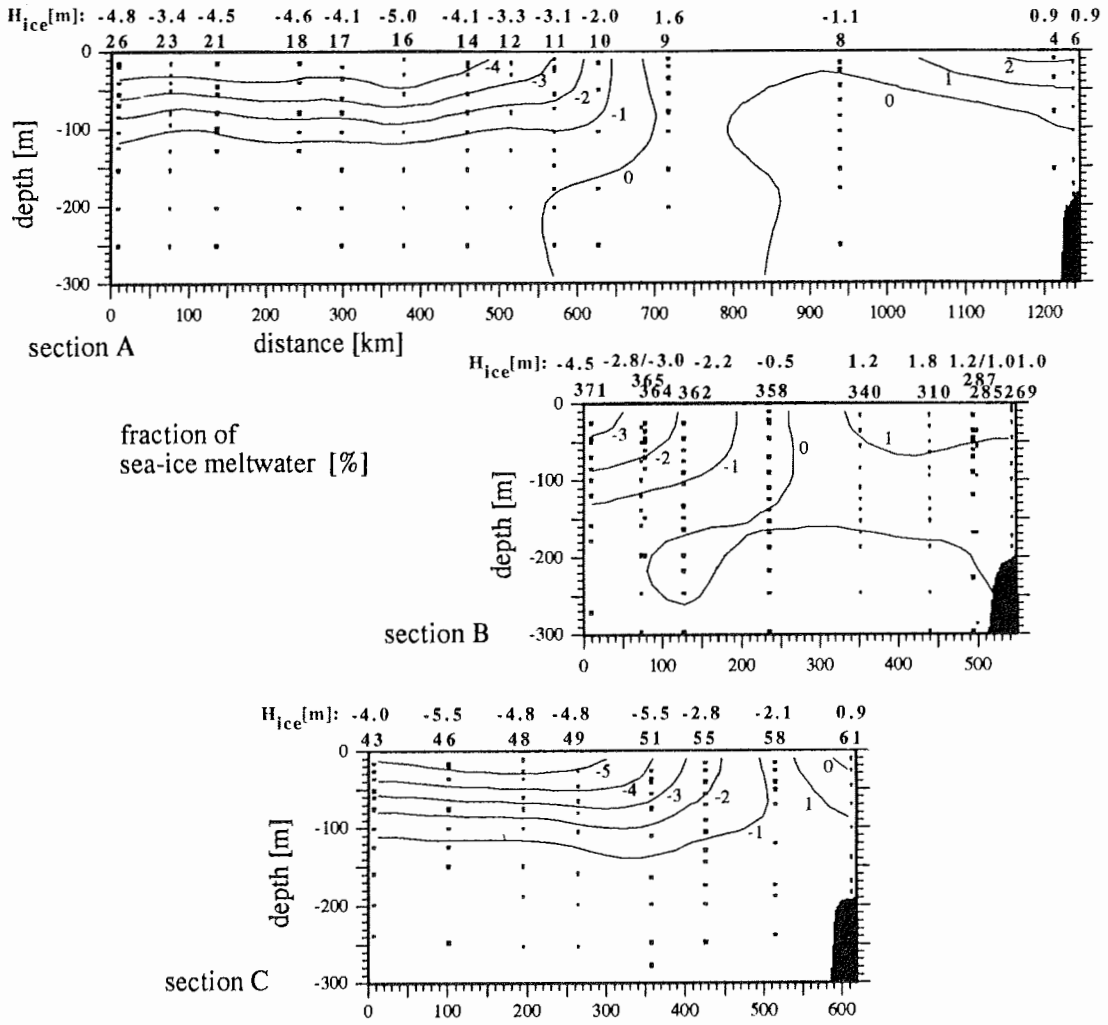
H_ice[m]: -4.8 -3.4 -4.5 -4.6 -4.1 -5.0 -4.1 -3.3 -3.1 -2.0 1.6 -1.1 0.9 0.9
26 23 21 18 17 16 14 12 11 10 9 8 4 6
depth [m]
0
-100
-200
-300
0 100 200 300 400 500 600 700 800 900 1000 1100 1200
section A
distance [km]
fraction of
sea-ice meltwater [%]
H_ice[m]: -4.5 -2.8/-3.0 -2.2 -0.5 1.2 1.8 1.2/1.0 1.0
371 365 364 362 358 340 310 287 285 269
depth [m]
0
-100
-200
-300
0 100 200 300 400 500
section B
H_ice[m]: -4.0 -5.5 -4.8 -4.8 -5.5 -2.8 -2.1 0.9
43 46 48 49 51 55 58 61
depth [m]
0
-100
-200
-300
0 100 200 300 400 500 600
section C

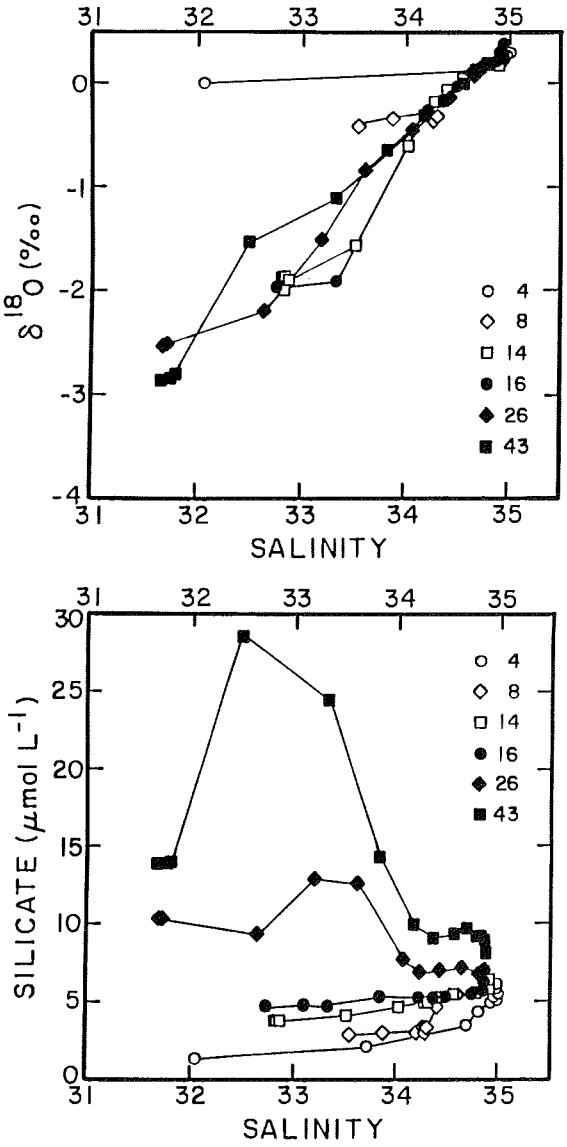

Figure 23: (a) δ^{18}O versus salinity for selected stations from ARCTIC 91. (b) Same as in a) for silicate versus salinity.

Section C north of Fram Strait shows sea–ice melting in the southeastern part and sea–ice formation in the northwestern part. The fractions of sea–ice meltwater and river–runoff reach more extreme values than in sections A and B; they amount to about $-6\,\%$ for sea–ice meltwater and about $14\,\%$ for river–runoff. In the northwestern part of section C halocline waters are observed with characteristics which are significantly different from those found at the northern ends of sections A and B. These waters probably originate in the Canadian Basin. This hypothesis is supported by the presence of elevated silicate values found at station 43 (Fig. 23 b). In the $\delta^{18}O$ versus salinity correlation of station 43 this influence is also seen in a relatively high $\delta^{18}O$ value compared to adjacent stations at a salinity of about 32.5 (Fig. 23 a).

The presence of water of Pacific origin will slightly distort the results of the mass balance calculation at station 43. The stations in the northern part of section A (stations 23, 26, 31) also show slightly elevated silicate values at salinities of around 33, which seems to indicate a small contribution of UHW to these waters. Based on these observations, the extent of the Siberian part of the Transpolar Drift can be located to be at the northern end of section A and at station 45 in section C. The halocline water of the Canadian Basin flows towards Fram Strait in a separate branch. The boundary between the halocline waters of the Eurasian and Canadian basins, which is basically the Lomonosov Ridge, is also reflected in the surface $\delta^{18}O$ values (Fig. 24). The surface waters of the Canadian Basin have lower $\delta^{18}O$ values compared to the Eurasian Basin. Interpretation of this observation requires quantification of the Pacific component contained in the halocline waters. This will be done in Chap. 6.3.

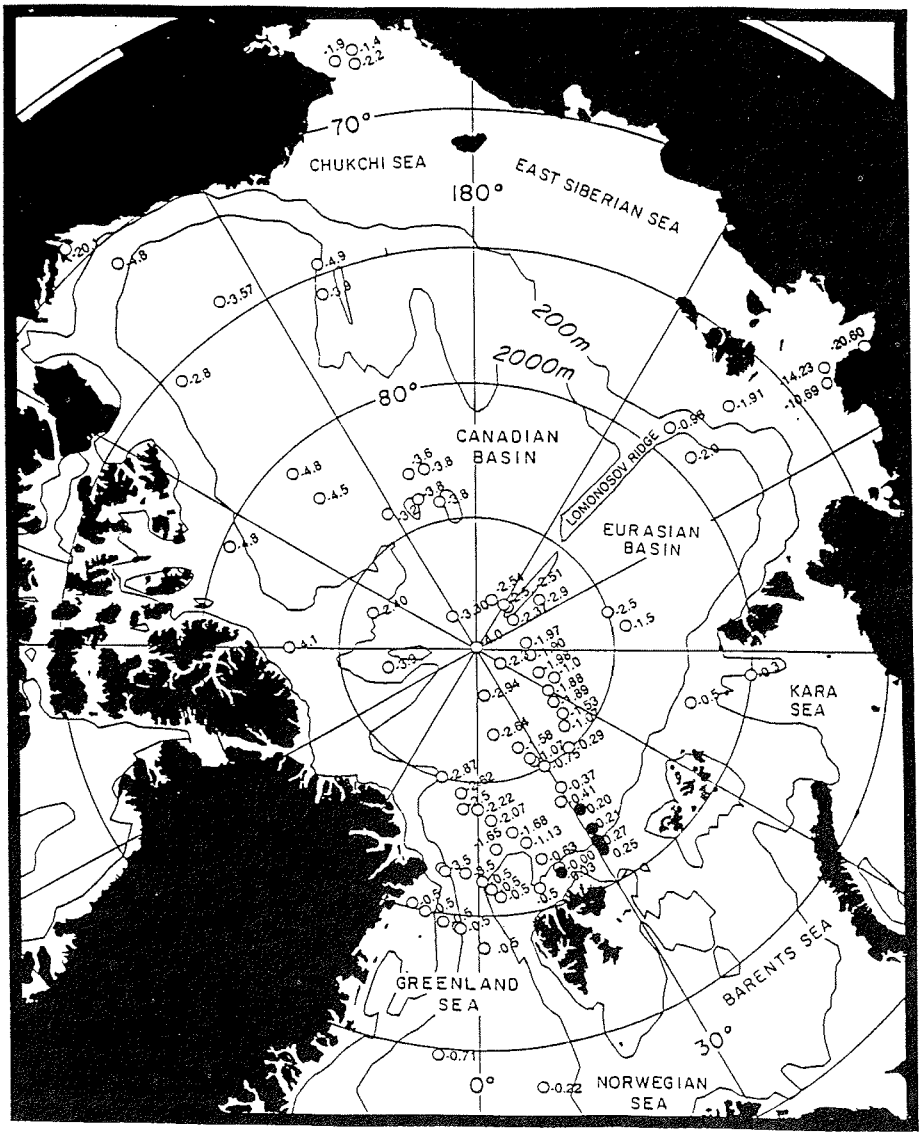

Figure 24: Geographic distribution of surface $\delta^{18}O$ values in the Arctic Ocean. Additional $\delta^{18}O$ data are taken from *Östlund and Hut* [1984]; *Östlund et al.* [1987]; *Macdonald and Carmack* [1991]; *Cooper and DeNiro* [1990]; *Donk and Mathieu* [1969]; *Vetshteyn et al.* [1974]. Deuterium values taken from *Friedman et al.* [1961] and *Redfield and Friedman* [1969] were converted to $\delta^{18}O$ values using the relationship $\delta^{18}O\ (^{o}/_{oo}) = 8 \cdot \delta D + 10$.

6.2 Water column inventories of sea–ice meltwater and river–runoff

The fractions of sea–ice meltwater and river-runoff water can be integrated from the surface down to the Atlantic layer, providing the total amount of river–runoff and sea–ice meltwater stored in the water column (values are indicated in Fig. 22). The uncertainty of the integration and the fraction calculation is about $\pm 0.5\,\mathrm{m}$ for the total inventory of sea–ice meltwater and river–runoff stored in the water column (determined by variation of the parameters for the fraction calculation and by variation of the intergration depth).

For a correct interpretation of the river–runoff and sea–ice meltwater inventories it has to be kept in mind, that these values represent the history of the water column. ¿From the $\delta^{18}\mathrm{O}$ signal we learn (in first order) how much river–runoff has been added to the water column, but this is not the actual amount of fresh water contained in the water column. Sea–ice might be melted or be formed out of the water column. The amount of freshwater actually contained in the water column is the value of sea–ice (H_{ice}) and river–runoff (H_{riv}) inventory combined ($H_{riv} + H_{ice}$).

The distribution of the inventory of sea–ice meltwater shows a sharp transition between melting and formation of sea ice over the Nansen Basin (Fig. 25 b). This front coincides with a strong gradient in the inventory of river–runoff (Fig. 25 a) and indicates their common source on the shelves: Most of the initial sea ice is formed on the shelves and it grows more slowly during its transit across the central Arctic basins [*Weeks and Ackley,* 1986].

While we know the major trajectories of the drifting sea ice [*Gordienko and Laktionov,* 1958; *Colony and Thorndike,* 1984], we know little about the advection and mixing of the halocline waters. From the distribution of sea–ice meltwater and river–runoff fractions it can be concluded that there are well defined lateral regimes. Although large amounts of river–runoff are flowing into the Kara and

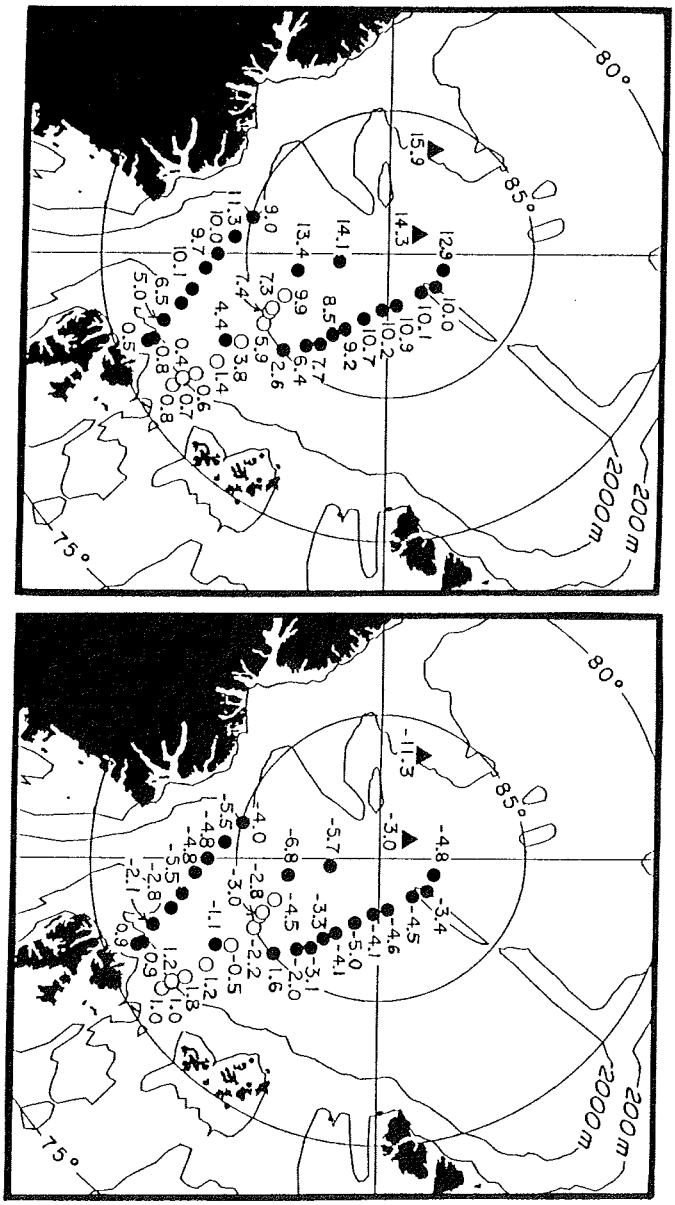

Figure 25: (a) Geographic distribution of the water column inventory of river–runoff (H_{riv}) contained in the halocline. The values for station 43, LOREX and CESAR are obtained using the 4–component mass balance calculation (see Chap 6.3), all other values are obtained using the 3–component mass balance calculation. (b) Same as in a) for sea–ice meltwater (H_{ice}).

Laptev seas, relatively little freshwater is found at that longitude directly north of the continental slope, as indicated by high surface $\delta^{18}O$ values just north of the Kara Sea [*Östlund and Hut,* 1984] (Fig. 24). Near the shelf break of the Laptev Sea, the surface $\delta^{18}O$ values are also relatively low (about $-2\,‰$; Fig. 24), but still higher than the maximum values found in the interior of the Arctic Ocean. This supports the concept that river–runoff generally does not cross directly northward to the shelf edge. The water might flow off the shelf in defined river plumes or it might be transported eastward in the Siberian Coastal Current and flow off the shelf as far east as the East Siberian or the Chukchi seas.

6.3 Quantification of the Pacific component in the Arctic Ocean Halocline

In the following approach silicate will be used as a tracer in a four– component mass balance to quantify the contribution of Bering Strait Inflow (BSI) to halocline water [*Bauch et al.*, 1994] :

$$f_a + f_b + f_r + f_i = 1 \tag{4}$$

$$f_a \cdot S_a + f_b \cdot S_b + f_r \cdot S_r + f_i \cdot S_i = S_m \tag{5}$$

$$f_a \cdot O_a + f_b \cdot O_b + f_r \cdot O_r + f_i \cdot O_i = O_m \tag{6}$$

$$f_a \cdot Si_a + f_b \cdot Si_b + f_r \cdot Si_r + f_i \cdot Si_i = Si_m \tag{7}$$

where f_a, f_b, f_r and f_i are the fractions of Atlantic water, Bering Strait Inflow (BSI) water, river–runoff and sea–ice meltwater in a halocline water parcel, and S_a, S_b, S_r, S_i, O_a, O_b, O_r,O_i and Si_a, Si_b, Si_r, Si_i are the corresponding salinities, $\delta^{18}O$ values and silicate concentrations, respectively. S_m, O_m and Si_m are the salinity, $\delta^{18}O$ value and silicate concentration measured in a specific halocline water parcel.

In the following, the limitations of this approach to quantify the Pacific component contributing to the freshwater balance of the Arctic Ocean are discussed. Additionally, the choice of the silicate values of the end members is discussed (all values in the four–component mass balance are listed in Table 5).

The water passing through Bering Strait has three components: Anadyr, Bering Shelf, and Alaskan Coastal water [*Coachman et al.*, 1975; *Walsh et al.*, 1989]. Based on salinity and nutrient distribution over the Chukchi Sea shelf [*Walsh et al.*, 1989] it can be concluded that Anadyr and Bering Shelf waters are the sources of nutrient rich water flowing off the shelf. This water mass is called UHW within the Arctic Ocean. Its salinity is about 33.1, similar to its source water masses Anadyr water

with a salinity of about 33 and Bering Shelf water with a salinity of about 32.5 [*Coachman et al.,* 1975]. The $\delta^{18}O$ value of BSI can be estimated to be about $-1.0\,‰$ on the basis of $\delta^{18}O$ and salinity measurements made in Bering Strait (*Macdonald et al.* [1989]; and data cited by *Björk* [1990]), in the northern Pacific (GEOSECS data) and from bottom salinity and $\delta^{18}O$ measurements in the western Bering and Chukchi seas [*Cooper and DeNiro,* 1990]. This value is only accurate within about $\pm 0.5\,‰$.

Alaskan Coastal water (ACW), the source water of Bering Summer Water (BSW), has a mean salinity of 31.5 [*Coachman et al.,* 1975]. Due to its relatively low density, it stays near the surface and is not in contact with the sediments to take up silicate by dissolution. It has no silicate signature and is therefore not accounted for in the mass balance calculation. From current measurements it can be estimated that ACW contributes less than 1/3 to the water flowing through Bering Strait, since the flow through Anadyr Strait is about twice as strong as the flow through Shpanberg Strait [*Walsh et al.,* 1989]. *Macdonald et al.* [1989] estimate that BSW makes up about 1/8 of the BSI found on the Beaufort shelf. Omission of about 1/3 of BSI in the mass balance calculation would lead to an error of the estimated river–runoff and sea–ice meltwater inventories of about 2 to 4 m and 0.3 m, respectively (estimated as half the difference between results of 3– versus 4–component mass balance; see discussion below). The actual error of the total river–runoff fraction migth be smaller, because part of the low salinity and $\delta^{18}O$ signal of BSW is caused by freshwater of the Yukon River, which joins the Alaskan Coastal Current on the Bering Sea shelf.

For determination of the silicate concentration of the components used in the mass balance, it has to be considered that the silicate concentration can be chnaged rapidly in ice–free shallow shelf seas by biological consumption during summer and dissolution from the sediments. Only off the shelves and beneath a permanent sea–ice cover theses factors are limited and the silicate concentration can be treated as

Table 5: Parameters used in the 4–component mass balance

	salinity	$\delta^{18}O$ [‰]	silicate [$\mu mol\, l^{-1}$]
Sea–ice meltwater	3	*surface**	1
River–runoff	0	-21	10
Atlantic water	34.92	0.3	6
Bering Strait Inflow	33	-1.0	40

* use $\delta^{18}O$ value of surface sample plus 2.1‰ for fractionation during sea–ice formation [*Melling and Moore,* 1994].

a conservative tracer. Therefore, the concentration of each component is specified as it flows off the shelf into the Arctic Ocean interior. The following silicate values were selected for the individual water masses contributing to the Arctic halocline (see also Tab. 5).

Atlantic water: $Si_a = 6\,\mu mol\, l^{-1}$ which is close to the value measured at the temperature maximum in the Eurasian Basin (ArkIV/3 and ARCTIC 91 silicate data [*Koltermann and Lüthje,* 1989]).

Sea–ice: $Si_i = 1\,\mu mol\, l^{-1}$ following *Macdonald et al.* [1989]. The choice of this value is not critical; if for example 5 instead of $1\,\mu mol\, l^{-1}$ is chosen, the results of each fraction change by less than 1 % (absolute) in all fractions.

River–runoff: $Si_r = 10\,\mu mol\, l^{-1}$ is adopted close to the average value observed in the Eurasians Basin containing river– runoff. $46\,\mu mol\, l^{-1}$ are measured in the Mackenzie River [*Macdonald et al.,* 1989] and estimates for the Siberian rivers are as high as $125\,\mu mol\, l^{-1}$ [*Codispoti and Owens,* 1975]. However, no correlation between river–runoff fraction and elevated silicate concentration is observed in our data sets (compare Figs. 22 a and 23 b). For this approach it can therefore

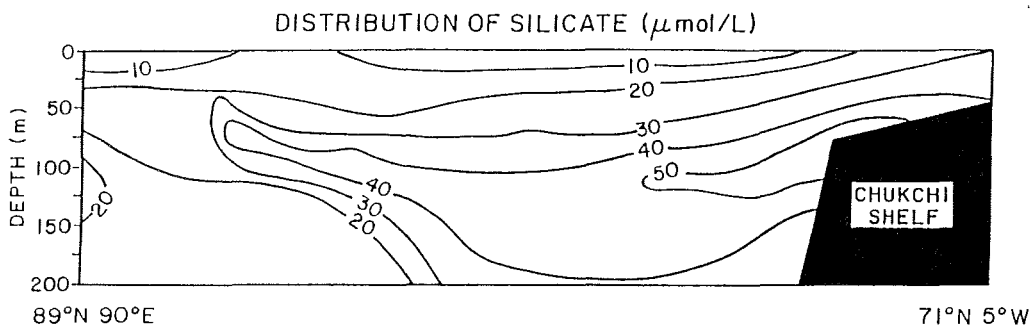

Figure 26: Silicate concentration along a section reaching from the Chukchi Sea into the Arctic Ocean interior (from approximately 71°N, 5°W to 89°N, 90°E). The section is taken from *Treshnikov* [1985].

be assumed that the high silicate concentration carried by the rivers have been reduced to about $10\,\mu mol\,l^{-1}$, i.e. to the level observed in the waters with the highers fraction of river–runoff.

Bering Strait Inflow: $Si_b = 40\,\mu mol\,l^{-1}$ is estimated for the average silicate concentration of BSI from a section by *Treshnikov* [1985], which shows a tongue of silicate–rich water reaching from the Chukchi Sea into the Arctic Ocean interior (Fig. 26).

Both river-runoff and Bering Strait Inflow cross the Arctic shelves and enter the interior basins. En route silicate levels decrease by the large seasonal growth of diatoms in surface waters [*Sambrotto et al.*, 1984; *Walsh et al.*, 1989]. To obtain silicate concentrations in river–runoff as low as $10\,\mu mol\,l^{-1}$, practically the entire amount of riverine silicate has to be deposited on the shelf by biological consumption. Considering the rapid biological processes found in the Arctic Ocean during the production season [*Sambrotto et al.*, 1984; *Walsh et al.*, 1989], and a mean residence

time of river–runoff on the shelves of approximately 3.5 ± 2 years (see Chap. 6.7), it seems possible that the initial silicate concentration can be reduced by the assumed amount.

However dissolution of silicate might occure over the shelves. For BSI much of this silicate decrease by biological consumption may be compensated by dissolution of silicate in shelf bottom waters [*Walsh et al.*, 1989].

Since none of the stations of the data set measured for this study has a fully developed silicate maximum such as those observed at locations in the Canadian Basin, data of the LOREX and the CESAR ice camp sites are used to test the balance equations ($\delta^{18}O$ and salinity data taken form *Östlund et al.* [1987]; silicate concentration for LOREX are taken from *Moore et al.* [1983], their Fig. 6, and for CESAR from *Jones and Anderson* [1986], their Fig. 3). At the CESAR Ice Camp station which was located over the Alpha Ridge in the Canadian Basin, Upper Halocline Water (UHW) is fully developed and a silicate maximum of about 40 $\mu mol\, l^{-1}$ is found at a salinity of about 33.2 at 120 m depth. At the LOREX Ice Camp station which was located over the Lomonosov Ridge in the Canadian Basin the silicate maximum of about 39 $\mu mol\, l^{-1}$ is found at a salinity of about 33.0 at 110 m depth. Station 43 from the ARCTIC 91 expedition has a silicate maximum of about 28.6 $\mu mol\, l^{-1}$ at a salinity of 32.5 at 50 m depth. Station 26 shows only a slight elevation in its silicate concentration of 13 $\mu mol\, l^{-1}$ at a salinity of 33.2 at 70 m depth.

At station 26 the fraction of BI at the depth of the silicate maximum is about 15 % and the fraction of Atlantic water is reduced to about 80 % (Fig. 27 a). Below the depth of the silicate maximum, the fraction of BSI is close to zero and practically pure Atlantic water is observed. At station 43, the fraction of BSI at the depth of the silicate maximum is about 70 % and the fraction of Atlantic water about 30 % (Fig. 27 b). At the LOREX Ice Camp the fraction of BSI at the depth of the silicate maximum is about 95 % and the fraction of Atlantic water is reduced to about 5 %

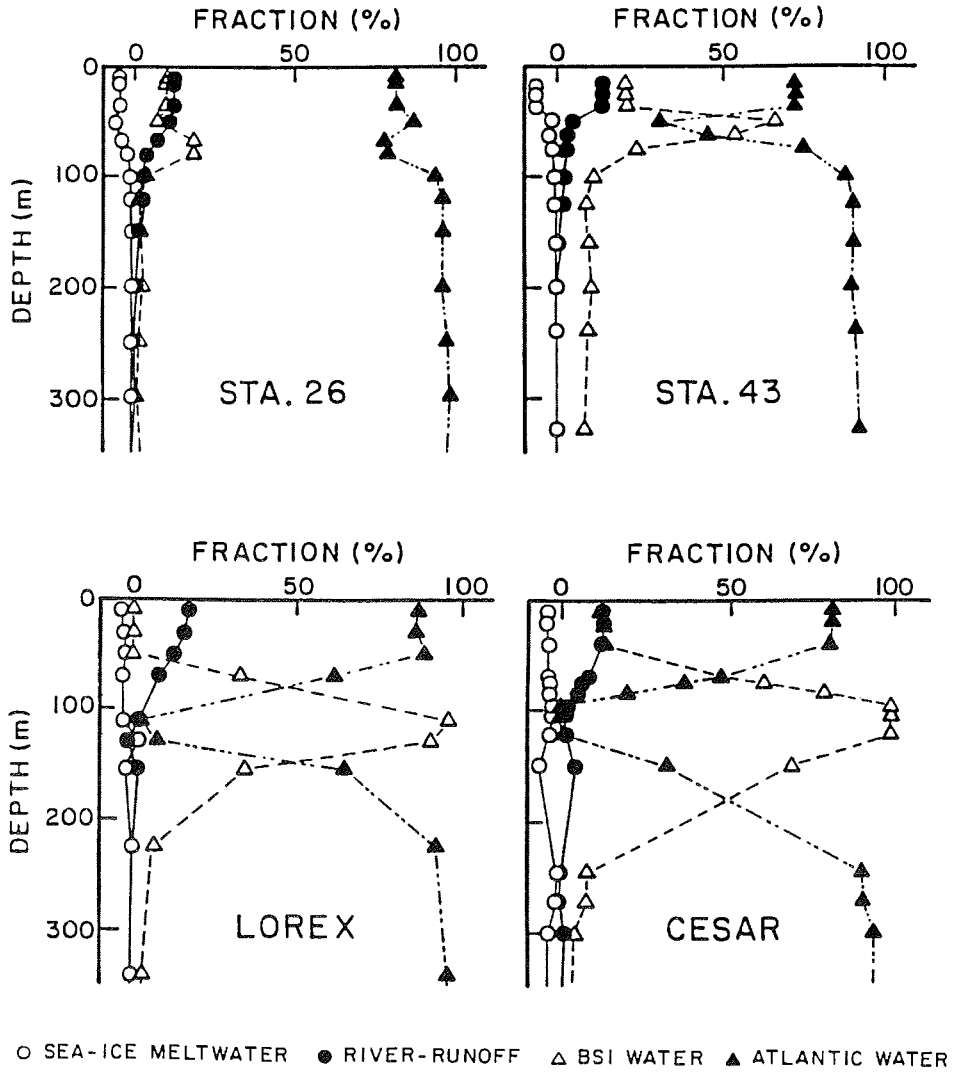

Figure 27: Fractions of sea–ice meltwater, river–water, Atlantic water and BSI water for stations 26 (a), 43 (b) and from LOREX (c) and CESAR (d). Calculations were done using the 4–component mass balance.

Table 6: Comparison of river–runoff and sea–ice meltwater inventories using the 3– and 4–component mass balance

	stat. 26		stat. 43		LOREX		CESAR	
	H_{ice}	H_{riv}	H_{ice}	H_{riv}	H_{ice}	H_{riv}	H_{ice}	H_{riv}
	[m]		[m]		[m]		[m]	
3-comp. calc.	-4.8	12.9	-4.3	12.0	-3.5	18.6	-11.7	23.7
4-comp. calc.	-4.9	12.1	-4.0	9.0	-3.0	14.3	-11.3	15.9
difference	0.1	-0.8	0.3	-3.0	0.5	-4.3	0.4	-7.8

H_{ice}, H_{riv} : sea-ice meltwater and river–runoff inventories.

(Fig. 27 c). At the CESAR Ice Camp the fraction of BSI at the depth of the silicate maximum is about 100 % and the fraction of Atlantic water is reduced to about 0 % (Fig. 27 d). The silicate concentrations in the Atlantic layer of station 43, LOREX and CESAR are higher than at station 26 and the other stations of the Eurasian Basin of the Arctic Ocean. As a result, the fraction of BSI water at the depth of the Atlantic layer differs significantly from zero. In the Canadian Basin the Atlantic layer might have acquired a higher silicate concentration due to diffusion from and mixing with the overlying UHW.

The influence of BSI water on the river–runoff and sea–ice meltwater inventories calculated from 3– and 4–component mass balances is illustrated in Table 6.

At station 26 the difference for the total amount of river–runoff using the 4–component and the 3–component mass balances remains close to the estimated uncertainty of the 3–component mass balance. The result for the total amount of sea–ice meltwater remains practically unchanged. At station 43 and at the LOREX Ice Camp, the difference in the river–runoff inventories is significant. At station 43, the river–runoff inventory estimated on the basis of the 4–component mass balance is about 9 m compared to about 12 m obtained from the 3–component mass balance.

Table 7: Estimate of the uncertainty in determining the sea-ice meltwater and river–runoff inventories using the 4–component mass balance

	H_{ice} [m] at station				H_{riv} [m] at station			
	26	43	LOREX	CESAR	26	43	LOREX	CESAR
results:	-4.9	-4.0	-3.0	-11.9	12.1	9.0	14.3	15.9
$\Delta Si_r : \pm 5 \mu mol\, l^{-1}$	±0.0	±0.0	±0.0	±0.1	±0.2	±0.1	±0.1	±0.2
$\Delta Si_b : \pm 5 \mu mol\, l^{-1}$	±0.0	±0.1	±0.1	±0.2	±0.3	±0.5	±0.5	±1.5
$\Delta O_b : \pm 0.5$ ‰	±0.4	±1.4	±2.4	±3.4	±0.5	±1.2	±2.2	±3.2

H_{ice}, H_{riv} : sea–ice meltwater and river–runoff inventories.

With this corrected result for station 43 the river–runoff inventories are more or less constant for the western part of section C (see Fig. 25). The largest differences in the river–runoff inventories is observed at the CESAR Ice Camp. Additionally, there is a noticeable difference in the results for the sea–ice meltwater inventory. Since the component of BSI watr which is omitted in the calculations is about 1/3 of the total inflow it can be estimated that the error is in first order about half of the listed differences.

The silicate values of the end members and the $\delta^{18}O$ of BSI are only known within a relative large uncertainty compared to the other parameters used in the calculations. Table 7 lists the changes in the river–runoff and sea–ice inventories as a function of these parameters. The range of each parameter variation reflects its estimated uncertainty.

It is evident that the greatest uncertainty is due to the $\delta^{18}O$ value of BSI water. It has to be determined more accurately by direct measurements from the Chukchi Sea.

6.4 Sea ice meltwater inventories: implications for sea–ice export through Fram Strait

Integration of the observed freshwater signal related to sea–ice formation along a section across Fram Strait can in principal be linked to export of sea–ice through this passage between the Arctic Ocean and the Greenland-Norwegian-Iceland seas. Calculation of a true sea–ice export rate through Fram Strait requires;

1. Knowledge of the distributions of the river–runoff and sea–ice meltwater fractions in the upper waters flowing southward through Fram Strait.

2. Quantification of the velocity profile at each station for which river–runoff and sea–ice meltwater fractions are available.

3. The assumption that the sea–ice and the surface waters which carry the $\delta^{18}O$ and salinity signals imprinted during sea–ice formation are following the same pathways from the shelf seas to Fram Strait.

With this information, both the export of river–runoff and sea–ice meltwater through Fram Strait could be calculated by integrating the product of the velocity and river–runoff or sea–ice meltwater fraction from the surface to the core of the Atlantic layer and along the southward flowing portion of the section.

Unfortunately, no detailed measurements of the current profile are available for the region of Fram Strait. Additionally, it is not known how closely the circulation of the upper waters carrying the sea–ice meltwater signal is coupled to that of sea–ice. Therefore, the evaluation of the sea–ice meltwater inventories are limitted to fairly rough first–order approximations. For these approximations, the following two scenarios are assumed:

1. The velocities of the upper waters in Fram Strait is used, determined by *Jonsson et al.* [1992] on the basis of current meter measurements. Assuming

that the velocities cited by these authors for the upper 78 to 262 meters are representative for the portion of section C which contains a negative sea–ice meltwater signal (i.e., assuming that the transition from positive to negative sea–ice meltwater fractions marks the transition from northward flowing Atlantic derived waters to southward flowing Arctic surface waters), the integral of the negative sea–ice meltwater fractions along the section ($2.45 \cdot 10^6$ m^2 can be multiplied by the mean velocity of 7.5 cm sec^{-1} [*Jonsson et al.,* 1992]. The result of such a calculation yields an export rate of the freshwater deficit caused by ice formation of about 0.18 Sv (6,300 km^3 year^{-1}; value corrected for the difference in densities of sea–water (about 1.0) and sea– ice (about 0.9)). The related flux of river–runoff through the section is about $2.47 \cdot 10^6$ m^2 times 7.5 cm sec^{-1}, or 0.19 Sv. These fluxes are upper limits because section C is well north of the latitude at which the current meters were deployed and it can be expected that the current velocities increase from the central Arctic Ocean towards Fram Strait where a considerable fraction of the surface waters feed into the comparably narrow East Greenland Current. This hypothesis is confirmed by the fact that our calculations yield a river–runoff flux of about 0.19 Sv, a value close to the sum of the total river discharge into the Arctic Ocean (about 0.1 Sv) and the P-E excess (about 0.03 to 0.08 Sv [*Aagaard and Carmack,* 1989; *Gorshkov,* 1983].

2. The inventory of river–runoff for the portion of the ARCTIC 91 section C (Fig. 13) where southward flow is assumed (H_{ice} negative) is calculated. Then this number ($4.92 \cdot 10^6$ m^2) is compared with the river discharge data to obtain a mean velocity of the river runoff contained in the upper waters flowing southward through Fram

   Strait. The result ($0.13\,Sv / 4.92 \cdot 10^6\,m^2$) yields an average velocity of about 2.6 $cm\,sec^{-1}$ for the river–runoff component leaving the Arctic Ocean through

Fram Strait. Assuming a constant ratio between the river–runoff fraction and the sea–ice meltwater fraction allows to estimate the export rate of the freshwater deficit related to ice–formation to be about 0.07 Sv (2,280 $km^3\,year^{-1}$).

In this calculation, the outflow of river–runoff through the Canadian Archipelago is neglected. This assumption makes the calculated velocity an upper limit (diversion of part of the river–runoff outflow through the Archipelago would decrease the velocity of river–runoff through Fram Strait). However, it seems likely that most of the sea–ice exits through Fram Strait while part of the river–runoff flows through the Canadian Archipelago. If the fraction in the upper waters of the Arctic Ocean are assumed to be in first order approximation more or less constant, the sea– ice export ratescalculated by this method should be fairly realistic.

The analytical uncertainty of this estimate is smaller than ± 0.02 Sv or $\pm 650\,km^3\,year^{-1}$ (determined on the basis of an error of $\pm 0.5\,m$ for the determination of the total river–runoff and sea–ice meltwater inventories). The systematic error introduced by the assumptions used in the calculations might be conciderably higher.

Previous estimates of sea–ice export rates through Fram Strait from ice drift observations and sea–ice thickness measurements range from 0.1 to 0.18 Sv for long–term averages (0.16 Sv, *Vinje and Finnekasa* [1986]; 0.10 Sv, *Hibler* [1979]; 0.18 Sv, *Koerner* [1983]; 0.13 Sv, *Wadhams* [1983]). The results of this study give an estimate for the sea–ice export rate through Fram Strait which have an upper limit of about 0.18 Sv and a lower limit of about 0.07 Sv.

Table 8 summarizes the sea–ice meltwater and river–runoff inventories calculated for section C and for two sections published by *Östlund and Hut* [1984] from YMER–80. The last three colums list the sea–ice export rates calculated by the discussed approaches. Since the YMER–80 results do not include the influence of BSI, the results for section C are listed for the 3–component mass balance (omitting BSI)

Table 8: Sea–ice meltwater and river–runoff inventories calculated for three sections across Fram Strait

section	average latitude [°N]	stations	length [km]	I_{ice}	I_{riv}	H_{ice}	H_{riv}	sea–ice export*	sea–ice export**	sea–ice export***
				$[10^6 m^2]$		[m]		[Sv]		[Sv]
including BSI influence (4–comp. calc.)										
ARCTIC 91	≈ 83	43...58	585	-2.45	4.92	-4.2	8.4	0.065	0.090	0.18
omitting BSI influence (3–comp. calc.)										
ARCTIC 91	≈ 83	43...58	585	-2.47	5.07	-4.2	8.7	0.063	0.088	0.19
Ymer–80	≈ 81	164...168	≈ 163	-0.78	1.77	-4.8	10.9	0.057	0.079	0.06
Ymer–80	≈ 80	159...152	≈ 350	-2.49	4.47	-7.1	12.8	0.072	0.100	0.19

I_{ice}, I_{riv} : Sea-ice meltwater and river–runoff inventories in the halocline integrated over the length of the sections.

H_{ice}, H_{riv} : average thickness of sea–ice meltwater and river–runoff layers

* sea–ice export based on a $P-E$ value of 0.03 Sv [*Aagaard and Carmack*, 1989] (second scenario).

** sea–ice export based on a precipitation value of 0.08 Sv [*Gorshkov*, 1983] (second scenario).

*** sea–ice export using a mean velocity of 7.5 cm sec^{-1} [*Jonsson et al.*, 1992] (first scenario).

and the 4–component mass balance (including BSI).

The effect of BSI on the sea–ice export rate is not significant. There is good agreement of the sea–ice export rates between the sections at varying latitudes for each scenario. There is a significant difference for Ymer–80 section at about 81°N latitude using a constant velocity of 7.5 cm sec^{-1} (first scenario). The relatively low value observed at this section is caused by its location in a narrower part of Fram Strait where the adopted velocity is probably most realistic. As a result the results between the two scenarios are at that location in relatively good agreement.

Table 9: Estimates of areas, fresh water layer thickness and fresh water volume in the Arctic Ocean interior

	area	H_{riv}	H_{ice}	V_{riv}	V_{ice}
	$[10^6 km^2]$	[m]		$[10^3 km^3]$	
Canadian Basin	3.2	13	-5	41.6	16.0
Eurasian Basin	1.9	7.5	-3.5	14.3	6.7
Arctic Ocean interior	5.1	11.0	-4.5	55.9	22.7

H_{ice}, H_{riv} : average thickness of sea–ice meltwater and river–runoff layers.

V_{ice}, V_{riv} : volume of sea–ice meltwater and river–runoff.

6.5 Water mass budget for the Arctic Ocean Halocline

Using the inventories of river–runoff and sea–ice meltwater, the freshwater storage of the Arctic Ocean halocline can be calculated. With the knowledge of the annual river discharge and the annual precipitation the mean residence time of the freshwater component in the Arctic Ocean can be determined. For the Canadian Basin, the thickness of the river–runoff and sea–ice meltwater layer was estimated in accordance with the results of ARCTIC 91 stations 43 and 26 and the LOREX and CESAR Ice Camps including the influence of water entering through Bering Strait (BSI). For the Eurasian Basin, river–runoff and sea–ice meltwater layer thicknesses were calculated using the results of the 3–component mass balance and an average value weighted by areas (Tab. 9).

With the estimated average river–runoff inventory (11 m) and the yearly river–runoff rate of 0.13 Sv (equivalent to 0.8m/yr), including a $P - E$ component of 0.03 Sv following *Aagaard and Carmack* [1989]), a freshwater mean residence time of 14 years is determined. Using a yearly river–runoff component of 0.18 Sv including a precipitation value of 0.08 Sv after *Gorshkov* [1983] a mean residence time of 11 years is determined. For an understanding of the balance it is important to note that the

total amount of river–runoff is not equivalent with the total amount of freshwater in the water column (which is equal to $H_{riv} + H_{ice}$). Freshwater is partly removed as sea–ice and exported with an rate independent from the water column. The derived mean residence time applies therefore for the river–runoff remaining in the water column and this is equivalent to the mean residence time of the freshwater actually found in the water column of the Arctic Ocean (ignoring the areas where sea–ice is melting). The mean residence time can also be adopted for the upper 50 m to 100 m of the halocline which are carrying the freshwater.

Mean ages derived from transient tracers point towards a faster renewal of the upper layers in the Eurasian Basin (e.g. *Wallace et al.* [1987]; *Schlosser et al.* [1990]; *Schlosser et al.* [1994]. Based on $\delta^{18}O$ and tritium measurements *Östlund and Hut* [1984] derive a freshwater mean residence time of 10 years within the Arctic Ocean. This values are reasonably close considering that the estimates are relatively rough, but it should be pointed out, that the estimate by *Östlund and Hut* [1984] involves qualitatively different results. *Östlund and Hut* [1984] do not detect a structure within the halocline and conclude that the horizontal mixing of the halocline waters occures on a much shorter time scale than the mean residence time. In contrast our results show a sharp boundary between the Eurasian and the Canadian basins and it can therefore be concluded that the lateral exchange is slow compared to the mean residence time and that the mean residence times might be different in each basin. The fresh water mean residence time of 14 years to 11 years is an average for the two basins. The main features of the circulation of the Arctic halocline are the Transpolar Drift in the Eurasian Basin and the Beaufort Gyre in the Canadian Basin. This circulation pattern suggests, that the mean residence time of the halocline in the Eurasian Basin is determined by the transfer time between the Siberian shelf areas and Fram Strait. In the Canadian Basin, on the other hand, the halocline water might be trapped in the Beaufort Gyre resulting in a longer mean residence time compared to the residence time in the Eurasian Basin. This

might be the reason that the average river water thickness in the Canadian Basin is significantly higher than in the Eurasian Basin. Since most of the river–runoff of the Arctic Ocean is entering the Siberian shelves, part of the Siberian river–runoff must flow eastwards and end up in the Beaufort Gyre.

6.6 Systematic error introduced by the choice of the $\delta^{18}O$ value of the river–runoff in the mass balance calculations

Brezgunov et al. [1983] published $\delta^{18}O$ values for the Siberian rivers Ob and Yenisey, which are significantly different from the value adopted for the Arctic river–runoff in the mass–balance calculations. From direct measurements of freshwater within the estuaries and by using salinity versus $\delta^{18}O$ regression lines *Brezgunov et al.* [1983] determine $\delta^{18}O$ values of about $-16.3\,‰$ for the Ob and $-17.5\,‰$ for the Yenisey river. However, *Brezgunov et al.* [1983] give no information about methods and measurement precision. Therefore these values were omitted. On the other hand an isotopically heavier value for the Ob and Yenisey rivers could be correct for the following reasons: (1) the drainage areas of both rivers reach further south than any of the other Arctic rivers (to about 45°N compared to about 55°N), and (2) the main source of precipitation for northern Eurasia lies towards the west of the continent, therefore the precipitation will be less depleted in the western regions, i. e. in the drainage areas of the Ob and Yenisey rivers.

In the following the systematic error is estimated by using an uniform $\delta^{18}O$ value of either $-21\,‰$ and $-20\,‰$ for river–runoff. Adopting a $\delta^{18}O$ value of about $-17\,‰$ for the combined runoff of Ob and Yenisey which is about one third of the total amount of Arctic river– runoff (about 1133 km^3yr^{-1} out of a total of 3303 km^3yr^{-1}; [*Treshnikov,* 1985]), the overall value of the Arctic river–runoff is about $-20\,‰$.

Using $-20\,‰$ versus $-21\,‰$ for the $\delta^{18}O$ value of river– runoff for most stations leads to a difference of about 0.5 m in sea–ice meltwater and in river runoff inventory.The error for most of the ARCTIC 91 stations is about 13% for the sea–ice meltwater and about 5% for the river–runoff inventories

The sea–ice export rate through Fram Strait using $-20\,‰$ for the $\delta^{18}O$ value

Table 10: Comparison of results using $-20\,‰$ versus $-21\,‰$ as $\delta^{18}O$ value for the river–runoff in the mass balance calculations

	result using -21 ‰	analytical error	result using -20 ‰	difference
H_{ice}, H_{riv}	-	$\approx \pm$ 0.5 m	-	$\approx$ 0.5 m
sea–ice export	0.06/0.08 Sv	$\approx \pm$ 0.02 Sv	0.08/0.10 Sv	0.02 Sv
mean residence time	11/14 yrs	-	11/14 yrs	$< 1yr$

of river–runoff is estimated to 0.08 Sv or 0.10 Sv compared to 0.06 Sv or 0.08 Sv calculated on the basis of a $\delta^{18}O$ value of $-21‰$. The estimate for the mean residence time of freshwater within the Arctic Ocean stays within $\pm 1\,yr$ at about 14 years or 11 years (see Tab. 10).

6.7 Mean residence time of river–runoff in the halocline and on the shelves of the Arctic Ocean

The principle approach used in this study to derive a mean residence time of river–runoff on the shelves is to compare tracer derived ages of halocline waters. In the Eurasian Basin, halocline waters consist of a mixture of Atlantic water and a freshwater component (river–runoff and sea ice meltwater), which are known to be formed on the shelves of the Arctic Ocean (e.g. *Aagaard et al.* [1981]; *Jones and Anderson* [1986]). Certain tracers delivered to the shelf by river–runoff start to 'age' at the time they enter the shelf. Other tracers are in contact with the atmosphere on the shelf and their clock is set to zero when they leave the shelf. We can use the difference of tracer derived ages which are set to zero at the time the runoff enters the shelves and when the shelf waters leave the shelf to determine the mean residence time of the river–runoff component on the shelf.

Östlund and Hut [1984] pointed out that the combination of salinity, tritium and ^{18}O can be used to determine the mean age of the river–runoff component. In a first step salinity and ^{18}O values are used to calculate the fractions of river–runoff and sea ice meltwater in the individual water samples (see Chap 6.1). In a second step the tritium concentration of the river–runoff component is calculated and this value is compared to the tritium concentrations as a function of time in the Siberian rivers estimated by *Östlund* [1982] to obtain the so–called 'tritium vintage age'. Applying this method to halocline waters yields an estimate of the mean time that has passed since the river–runoff fraction contained in a water parcel of the halocline has entered the shelf. This time is a measure for the total of the times spent on the shelf and the travel time from the shelf edge to the sampling site.

The tritium/^{3}He age is set to zero in a different way. ^{3}He formed in the shelf waters by tritium decay is lost to a large degree to the atmosphere by gas exchange. Thus, the tritium/^{3}He age is close to zero for shelf waters. The 'tritium/^{3}He clock'

is started at the time when the shelf waters flow into the interior basin and gas exchange with the atmosphere is suppressed. Tritium/^{3}He ages of the Arctic halocline should therefore be lower than the tritium vintage ages. The same should hold for all ages derived from gases dissolved in sea water (e.g. CFCs). The few published data are in agreement with this concept (e.g. *Östlund and Hut* [1984]; *Östlund et al.* [1987]; *Schlosser* [1985]; *Schlosser et al.* [1990]; *Wallace and Moore* [1985]; *Wallace et al.* [1987]; *Wallace et al.* [1992]).

6.7.1 Tritium results

Tritium measurements were made for samples taken during ArkIV/3 [*Schlosser et al.*, 1993; *Bönisch*, 1991] (for station locations see Fig. 13). The tritium section (Fig. 28 a) shows a similar pattern as the δ^{18}O section (see Fig. 16 a, section B) with maximum concentrations of about 10 TU in the surface waters of the northernmost station (371) and relatively low concentrations on the Barents Shelf (about 3.5 TU at station 269). The tritium concentrations in the Atlantic water are fairly homogeneous between the Barents Shelf and the northern boundary of the Nansen Basin with values of about 3.3 to 4.5 TU.

The apparent ^{3}H/^{3}He–age of the surface waters (Fig. 28 b) increases from the Barents Shelf (about 1 yr) towards the northern Nansen Basin where they reach values between about 3 and 5 yrs at station 371. There is an intermediate ^{3}H/^{3}He–age maximum at stations located in the central Nansen Basin which is caused by the fact that relatively young Atlantic water underlies relatively old water of the lower halocline. This feature disappears at stations in the northern Nansen Basin (e.g. sta. 371) where the age of the Atlantic water is higher than further south. At these stations, the ^{3}H/^{3}He–age increases more or less monotonically with depth.

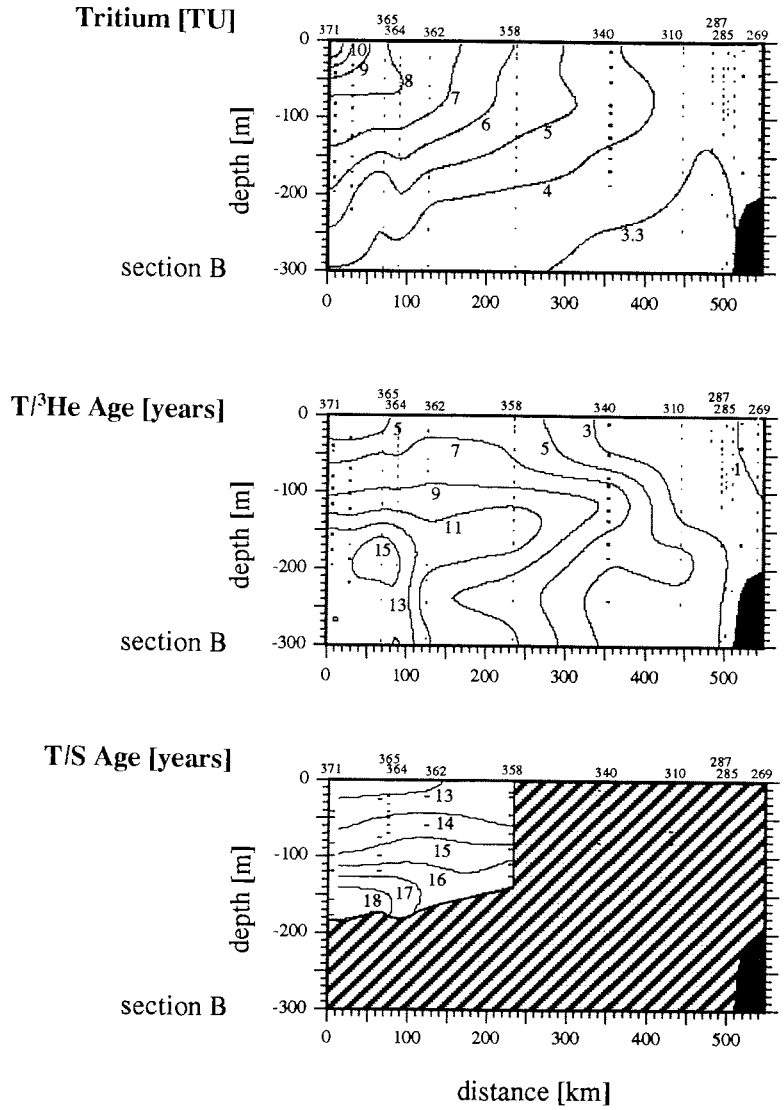

Figure 28: (a) Tritium section of the upper 250 meters for a section extending from the Barents Shelf (sta. 269) to the Gakkel Ridge (Sta. 371; for geographical position of the stations, see section B in Fig. 13). (b) Same as a) for tritium/^{3}He ages. (c) Same as a) for tritium vintage ages. The part of the section in which the river–runoff component used to determine the tritium vintage age is insignificant is shaded.

6.7.2 Tritium vintage ages of the freshwater component

The tritium balance of the halocline waters is given by the following equation:

$$f_a \cdot T_a + f_r \cdot T_r + f_i \cdot T_i = T_m \tag{8}$$

where T_a, T_r, T_i and T_m mean the tritium concentrations of the Atlantic water, the river–runoff, the sea–ice meltwater and the measured halocline water, respectively. As both T_a and T_m are known and T_i can be assumed to be the same as the surface water tritium concentration measured at the individual stations, equation (8) can be resolved for the tritium concentration of the river–runoff component T_r. Comparison of this tritium concentration with the time dependent tritium curve for river–runoff principally allows to estimate the 'vintage' of the river–runoff. This method was used by *Östlund and Hut* [1984] to estimate the age of the freshwater component of the Arctic halocline. In this estimate a values of 3.25 TU for T_a is used and the surface values measured at the individual stations for T_i is used (range: 3.7 TU at station 269 to 10 TU at station 371). The calculated tritium concentrations of the freshwater component range from about 20 TU to about 215 TU (see Table B.1 in the appendix). A curve for tritium in river–runoff was estimated by *Östlund et al.* [1982] and extended to 1987 for this study, using tritium measurements in precipitation published by the International Atomic Energy Agency. Straightforward comparison yields 'freight train' ages of the river–runoff component of the freshwater between 9 and 20 years with a general trend of increasing ages with increasing depth (Fig. 28 c and Table B.1 in appendix). This range is significantly higher than the values obtained by *Östlund and Hut* [1984] and is similar to the range obtained using other tracers such as CFCs (e.g. *Wallace and Moore* [1985]; *Wallace et al.* [1987]) or tritium/^{3}He (e.g. *Östlund et al.* [1982]; *Schlosser et al.* [1990]; *Wallace et al.* [1992]).

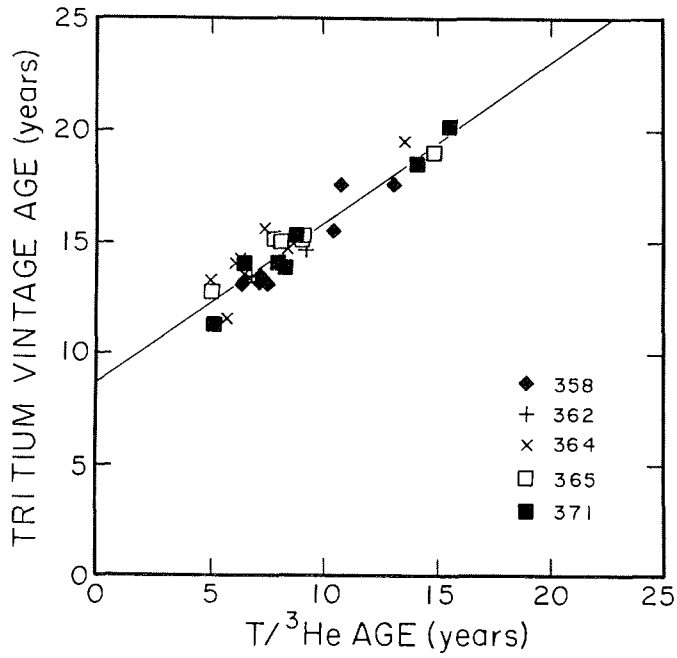

Figure 29: Tritium vintage age versus tritium/^{3}He age for the upper water column (S>34.5).

6.7.3 Comparison of tritium vintage ages and tritium/^{3}He ages

The ages of the freshwater component derived from the tritium data are systematically higher than the tritium/^{3}He ages (Fig. 29). This difference can be interpreted as an indicator of the mean residence time of the freshwater component on the shelf. Fig. 29 suggests a mean residence time of about 8 years. As the freshwater component of the shelf waters leaving the shelves contains a mixture of river–runoff discharged during more than one year, and the tritium concentration in runoff is a non–linear function of time, the difference between the two ages might be mislead-

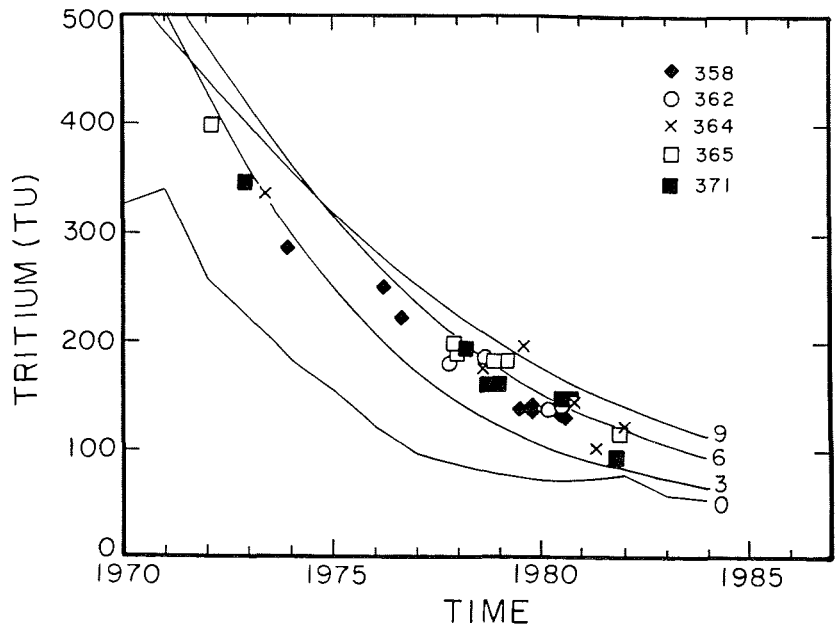

Figure 30: Tritium concentrations as a function of time in the runoff component of shelf water for different residence times of the shelf water (1–box model). According to their $^3H/^3He$–age, the calculated tritium values in the runoff component are included in the plot at the time 1987 minus the tritium/^{3}He age for samples with salinities above 34.5. For further explanation, see text.

ing if interpreted in a straightforward manner. Therefore the tritium concentration of the freshwater component of the shelf water was calculated for different storage times of the river–runoff on the shelf. For this calculation the tritium curve for Arctic runoff was used as input function of a well–mixed reservoir (1–box model). The resulting curves are plotted in Fig. 30. Assuming that the tritium/^{3}He age reflects the time that has passed since the shelf waters entered the halocline, the tritium concentration of the runoff component contained in the halocline waters can be plotted on the tritium curve at the time the water left the shelf (1987 minus

tritium/^{3}He age; Fig. 30). Most of the tritium points fall between the curves calculated for mean residence times of the freshwater component on the shelf of 3 and 6 years, respectively, indicating a mean residence time of the river–runoff component of 3 to 6 years.

In most cases the tritium/^{3}He age of the shelf water is not zero due to limited exchange with the atmosphere. Therefore, the difference between the tritium age and the tritium/^{3}He age has to be corrected to obtain a meaningful estimate of the mean residence time of the river–runoff on the shelf. At stations on the shelf and close to the continental slope (269, 280 and 287) tritium/^{3}He ages in the range of about 0.5 to 1.5 years are observed. By correcting the difference between the tritium ages and the tritium/^{3}He ages for this initial tritium/^{3}He age, a best estimate is observed for the mean residence time of the runoff component of about 3.5 ± 2 years. The scatter in the data reflects variations in both the mean residence times and the initial tritium/^{3}He ages of the shelf waters.

The halocline waters sampled during the 87 *Polarstern* cruise are probably derived from the Barents and Kara seas (see Chap. 2). Further studies with more complete data sets covering both the shelf areas and the halocline waters of the central Arctic Basin are needed to estimate mean residence times of river–runoff on each shelf that feeds water into the halocline.

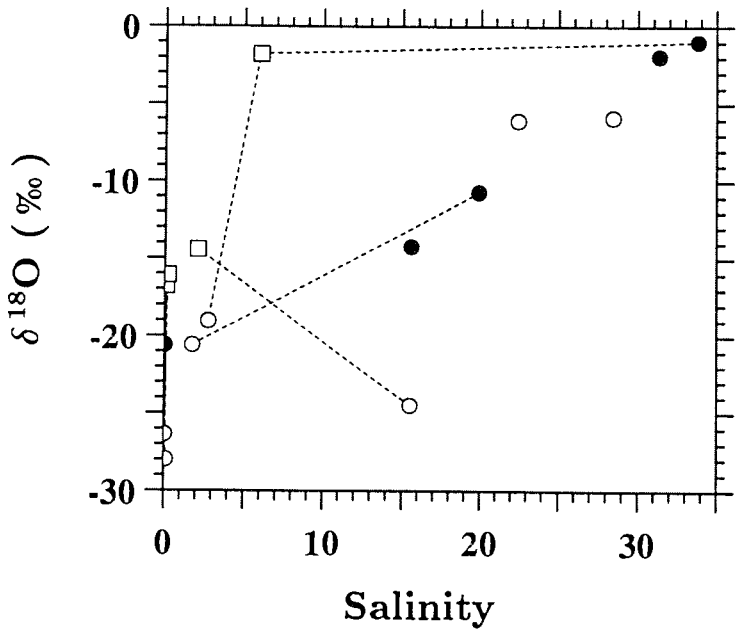

Figure 31: $\delta^{18}O$ versus salinity for surface water samples (full dots), sea-ice samples (open squares) and snow samples (open dots) in the Laptev Sea. Samples taken at the same location are connected with a dotted line.

6.8 Sea–ice formation and river–runoff distribution in the Laptev Sea

The salinity versus $\delta^{18}O$ values of the surface water samples are roughly linearly related, with a $\delta^{18}O$ value of $-20.6\,‰$ for zero salinity and about $0.3\,‰$ at a salinity of 34.92 (Fig. 31).

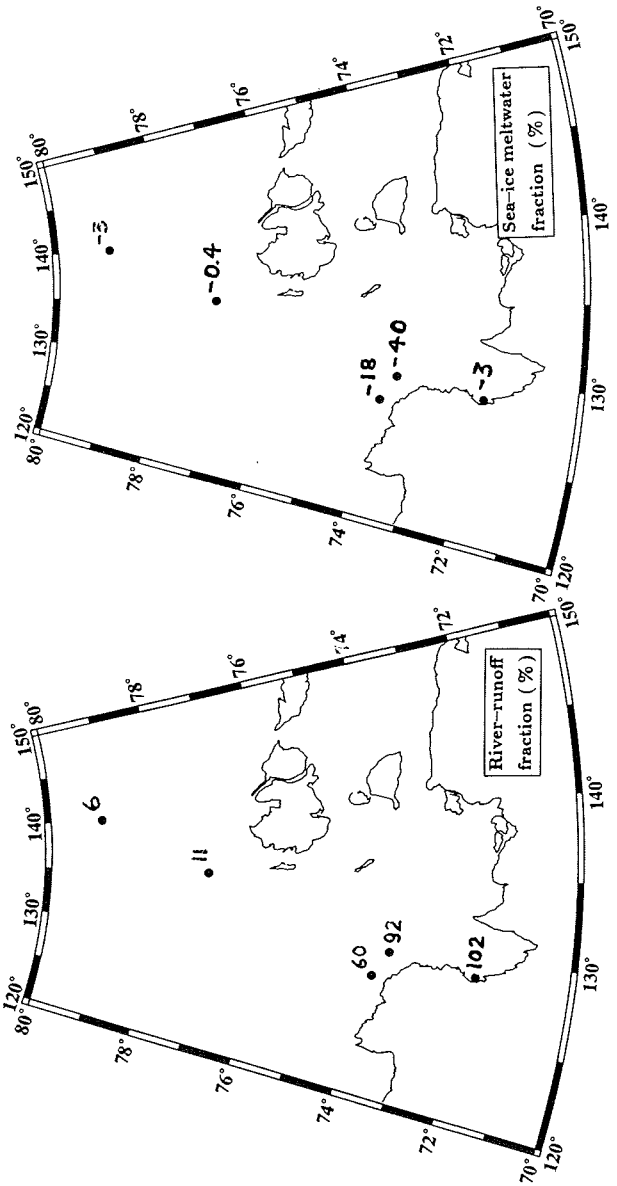

Figure 32: (a) River–runoff fractions of surface water samples are indicated next to the sampling location. (b) Same as a) for sea–ice meltwater fractions.

Table 11: Results of 3–component mass balance for Laptev Sea surface water samples

ref. no.	salinity	$\delta^{18}O$ [‰]	f_{ice} [%]	f_{riv} [%]
3	0.05	−20.60	−3	102
5	15.54	−14.23	−40	92
6	19.90	−10.69	−18	60
14	31.35	−1.91	−0.4	11
17	33.82	−0.98	−3	6

The 3-component mass balance (see Chap. 6.1) was applied, but with an $\delta^{18}O$ value of −20.6 ‰ for river–runoff instead of −21 ‰. From south to north the fraction of river–runoff in the surface water is decreasing (see Fig. 32 a and Tab. 11). At 79 °N (ref.no. 17) the fraction of river–runoff is only 6 % ; this value is low compared to 15-13 % found in surface samples of stations in the Trans Polar Drift near the north pole (ARCTIC 91 stations 26 and 31). This discrepancy supports the idea that the river–runoff from the Lena River is deflected towards the east and that its influence is relatively small directly north at the shelf break of the Laptev Sea. The eastward flow of Lena River discharge can also be observed in the dissolved silica distribution [*Treshnikov,* 1985] which shows the highest value at the Lena River delta and a stronger gradient towards the north than towards the east. Also the distribution of freshwater ice near the river delta was found to extend about 100 km in eastward direction from the delta [*Dethleff et al.,* 1993].

The sea-ice meltwater fractions are all negative and indicate formation of sea ice (see Fig. 32 b). The fractions removed for sea–ice formation increases from south to north. Similar to the river–runoff fractions the fraction removed for sea–ice formation is relatively small near the shelf break compared to the values found in the central Eurasian Basin. The calculated fractions of sea–ice formation are very high at about 74 °N (ref.no.5 and 6; see Fig. 14). The high fractions removed

for sea–ice formation are found at the location of the polynia observed in the Laptev Sea. This polynia is a recuring phenomena. During the E.S.A.R.E. 92 expedition [*Dethleff et al.,* 1993] the polynia was about 20 km wide, 1800 km long and it was located between the border of the fast ice edge and the drift ice at about 20 to 30 m water depth. Large amounts of sea ice were produced and continuously advected offshore [*Dethleff et al.,* 1993].

The surface salinity gradient observed is strong compared to literature data. *Gorshkov* [1983] gives a range of 15 to 30 (for winter conditions) compared to 0 and 34 over the same geographical area.

There are only two locations where both a surface water sample and an ice sample were collected. One of them is located in the Lena river delta (ref. no. 3): both water and ice are fresh and the difference in $\delta\,^{18}O$ values is 4.6 ‰. The maximal fractionation during sea–ice formation is 2.8 ‰ under equilibrium conditions [*Beck and Münnich,* 1988]. Therefore the ice must have been formed out of isotopically heavier water than that found at the sampling site. The water, out of which the ice formed, cannot be a mixture of river–runoff and sea water since the ice is fresh. The second location, where a surface water sample and an ice sample were collected is near the shelf break at 79 °N (ref. no. 17): the salinities are 33.8 and 6.0, respectively, and the $\delta\,^{18}O$ values are −0.98 ‰ and −1.91 ‰ respectively. The isotopic difference between water and sea–ice sample is only about 0.9 ‰. It is possible that the sea ice formed under non equilibrium conditions from the water found at that location.

The snow samples show that precipitation in that area are as low as −29 ‰. The snow samples with salinities different from zero are contaminated and cannot be interpreted.

6.9 Estimate of fresh water content of the Siberian shelves

The concept used earlier for the halocline of the Eurasian Basin (see Chap. 6.1) can be applied to the Siberian shelves. The waters of the Barents and Kara seas and possibly the Laptev Sea will be in first order a mixture of Atlantic water, river runoff and sea–ice meltwater. The Barents and Kara seas have a direct inflow of Atlantic water. The Laptev Sea might exchange with the adjacent seas, the Kara and East Siberian seas and with the Arctic Ocean halocline. The waters of the East Siberian Sea will be influenced the adjacent seas and part of this water might be of Pacific origin entering via the Chukchi Sea. There are temperature, salinity and nutrient data available from the Siberian shelves. In this study salinity data from the National Oceanographic Data Center (NODC) were used to calculate mean salinities of the shelf seas. A simple box model calculation was made as a consistency check: it uses a simplified concept of Atlantic water and fresh water on the Siberian shelves. Since there are no isotope data available, it is not possible to distinguish between river–runoff and sea–ice meltwater, and the impact of sea–ice formation will be omitted in this approach.

6.9.1 Calculation of mean salinities of the Siberian shelves from NODC data

Although the data base of the National Oceanographic Data Center (NODC) is relatively sparse in its coverage of the Arctic Ocean, it contains a significant amount of data from the Siberian shelves. In this study, data from stations with CTD/Nansen casts were used (see Fig. 33). The salinity data have a precision of at least ± 0.01. The area of the Barents Sea (30°E to 55°E) is very well covered. The Kara Sea (55°E to 100°E) is less extensively sampled. The Laptev Sea (100°E to 155°E) and the East Siberian Sea (155°E to 180°E) are covered to a water depth of about 50 m, but sampling across the shelf break is missing.

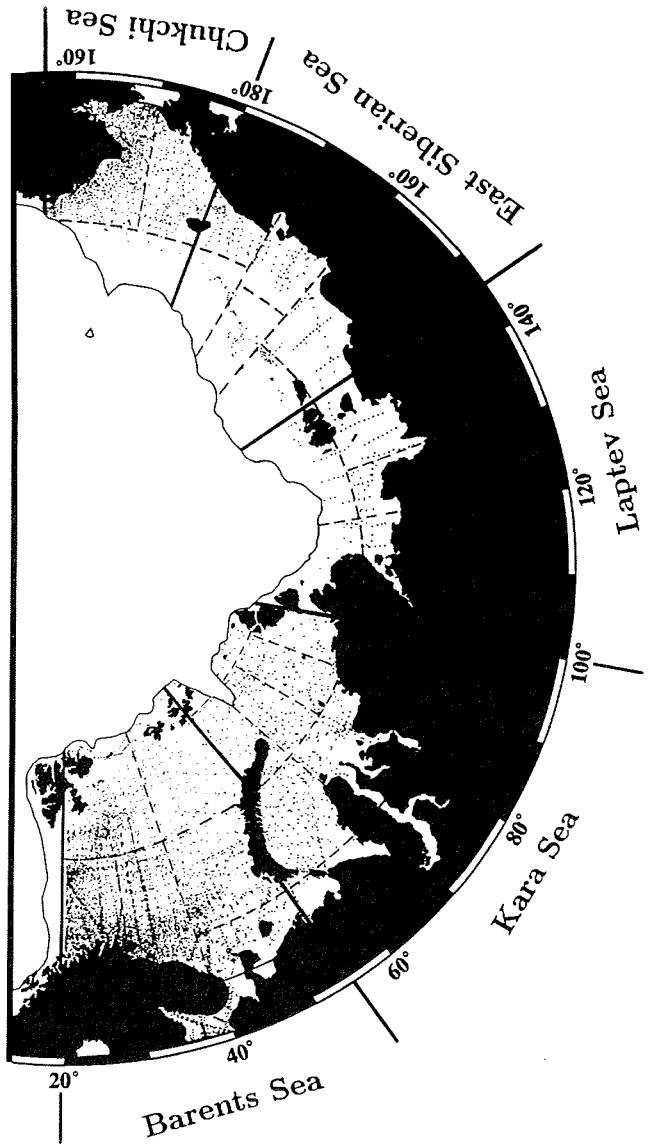

Figure 33: Geographic position of CTD Nansen cast stations from the NODC database. The heavy lines mark the borders taken between the shelf areas and the light lines the chosen sub-areas. The 500 m isobath is indicated.

Table 12: Mean salinities of the Siberian shelves calculated from NODC data

	salinity	depth [m]	area $[km^2]$	volume $[km^3]$
Barents Sea	34.75	163	1,378,000	224,019
Kara Sea	33.69	100	866,000	86,909
Laptev Sea	27.81	28	578,000	16,273
East Siberian Sea	29.42	32	898,000	28,847
Chukchi Sea	32.02	45	639,000	28,517

For calculation of the mean salinity each area was divided in 5 to 6 smaller areas of approximately equal size (see Fig. 33). Where possible these areas were chosen in a way that the data coverage was evenly distributed and regions with similar bathymetry were grouped together. The size of each area was calculated using the bathymetry of the ETOPO-5 global raster data base (National Geophys. Data Center, Boulder, CO), by omitting all islands and allowing bottom depths of up to 500 m. This relatively deep isobath was chosen in order to include the relatively deep parts of the Barents Sea.

The salinity of each station was integrated to a depth of 200 m. If the bottom depth was larger than 200 m (but smaller than 500 m), the integration was cut off in order to put not too much emphasis on the deeper stations located at the shelf break. This is important with respect to the Laptev and East Siberian seas, where there is no data coverage for the shelf break. For each area the mean salinity weighted by the depth of each station was calculated. Finally, the mean salinity of the entire shelf was calculated weighing over the mean depth and the size of each area (see Tab. 12).

6.9.2 'Freight train' approach box model of the Siberian shelves

In the following box model Atlantic water (with a salinity of 35.2) enters the shelf seas in the Barents Sea and flows from there to the east. The individual shelf seas are represented by well mixed boxes with a mean salinity to which fresh water (either sea–ice meltwater or river–runoff) and sea water with the salinity of the adjacent eastern shelf sea is added. For the case of the East Siberian Sea water from the east was allowed to spread westwards (see Fig. 34). Using the mean salinity of each shelf sea, the fraction of fresh water and of sea water with the salinity of the adjacent eastern shelf sea was calculated; the same procedure was also used for Atlantic water. For the East Siberian Sea, the fractions of Laptev Sea and Chukchi Sea waters were calculated. With a mean residence time of shelf water of about 3.5 years (see Chap. 6.7.3), annual transport rates were estimated (see Tab. 13 and Fig. 34). The transport of shelf waters into the Arctic Ocean are calculated from mass conservation.

The $\delta^{18}O$ values listed in Table 13 are calculated from the $\delta^{18}O$ values of the different water masses. The freshwater component was assumed to be sea–ice meltwater in the Barents Sea, with a $\delta^{18}O$ value of -2‰ (estimated mean $\delta^{18}O$ values in Barents Sea sea–ice using measurements from ice cores [*Pfirman et al.*, 1993*a*]), and river–runoff with a $\delta^{18}O$ value of -21‰ in the Kara and Laptev seas. The $\delta^{18}O$ value of the Chukchi Sea was estimated to about -1 ‰ after measurements published by *Cooper and DeNiro* [1990].

The 'freight train' approach is thought as a consistency test and first order approximation. The concept might be unfeasible for the Laptev Sea and East Siberian Sea, because the assumed flow pattern might be unrealistic. Besides the problem of the simplified concept, a significant systematic error will be the omission of sea–ice formation. The brine which is released during sea–ice formation will produce a higher salinity in the water column. In the areas with net sea–ice formation like

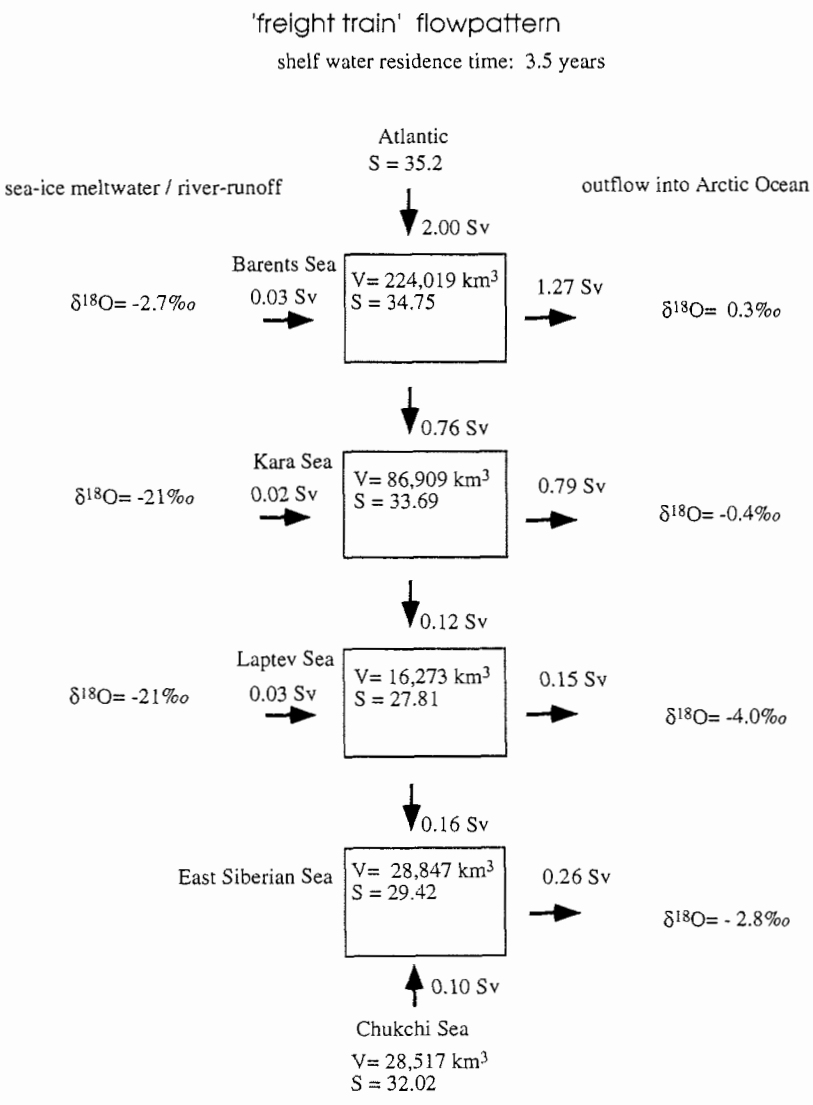

Figure 34: Flow scheme of 'freight train' approach box model. Each shelf region is represented by a well mixed box. The mean salinity (S) and the volume (V) of each shelf is indicated in each box.

Table 13: Transport rates from 'freight train' approach box model (see also Fig. 34).

	volume [km^3]	depth [m]	fraction [%]	$\delta\,^{18}O$ [‰]	flow [Sv]
Barents Sea					
from Atlantic	221130	161	99	0.324	2.00
fresh	2889	2	1	−2	0.03
total	224019	163	100	0.3	
Kara Sea					
from Barents Sea	84268	97	97	0.3	0.76
fresh	2641	3	3	−21	0.02
total	86909	100	100	−0.4	
Atlantic	83181	96	96		0.75
fresh rel. to Atl.	3728	4	4		0.03
Laptev Sea					
from Kara Sea	13431	23	82	−0.4	0.12
fresh	2842	5	18	−21	0.03
total	16273	28	100	−4.0	
Atlantic	12855	22	79		0.12
fresh rel. to Atl.	3418	6	21		0.03
East Siberian Sea					
from Laptev Sea	17770	20	62	−4.0	0.16
from Chukchi Sea	11077	12	38	−1	0.10
total	28847	32	100	-2.8	

the Laptev Sea and the Kara and East Siberian seas, the fraction of Atlantic water is overestimated and the fraction of river–runoff underestimated. Therefore, the estimated isotope values are a lower limit.

There are only a few estimates for transport rates on the Siberian shelves. Based on two month of current measurements between Norway and Bear Island, *Blindheim* [1989] calculated the water transport in and out of the southwestern Barents Sea to be about 3 Sv and 1 Sv, respectively. Based on a one year current meter array between Novaya Zemlya and Frans Josef Land, *Loeng et al.* [1993] estimate an outflow varying from 0.7 to 3.2 Sv with an average of about 2 Sv. *Rudels* [1987] estimated a transport of 1.2 Sv of Atlantic water into the Arctic Ocean from the Barents and Kara seas based on mass balance considerations. According to the 'freight train' approach box model estimate, about 2 Sv of Atlantic water enter the Barents Sea from the west. About 2.1 Sv are transported from the Kara and Barents seas into the Arctic Ocean. These results are in reasonable agreement with the transport estimates by *Loeng et al.* [1993] and *Blindheim* [1989]. The flow of river–runoff into the Siberian shelf seas adds up to 0.05 Sv. This is smaller than the value of 0.07 Sv found from long–term measurements for the Siberian rivers [*Treshnikov,* 1985]. The difference is due to the systematic errors introduced by the omission of sea–ice formation and brine release. The transport rates between the shelf areas are indirectly affected by this systematic error.

The long term averages of river-runoff [*Aagaard and Carmack,* 1989; *Treshnikov,* 1985] can be compared with the calculated freshwater content in each shelf sea and an estimate of the mean residence time of the water on the shelf can be obtained: the freshwater content relative to Atlantic water has to be divided by the total river-runoff into the shelf sea and the westward areas (see Tab. 14). The fraction of river–runoff in the shelf sea located to the west, which leaves the shelf and flows into the Arctic Ocean, is omitted. For the Kara, Laptev and East Siberian seas a mean residence time of shelf waters of about 2 to 3 years is estimated. This estimate is a

Table 14: Estimate of shelf water mean residence time from 'freight train' approach box model

	R_Σ $[km^3]$	$V_{fresh-atl}$ $[km^3]$	τ [yrs]
Kara Sea	1373	3728	2.7
Laptev Sea	1998	3418	1.7
East Siberian Sea	2157	4734	2.2

$V_{fresh-atl}$: calculated freshwater volume relative to Atlantic water (see Tab. 13).

τ: mean residence time of shelf water calculated by $\tau = \frac{V_{fresh-atl}}{R_\Sigma}$

R_Σ: mean annual river discharge into shelf area and westward laying shelf area [*Aagaard and Carmack*, 1989; *Treshnikov*, 1985]

lower limit, due to the omission of sea–ice formation. It is in reasonable agreement with the shelf water residence time of 3.5 ± 2 years estimated earlier (see Chap. 6.7.3).

The salinity versus δ^{18}O correlation in the Arctic Ocean Halocline can also be used for a rough estimate of the δ^{18}O value on the shelves. The salinity versus δ^{18}O correlation is non–linear due to freezing/melting processes, but for this purpose it will be described by the smoothed correlation $\delta^{18}\mathrm{O}\ (‰) = salinity - 34.7$ (from data in the Eurasian Basin). Using the mean salinity of the shelves calculated above (see Tab. 12), a mean δ^{18}O is calculated (see Tab. 15). The estimates obtained for δ^{18}O_*slope* are systematically lower, than the estimates for δ^{18}O_*box*. The omission of sea–ice formation causes δ^{18}O_*box* to be systematically too high. The estimate of δ^{18}O_*slope* on the other hand might be systematically too low, because it applies the average relation of river–runoff fraction to sea–ice meltwater fraction from an area of net sea–ice formation (the central Eurasian Basin) to the shelf seas, where this relation might be different and the fraction of sea–ice melting higher. There are only a few δ^{18}O measurements available from the Siberian shelf seas which cannot

Table 15: Comparison of $\delta^{18}O$ estimates for the Siberian shelves

	$\delta^{18}O\_box$ [‰]	$\delta^{18}O\_slope$ [‰]
Barents Sea	0.3	0.05
Kara Sea	−0.4	−1.0
Laptev Sea	−4.0	−6.9
East Siberian Sea	−2.8	−5.3
Chukchi Sea	−1.0	−2.7

$\delta^{18}O\_box$: $\delta^{18}O$ value calculated from 'freight train' approach box model.

$\delta^{18}O\_slope$: $\delta^{18}O$ value calculated from mean slope of salinity and $\delta^{18}O$ correlation in Eurasian Basin $\delta^{18}O$ (‰) = $salinity - 34.7$

be considered representative for the entire shelf sea. In the Barents Sea a $\delta^{18}O$ of about 0.1‰ was measured in the passage between Novaya Zemlya and Frans–Josef–Land (see Chap. 5.4 and Tab. A.4 in the appendix). At the shelf break of the Kara Sea two surface $\delta^{18}O$ values of −0.3‰ and −0.5‰ were observed [*Östlund and Hut,* 1984]. Four $\delta^{18}O$ values of surface water samples from the Laptev Sea were determined (see Chap. 5.3 and Tab. A.3 in the appendix). While the $\delta^{18}O$ values measured near the shelf break are about −1‰ and −2‰ the $\delta^{18}O$ values near the river delta are about −11‰ and −14‰. It is impossible to estimate an average $\delta^{18}O$ value for the entire area based on these spare values. On the basis of the few available $\delta^{18}O$ measurements from the shelf seas no evaluation of the two estimates $\delta^{18}O\_box$ and $\delta^{18}O\_slope$ can be done.

6.10 Sources of Arctic Ocean deep and bottom waters

The $\delta^{18}O$ profiles show only small variations below the Atlantic–derived layer. The stations in the central Arctic basins show a slight increase in $\delta^{18}O$ ($\approx 0.03\,‰$) below about 2600 m depth (the sill depth of Fram Strait). Average values of $\delta^{18}O$ and salinity were calculated for the depth intervals between 1000 and 2600 m and between 2600 m and the bottom (Fig. 35 a; open symbols: 1000 to 2600 m; full symbols: 2600 m to bottom depth; the error bars represent the standard errors of the mean values: $\frac{\sigma_{n-1}}{\sqrt{n-1}}$; see also Tab. 16).

Stations 79 and 617, located in the Norwegian Sea and in the Greenland Sea, respectively, do not show any significant increase in salinity or $\delta^{18}O$ with depth (see also Tables 16 and 17). For all stations in the Arctic Ocean, there is a trend of a $\delta^{18}O$ increase between the upper (1000 to 2600 m; open symbols in Fig. 35 a) and the lower (2600 m to bottom: full symbols in Fig. 35 a) depth intervals of about $0.03\,‰$. The deep waters in the Norwegian Sea fall on a mixing line between the deep Eurasian Basin and Greenland Sea waters. The values of Station 26 located in the Makarov Basin (Canadian Basin) do not fall on that mixing line. At this station, a shift to higher salinities and lower $\delta^{18}O$ values is observed.

A salinity balance shows that Eurasian Basin Bottom Water (EBBW; water below 2600 m depth) contains about $5\,‰$ of freshwater, relative to the Atlantic inflow (surface to 500 m depth at station 79 in the Norwegian Sea; Fig. 35 b). There is no decrease in $\delta^{18}O$ between inflowing Atlantic water and EBBW, indicating that the freshwater which contributes to EBBW must be derived from melting of sea–ice. The $\delta^{18}O$ values of Atlantic inflow and EBBW are within about 2 σ. If the contribution of river–runoff is calculated on the basis of this difference of 2 σ, a river–runoff fraction of $1\,‰$ is obtained. This possible small contribution of river–runoff to EBBW is still consistent with the hypothesis that the fresh water contributing to EBBW is derived from sea–ice meltwater, since sea–ice formed from shelf waters

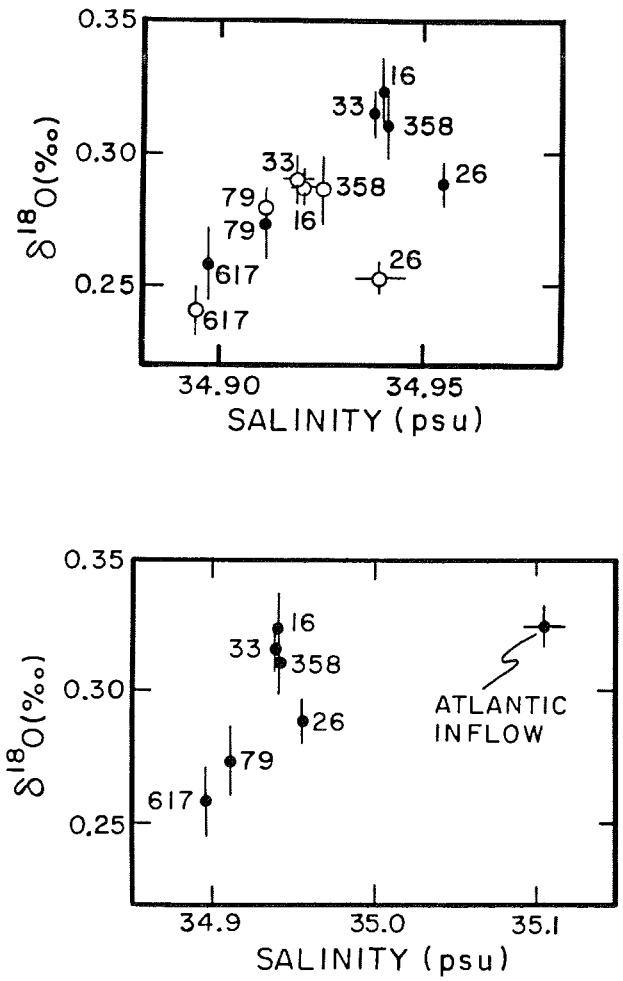

Figure 35: (a) $\delta^{18}O$ versus salinity plot for deep (1000 to 2600 m depth; open circles) and bottom (2600 m to bottom depth; full circles) waters. (b) $\delta^{18}O$ versus salinity plot for bottom waters and Atlantic Inflow.

Table 16: Station averages over deep and bottom intervals

station	interval [m]	$\delta^{18}O$ [‰] mean	error	salinity mean	error	n
358	1000-2600	0.286	0.013	34.925	0.001	12
	2600-bottom	0.310	0.012	34.941	0.001	12
16	1000-2600	0.287	0.007	34.920	0.003	9
	2600-bottom	0.323	0.014	34.940	0.001	10
33	1000-2600	0.290	0.009	34.919	0.004	6
	2600-bottom	0.315	0.009	34.938	0.002	8
26	1000-2600	0.253	0.006	34.939	0.006	9
	2600-bottom	0.288	0.008	34.955	0.000	9
617	1000-bottom	0.241	0.009	34.920	0.003	8
79	1000-bottom	0.279	0.006	34.940	0.001	14

Table 17: Properties of deep and bottom water masses

	$\delta^{18}O$ [‰]	error	salinity	error
EBDW	0.278	0.007	34.922	0.001
EBBW	0.305	0.008	34.940	0.001
GSDW	0.248	0.007	34.896	0.001
NSDW	0.276	0.007	34.911	0.001
Atl.inflow	0.324	0.008	35.105	0.014

EBDW: average of 1000-2600 m interval samples from stations 358, 16 and 33.

EBBW: average of 2600 m-bottom interval samples from stations 358, 16 and 33.

GSDW: average of 1000 m-bottom interval samples from station 617.

NSDW: average of 1000 m-bottom interval samples from station 79.

Atl.inflow: average of upper 500 m from samples in the Norwegian Sea (8 values from station 79).

containing river–runoff will indirectly carry a slight river $\delta^{18}O$ signal (e.g. the mean $\delta^{18}O$ value of ice cores taken within the Barents Sea is $-2.6\,‰$ [*Pfirman et al.*, 1993*b*]).

The bottom waters of the Makarov Basin and the Greenland and Norwegian seas are slightly depleted in $\delta^{18}O$ relative to Atlantic Water. The bottom water found at station 26 contains about $5\,‰$ of freshwater (calculated from a salinity balance). About $2\,‰$ of this freshwater might be derived from river–runoff (calculated from a $\delta^{18}O$ balance). This means that up to about 50 % of the freshwater is derived from river–runoff with a $\delta^{18}O$ value of $-21\,‰$.

Comparison of $\delta^{18}O$ values of the deep and bottom waters of the central Arctic Ocean with those observed in the surface shelf waters (Fig. 24) indicate that the main source region of EBBW are in the Barents and Kara seas (assuming steady–state conditions for deep and bottom water formation). The higher river–runoff fraction in the Canadian Basin indicates that at least a small part of CBDW has its source on the shelves east of the Barents and Kara seas. For all this conclusions steady state conditions for deep and bottom water formation are assumed. A somewhat speculative hypothesis is that the deep and bottom waters were formed at times (e.g. the last warm period during the middle ages) when the isotopic composition of the Atlantic Water was shifted to a higher $^{18}O/^{16}O$ ratios and that we presently see the remnants of bottom waters formed under different climatic conditions.

7 Conclusions

Balances of mass, salinity and $\delta^{18}O$ allow quantification of the fractions of the individual water masses contributing to the Arctic halocline. In the Eurasian Basin the relative contributions of the different freshwater sources can be determined relative precisely. In the Canadian Basin the mass balance calculation has to include BSI water in order to obtain a complete analysis of the halocline waters. Using silicate as an additional parameter in a four–component mass balance accounts for part of the Pacific component feeding into the upper halocline. The relatively low salinities and low $\delta^{18}O$ values in the Canadian Basin are caused by BSI water, as well as by larger river–runoff and sea–ice meltwater fractions. For a more precise quantitative determination of the freshwater sources and content in the Canadian Basin, the parameters of the mass balance calculations have to be determined more accurately. This can be done in an oceanographic study which includes $\delta^{18}O$ and silicate measurements in the western Chukchi Sea where the UHW acquires its properties and where it flows off the shelf.

A mean residence time of river–runoff on the shelves can be estimated by comparing tritium 'vintage' ages and tritium/^{3}He ages. The method to derive a tritium 'vintage' age only works as long as the gradient in the tritium concentration of river–runoff is steep enough. Given the presently nearly constant tritium concentration in Siberian river–runoff, this method cannot be applied in future studies.

Comparison of the $\delta^{18}O$ values of EBBW, Atlantic Water and shelf waters allows to estimate the river–runoff content relative to the freshwater content in this water mass. The sources of EBBW can be located to be in the Barents and Kara seas. The source region of CBBW supplies a slightly larger amount of river–runoff and cannot be located with the help of the present $\delta^{18}O$ data set.

The sea–ice meltwater inventories calculated for the Arctic Ocean can be directly converted into export rates through Fram Strait once better current measurements

are available for Fram Strait and the coupling between the circulation of sea–ice and surface waters is better known.

On the basis of a freshwater balance of the entire halocline of the Arctic Ocean, an average mean residence time of the river–runoff within the Arctic Ocean is calculated. The freshwater distribution within the Arctic Ocean reveals distinct regimes of the halocline. These regimes can be used to outline pathways and transport mechanisms within the halocline. A direct application of this knowledge is the prediction of the transport of pollutants which are released to the Siberian shelves by river–runoff. The $\delta\,^{18}O$ distribution suggests, that the river-runoff from the Siberian shelves is not spreading into the Arctic Ocean interior directly, but flows initially eastwards or flows off the shelves in plumes.

For a further understanding of the Arctic Ocean a better oceanographic data coverage is needed. However, the presently existing observational data and accumulated knowledge can allready be used to validate the large–scale features of models simulating the circulation in the Arctic Ocean.

References

Aagaard, K., A synthesis of the Arctic Ocean circulation., *Papp. P.-v. Reun. Cons. int. Explor. Mer.*, *188*, 11–22, 1989.

Aagaard, K., and E. C. Carmack, The role of sea ice and other fresh water in the Arctic circulation, *Journal of Geophysical Research*, *94* (C10), 14,487–14,498, 1989.

Aagaard, K., L. K. Coachman, and E. C. Carmack, On the halocline of the Arctic Ocean., *Deep-Sea Research*, *28*, 529–545, 1981.

Aagaard, K., J. H. Swift, and E. C. Carmack, Thermohaline circulation in the Arctic Mediterranean seas., *Journal of Geophysical Research*, *90* (C3), 4833–4846, 1985.

Anderson, L. G., and M. L. Carlson, editors, *International Arctic Ocean Expedition 1991. Icebreaker Oden. A Cruise Report.* Swedish Polar Research Secretariat, Box 50005, S-104 05 Stockholm, Sweden, 1991.

Anderson, L. G., E. P. Jones, K. P. Koltermannn, P. Schlosser, J. H. Swift, and D. W. R. Wallace, The first oceanographic section across the Nansen Basin in the Arctic Ocean, *Deep-Sea Research*, *36* (3), 475–482, 1989.

Bauch, D., P. Schlosser, and R. Fairbanks, Freshwater balance and the sources of deep and bottom waters in the Arctic Ocean inferred from the distribution of $H_2^{18}O$, *submitted to Progress in Oceanography*, 1994.

Beck, N., and K. O. Münnich, Freezing of water: isotopic fractionation, *Chem. Geol.*, *70*, 168, 1988.

Björk, G., The vertical distribution of nutrients and oxygen 18 in the upper Arctic Ocean, *Journal of Geophysical Research*, *95* (C9), 16025–16036, 1990.

Blindheim, J., Cascading of Barents Sea bottom water into the Norwegian Sea., *Rapp. P.-V. Teun. Cons. Int. Explor. Mer*, *188*, 49–58, 1989.

Bönisch, G., Spurenstoffuntersuchungen zur Tiefenwasserbildung und -zirkulation im Europäischen Nordmeer, Ph.D. thesis, Inst. für Umweltphysik, INF 366, Heidelberg, Germany., 1991.

Bönisch, G., and P. Schlosser, Deep water formation and exchange rates in the Greeland/Norwegian

seas and in the Eurasian Basin of the Arctic Ocean derived from tracer balances, *submitted to Progress in Oceanography*, 1994.

Bottinga, Y., *reported in: I. Friedman and J. R. O'Neil, Data of Geochemistry, Geol. Survey Prof. paper 440-KK.* 1973.

Brezgunov, V. S., V. Debol'skii, V. V. Nechaev, V. I. Ferronskii, and T. V. Yakimova, Characteristics of the formation of the oxygen isotope composition and salinity upon mixing of sea and river waters in the Barents and Kara seas., *Water Resour., transl of Vodn. Resur.*, *9* (4), 335–344, 1983.

Broecker, W. S., "NO", a conservative water-mass tracer, *Earth Planet. Sci. Lettt.*, *23*, 100–107, 1974.

Coachman, L. K., and K. Aagaard. 1974. *Physical oceanography of Arctic and submarine Seas.* volume Marine Geology and Oceanography of the Arctic Seas, chapter 1, 1–72. Springer, New York.

Coachman, L. K., and K. Aagaard, Transport through Bering Strait: Annual and interannual variability., *Journal of Geophysical Research*, *93* (C12), 15,535–15,539, 1988.

Coachman, L. K., and C. A. Barnes, The movement of Atlantic Water in the Arctic Ocean., *Arctic*, *16* (1), 8–16, 1963.

Coachman, L. K., K. Aagaard, and R. B. Tripp, *Bering Strait: The regional physical oceanography.* University of Washington Press, 1975.

Codispoti, L. A., and T. G. Owens, Nutrient transport through Lancaster Sound in relation to the Arctic Ocean's reactive silicate budget and the outflow of Bering Strait waters, *Limnology and Oceanography*, *20*, 115–119, 1975.

Colony, R., and A. Thorndike, An estimate of the mean field of Arctic sea ice motion., *Journal of Geophysical Research*, *89* (C6), 10623–10629, 1984.

Cooper, L. W., and M. J. DeNiro, Oxygen isotope compositions of bottom seawater and tunicate cellulose used as indicator of water masses in the northern Bering and Chukchi seas, *Limnol. Oceanogr.*, *35* (5), 1182–1195, 1990.

Craig, H., Standard for reporting concentration of deuterium and oxygen–18 in natural waters, *Science*, *133*, 1833–1834, 1961.

Dethleff, D., D. Nürnberg, E. Reimnitz, M. Saarso, and Y. P. Savchenko, East Siberian Arctic Region Expedition '92: The Laptev Sea – Its significance for the Arctic sea–ice formation and transpolar sediment flux, *Berichte zur Polarforschung, AWI, D-2850 Bremerhaven, Germany*, *120*, 1993.

Donk, J. v., and G. Mathieu, Oxygen isotope compositions of foraminifera and water samples from the Arctic Ocean, *Journal of Geophysical Research, 74* (13), 3396–3407, 1969.

Epstein, S., and T. Mayeda, Variation of oxygen–18 content of waters from natural sources., *Geochem. Cosmochim. Acta, 4*, 213–224, 1953.

Fairbanks, R. G., The origin of continental shelf and slope water in the New York Bight and Gulf of Maine: Evidence from $H_2{}^{18}O/H_2{}^{16}O$ ratio measurements, *Journal of Geophysical Research, 87* (C8), 5,796–5,808, 1982.

Finnigan MAT, *Operating Manual for M251, part nr. 16110, issue 7/85.* Finnigan MAT, 1985.

Fissel, D. B., D. D. Lemon, H. Melling, and R. A. Lake, Non-tidal flows in the Northwest Passage, *Can. Tech. Rep. Hydrogr. Ocean Sci., 98*, Inst. of Ocean Sci., Sidney, B.C. Canada, 1988.

Foldvik, A., K. Aagaard, and T. Tørressen, On the velocity field of the East Greenland Current., *Deep-Sea Research, 35* (8), 1335–1354, 1988.

Friedman, I., B. Schoen, and J. Harris, The deuterium concentration in Arctic sea ice, *Journal of Geophysical Research, 66* (6), 119–122, 1961.

Garlick, G. D. 1969. *Handbook of Geochemistry.* edited by K. H. Wedepohl, volume 8B, chapter The stable isotopes of oxygen. Springer, Berlin Heidelberg New York.

Gat, J. R., and R. Gonfiantini, Stable isotope hydrology, deuterium and oxygen–18 in the water cycle., Technical Report 210, International Atomic Energy Agency, Vienna, 1981.

Gordienko, P. A., and A. F. Laktionov. 1958. *Annals of the International Geophysical Year.* edited by A. Gordon , and F. W. G. Baker, volume XLVI, chapter Circulation and Physics of the Arctic Basin Waters., 94–112. Pergamon Press.

Gorshkov, S. E., *World Ocean Atlas, vol. 3, Arctic Ocean (in Russian), 189 pp.* Pergamon, New York, 1983.

Hanzlick, D., The West Spitzbergen Current: transport, forcing and variability, Ph.D. thesis, Univ. of Washington 127pp., 1983.

Hibler, W. D., A dynamic thermodynamic sea ice model for climate studies, *J. Phys. Oceanogr., 89* (4), 1979.

Hoefs, J., *Stable Isotope Geochemistry.* Springer, Berlin Heidelberg New York, 1987.

IAEA, World survey of isotope concentration in precipitation, Technical Report Series Nos. 69, 117, 129, 147, 165, 192, 226, 264, 311, International Atomic Enery Agency, Vienna, 1969, 1970, 1971, 1973, 1975, 1979, 1983, 1986, 1990.

Jones, E. P., and L. G. Anderson, On the origin of the chemical properties of the Arctic Ocean Halocline., *Journal of Geophysical Research, 91* (C9), 10,759–10,767, 1986.

Jones, E. P., L. G. Anderson, and D. W. R. Wallace, Tracers of near-surface, halocline and deep waters in the Arctic Ocean: Implications for circulation, *Journal of Marine Systems*, *2*, 241–255, 1991.

Jonsson, S., A. Foldvik, and K. Aagaard, The structure and atmospheric forcing of the mesoscale velocity field in Fram Strait, *Journal of Geophysical Research*, , 2939–2952, 1992.

Kinney, P., M. E. Arhelger, and D. Burrell, Chemical characteristics of water masses in the Amerasian Basin of the Arctic Ocean, *Journal of Geophysical Research*, *75*, 4097–4104, 1970.

Koerner, R. M., The mass balance of the sea ice in the Arctic Ocean., *Journal of Glaciology*, *12* (65), 173–178, 1983.

Koltermann, K. P., and H. Lüthje, *Hydrographischer Atlas der Grönland und Nördlichen Norwegischen See (1979–1987)*. Deutsches Hydrographisches Institut, Hamburg, pp274, 1989.

Krouse, H. R., and J. R. Mackay, Application of $H_2{}^{18}O$ / $H_2{}^{16}O$ abundances to the problem of lateral mixing in the Liard-Mackenzie river system., *Can. J. of Earth Sc.*, *8*, 1107, 1971.

Loeng, H., V. Ozhigin, B. Ådlandsvik, and H. Sagen, Current measurements in the northeastern Barents Sea, *Ices Statutory Meeting 1993, C. M. 1993/C:41 Hydrographic Commitee*, 1993.

Macdonald, R. W., and E. C. Carmack, The role of large-scale under-ice topography in separating estuary and ocean on an Arctic shelf, *Atmosphere-Ocean*, *29* (1), 37–53, 1991.

Macdonald, R. W., E. C. Carmack, F. A. McLaughlin, K. Iseki, D. M. Macdonald, and M. C. O'Brien, Composition and modification of water masses in the Mackenzie Shelf estuary, *Journal of Geophysical Research*, *94* (C12), 18057–18070, 1989.

Melling, H., and E. L. Lewis, Shelf drainage flows in the Beaufort sea and their effect on the Arctic Ocean pycnocline., *Deep-Sea Research*, *29*, 967–986, 1982.

Melling, H., and R. Moore, Modification of halocline source waters during freezing on the beaufort sea shelf, *Continental Shelf Research, in press*, 1994.

Midttun, L., Formation of dense bottom water in the Barents Sea., *Deep-Sea Research*, *32* (10), 1233–1241, 1985.

Moore, R. M., M. G. Lowings, and F. C. Tan, Geochemical profiles in the central Arctic Ocean: Their relation to freezing and shallow circulation., *Journal of Geophysical Research*, *88* (C4), 2667–2674, 1983.

Mosby, H., Water, salt and heat balance of the North Polar Sea and the Norwegian Sea., *Geofys. Publ.*, *24*, 289–313, 1962.

Nürnberg, D., and E. Groth, Expedition to Novaja Zemlja and Franz Josef Land with RV "Dalnie Zelentsy", *Berichte zur Polarforschung, AWI, D-2850 Bremerhaven, Germany*, *120*, 1993.

O'Neil, J. R., and L. H. Adami, *reported in: I. Friedman and J. R. O'Neil, Data of Geochemistry, Geol. Survey Prof. paper 440-KK.* 1969.

Östlund, G., The residence time of the freshwater component in the Arctic Ocean., *Journal of Geophysical Research, 87* (C3), 2035–2043, 1982.

Östlund, G., Z. Top, and V. E. Lee, Isotope dating of waters at Fram III, *Geophys. Res. Lett., 9*, 6,373–6,381, 1982.

Östlund, H. G., G. Possnert, and J. H. Swift, Ventilation rate of the deep Arctic Ocean from carbon 14 data., *Journal of Geophysical Research, 92* (C4), 3769–3777, 1987.

Östlund, H. G., and G. Hut, Arctic Ocean water mass balance from isotope data., *Journal of Geophysical Research, 89* (C4), 6373–6381, 1984.

Pfirman, S., J.-C. Gascard, I. Wollenburg, P. J. Mudie, and A. Abelman, Particleladen Eurasian Arctic sea ice, observations from July and August 1987., *Polar Res., 7*, 59–66, 1989.

Pfirman, S. L., D. Bauch, and T. Gammelsrød. 1993*a*. The northern Barents Sea: Water mass distribution and modification. in *The Role of the Polar Oceans in Shaping the Global Environment. AGU Monograph,* . submitted.

Pfirman, S. L., H. Eiken, D. Bauch, R. Colony, M. A. Lange, I. Wollenburg, and R. Fairbanks, Sediment-laden Siberian Sea ice in the Barents Sea, 1993*b*, to be submitted.

PSSP, Polarstern Shipboard Scientific Party. Breakthrough in Arctic deep sea research: the RV Polarstern expedition 1987., *EOS, Trans. Amer. Geophys. Union, 665*, 676–678, 1988.

Redfield, A. C., and I. Friedman, The effect of meteoric water, melt water and brine on the composition of polar sea water and of the deep waters of the ocean., *Deep-Sea Research, 16*, 197–214, 1969.

Roether, W., Water-CO_2 exchange set-up for the routine ^{18}Oxygen assey of natural waters, *Intern. Journal of Applied Radiation and Isotopes, 321*, 379–387, 1970.

Rudels, B., On the mass balance of the polar ocean, with special emphasis on the Fram Strait., *Norsk Polarinstitutt Skrifter, 188*, 1–53, 1987.

Sambrotto, R. N., J. J. Goering, and C. P. McRoy, Large yearly production of phytoplankton in the western Bering Strait, *Science, 225*, 1147–1150, 1984.

Schlosser, P., D. Bauch, R. Fairbanks, and G. Bönisch, Arctic river–runoff: mean residence time on the shelves and in the halocline, *Deep-Sea Research, in press*, 1993.

Schlosser, P., G. Bönisch, B. Kromer, H. Loosli, Bühler, R. Bayer, Bonati, and K. P. Koltermann, Mid 1980s distribution of tritium, ^{3}He, ^{14}C and ^{39}Ar in the Greenland/Norwegian seas and the Nansen Basin of the Arctic Ocean: Implication for large–scale circulation patterns, *submitted to*

Progress in Oceanography, 1994.

Schlosser, P., Ozeanographische Anwendungen von Spurenstoffmessungen im Mittelmeerausstrom und im Europäischen Nordmeer, Ph.D. thesis, Universität Heidelberg, 1985.

Schlosser, P., G. Bönisch, B. Kromer, K. O. Münnich, and K. P. Koltermann, Ventilation rates of the waters in the Nansen Basin of the Arctic Ocean derived from a multitracer approach, *Journal of Geophysical Research, 95* (**C3**), 3265–3272, 1990.

Smethie, W. M., D. W. Chipman, J. H. Swift, and K. P. Koltermann, Chlorofluoromethanes in the Arctic Mediterranean seas: evidence for formation of bottom water in the Eurasian Basin and deep-water exchange through Fram Strait., *Deep–Sea Research, 35*, 347–369, 1988.

Swift, J. H., T. Takahash, and H. D. Livingston, The contribution of Greenland and Barents Sea to the deep water of the Arctic Ocean, *Journal of Geophysical Research, 88* (**C10**), 5981–5986, 1983.

Treshnikov, A. F., *Arctic Atlas (in Russian) 204pp.* Arkt.Antarkt. Nauchno Issled. Inst. Moscow, 1985.

Vetshteyn, V., G. A. Malyuk, and V. P. Russanov, Oxygen-18 distribution in the central Arctic Basin., *Oceanology, 14*, 514–519, 1974.

Vinje, T., and O. Finnekasa, The ice transport through Fram Strait, *Norsk-Polarinstitutt Skrifter, 186*, 4–39, 1986.

Wadhams, P., Sea ice thickness distribution in Fram Strait., *Nature, 305*, 108–111, 1983.

Wallace, D. W. R., R. M. Moore, and E. Jones, Ventilation of the Arctic Ocean cold halocline: rates of diapycnal and isopycnal transport, oxygen utilization and primary production inferred using chlorofluoromethane distributions., *Deep–Sea Research, 34* (**12**), 1957–1979, 1987.

Wallace, D. W. R., P. Schlosser, M. Krysell, and G. Bönisch, Halocarbon and tritium/^3He dating of water masses in the Nansen Basin, Arctic Ocean, *Deep–Sea Research, 39* (**Suppl. 2**), S435–S458, 1992.

Wallace, D. W. R., and R. M. Moore, Vertical profiles of CF_2Cl_2 (F-12) and CCl_3F in the Central Arctic Ocean, *Journal of Geophysical Research, 90*, 1155–1166, 1985.

Walsh, J. J., C. P. McRoy, L. K. Coachman, J. Goering, J. Nihoul, T. E. Whitledge, T. H. Blackburn, P. L. Parker, C. D. Wirick, P. G. Shuert, J. M. Grebmeier, A. M. Springer, R. D. Tripp, D. A. Hansell, S. Djenidi, E. Deleersnijder, K. Henriksen, B. A. Lund, P. Anderson, F. E. Müller-Karger, and K. Dean, Carbon and nitrogen cycling within the Bering/Chukchi seas: Source regions for organic matter effecting AOU demands of the Arctic Ocean, *Progress in Oceanography, 22*, 277–359, 1989.

Weeks, W. F., and S. F. Ackley. 1986. *The growth, structure, and properties of sea ice.* edited by N. Untersteiner, volume The Geophysics of Sea Ice., chapter 1, 9–164. University of Washington, Seattle, Washington.

Wilson, C., and D. W. R. Wallace, Using the nutrient ratio NO/PO as a tracer of continental shelf waters in the central Arctic Ocean, *Journal of Geophysical Research, 95* (C12), 22,193–22,203, 1990.

A Tritium concentration in Arctic river–runoff

The curve of tritium concentrations in Arctic river–runoff versus time is given by *Östlund* [1982] for the years from 1953 to 1977. Using his method which is in the following briefly described these curve was extended to the year 1984.

Monthly tritium concentrations in Arctic precipitation are available from publications of the *International Atomic Energy Agency* [*IAEA*, 1969, 1970, 1971, 1973, 1975, 1979, 1983, 1986, 1990]. The precipitation stations selected were those north of 50°N and some more southern stations that represent sources of runoff to the Arctic Ocean (see Tab. 18). For each station, yearly averages were calculated, weighted by the amount of precipitation. The yearly averages, plotted on a logarithmic scale versus year, show similarity between the stations: the curves are all of the same shape. Thus the data from each station can be made to fit another location by applying a factor specific for that station. The Ottawa station has the longest uninterrupted data set. Therefore it was selected as standard for the calculation of the adjustment factors. The uncertainty in these factors F_{ott} are all below 20% (see column 6 in Tab. 18).

In a next step all stations were selected, which are continental and feed into the runoff of the Arctic Ocean (marked A and S in Table 18 for the American and Siberian sectors, respectively). The average Ottawa factor F_{ott} for the A stations is 1.48 $\pm$ 0.12, and for the S stations 1.61 $\pm$ 0.13, so an overall Arctic factor F_{arc} of 1.48 $\pm$ 0.12 was adopted. The yearly precipitation averages were then multiplied by F_{arc}/F_{ott}, and a gross average was calculated, representing the 'best' tritium concentration in continental precipitation that feed into Arctic Ocean runoff (see column 2 in Tab. 19).

In order to account for the storage and interaction with groundwater a simple model was used to compute tritium concentrations in river–runoff by fitting the model to the few available river data. A one–box model for the hydrological system

Table 18: Arctic precipitation stations (after *Östlund* [1982])

		Location		Ottawa Factor	
Class	Station Name	Latitude	Longitude	Value	Error (±)
	Adak	52°N	177°W	0.36	0.04
	Bethel	61°N	162°W	0.75	0.05
A	Barrow	71°N	157°W	1.05	0.20
	Anchorage	61°N	150°W	0.75	0.05
A	Whitehorse	61°N	135°W	1.20	0.07
A	Edmontton	54°N	114°W	1.75	0.07
A	Fort Smith	60°N	112°W	1.70	0.07
	Ottawa	45°N	76°W	1.00	0.00
A	Thule	77°N	69°W	1.80	0.10
A	Goose Bay	53°N	60°W	1.15	0.05
	Groennedal	61°N	48°W	0.70	0.05
	Reykjavik	64°N	22°W	0.40	0.05
A	Nord, Greenland	82°N	17°W	1.70	0.10
	Lista	58°N	7°E	0.45	0.03
	Isfjord	78°N	14°E	0.55	0.03
	Huddinge	59°N	18°E	0.71	0.03
S	Archangelsk	65°N	41°E	1.00	0.20
S	Perm	58°N	56°E	1.40	0.20
S	Salehard	66°N	66°E	1.40	0.20
S	Omsk	55°N	73°E	1.50	0.20
S	Novosibirsk	55°N	83°E	1.60	0.30
S	Enisejsk	58°N	92°E	1.90	0.15
S	Irkutsk	52°N	104°E	2.10	0.20
S	Skovorodino	54°N	124°E	1.70	0.20
S	Jakutsk	62°N	130°E	1.80	0.20
	Petropavlosk	53°N	159°E	0.60	0.20

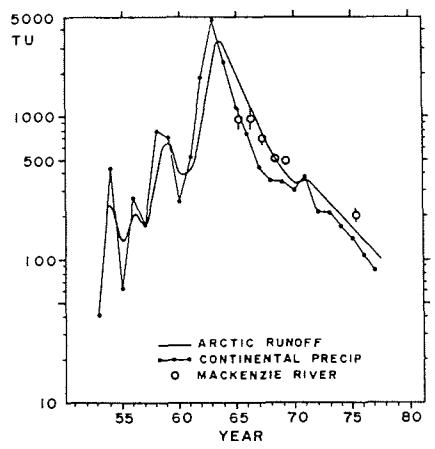

Figure 36: Calculated yearly tritium concentrations of runoff to the Arctic Ocean plotted at mid years taken from *Östlund* [1982] (for explanation see text). The runoff parameter was selected to fit the available experimental data from the Mackenzie River (r=0.5).

was assumed, with constant quantity V of resident groundwater, with a tritium concentration of G. The tritium inventory is depleted by decay with the radioactive decay constant λ ($= 0.0565\,yr^{-1}$) and by runoff at a rate of dV/dt and is replaced by precipitation with a tritium concentration of P at a rate of dV/dt.

$d(VG) = PdV - GdV - VG\lambda dt.$

with $r = (dV/V)/dt$ as fractional recharge and runoff per year

$dG = (Pr - Gr - G\lambda)dt$

Assuming that the groundwater reservoir mixes and exchanges only once a year in a short summer season a series of yearly values was formed. Between the recharge and runoff events the tritium in the residual groundwater decays until the next years event. A runoff ratio r is selected to best fit the few available data from the Mackenzie river (see Fig. 36). A value for r of 0.5 fits the data best, and the model data for tritium in Arctic runoff are listed in column 3 in Table 19. For further reference see *Östlund* [1982].

Table 19: Reconstructed Arctic precipitation and runoff history

year	Tr [TU] precipitation	Tr [TU] runoff
1953	41	21
1954	432	225
1955	62	131
1956	276	196
1957	177	175
1958	795	475
1959	725	573
1960	252	380
1961	522	430
1962	1859	1120
1963	4484	2739
1964	2411	2421
1965	1143	1645
1966	762	1111
1967	434	710
1968	354	492
1969	357	397
1970	300	326
1971	392	341
1972	213	258
1973	216	222
1974	170	184
1975	148	151
1976	104	119
1977	84	95
1978	86	85
1979	76	76
1980	76	72
1981	82	72
1982	90	77
1983	47	58
1984	58	55

B Tables

B.1 Table of measurements from 1987 *Polarstern* (ArkIV/3; section B)

The hydrographic parameters together with the $\delta^{18}O$, tritium, and ^3He measurements of halocline waters (salinity <34.5) from the 1987 *Polarstern* section (section B) are listed. The fractions of Atlantic water (f_a), sea–ice meltwater (f_i) and river–runoff (f_r) and the calculated ^3He in river–runoff ($^3H_{runoff}$) and the tritium vintage age (vint. age) are also included.

Sta	depth [m]	Θ [°C]	sal	$\delta^{18}O$ [‰]	^3H [TU]	f_i [%]	f_r [%]	f_a [%]	$^3H_{runoff}$ [TU]	vint. age [yrs]	$^3H/^3He$–age [yrs]
269	3	-1.66	34.094	0.252	3.66	2.1	0.4	97.5	75	11.7	0.4
269	9	-1.66	34.108	0.110	3.43	1.4	1.0	97.6	15	-	0.3
269	20	-1.64	34.154	0.241	3.55	1.9	0.5	97.6	51	8.7	0.4
269	40	-1.14	34.450	0.140	3.53	0.6	0.8	98.6	31	-	0.7
285	31	-1.70	34.202	0.220	3.41	1.7	0.5	97.8	22	-	1.5
287	10	-1.75	34.077	0.274	-	2.3	0.3	97.4	-	-	-
287	31	-1.71	34.180	0.241	3.53	1.8	0.5	97.7	48	-	0.9
287	40	-1.58	34.248	0.218	3.24	1.5	0.5	97.9	-	-	0.7
287	49	-1.22	34.465	0.279	2.81	1.2	0.2	98.6	-	-	1.0
310	10	-1.82	34.188	0.210	3.57	1.7	0.6	97.8	46	-	1.6
310	29	-1.83	34.217	0.218	3.66	1.6	0.5	97.9	64	10.8	1.6
310	49	-1.83	34.323	0.193	-	1.2	0.6	98.2	-	-	-
310	64	-1.79	34.380	0.245	3.61	1.3	0.4	98.3	77	11.8	2.1
310	80	-1.81	34.398	0.250	3.56	1.2	0.4	98.4	69	11.2	1.6
310	94	-1.78	34.437	0.236	3.42	1.1	0.4	98.5	30	-	1.2
340	10	-1.83	34.076	0.119	4.07	1.6	1	97.5	77	11.8	2.4
340	30	-1.83	34.133	0.099	4.02	1.3	1.1	97.6	68	11.1	-
340	50	-1.84	34.181	0.124	4.51	1.3	0.9	97.8	126	15.5	2.2
340	80	-1.55	34.351	0.088	4.89	0.6	1.1	98.3	151	18.2	7.2
358	15	-1.79	34.028	-0.380	6.03	-0.7	3.1	97.5	91	13.1	6.4
358	20	-1.79	34.044	-0.343	5.89	-0.5	3	97.5	91	13.1	7.5
358	44	-1.84	34.199	-0.215	5.42	-0.4	2.4	98	93	13.3	6.5
358	69	-1.86	34.232	-0.273	5.69	-0.7	2.6	98.1	95	13.5	7.2

Sta	depth [m]	Θ [°C]	sal	$\delta^{18}O$ [‰]	^3H [TU]	f_t [%]	f_r [%]	f_a [%]	$^3H_{runoff}$ [TU]	vint. age [yrs]	$^3H/^3He$-age [yrs]
358	89	-1.86	34.235	-0.300	5.68	-0.8	2.7	98.1	91	13.2	7.2
358	109	-1.49	34.324	-0.033	5.44	0.1	1.6	98.3	139	17.6	10.8
358	124	-1.241	34.383	0.026	4.90	0.3	1.3	98.4	125	15.5	10.4
358	138	-0.72	34.450	0.048	4.93	0.2	1.2	98.6	139	17.6	13.1
362	20	-1.81	33.868	-0.745	7.56	-2	4.8	97.2	95	13.4	6.8
362	40	-1.85	34.112	-0.630	-	-2.1	4.3	97.9	-	-	-
362	59	-1.85	34.168	-0.592	7.43	-2.1	4.1	98	108	14.6	9.2
362	74	-1.85	34.181	-0.562	7.66	-2	3.9	98.1	118	15.2	8.3
362	89	-1.83	34.206	-0.520	-	-1.9	3.8	98.1	-	-	-
362	104	-1.81	34.216	-0.455	-	-1.6	3.5	98.1	-	-	-
362	132	-1.36	34.301	-0.030	-	0.2	1.6	98.2	-	-	-
362	147	-1.12	34.351	0.015	-	0.3	1.4	98.3	-	-	-
362	162	-0.52	34.449	-0.030	-	-0.2	1.5	98.7	-	-	-
364	21	-1.80	33.607	-1.103	7.75	-3	6.5	96.5	75	11.6	5.7
364	40	-1.84	33.905	-0.839	8.43	-2.6	5.3	97.3	104	14.2	6.3
364	59	-1.84	33.960	-0.793	7.93	-2.5	5	97.5	99	13.7	6.5
364	83	-1.85	34.123	-0.599	7.57	-2	4.2	97.9	110	14.8	8.4
365	25	-1.81	33.580	-1.065	8.42	-2.7	6.3	96.4	88	12.8	5.1
365	49	-1.84	34.083	-0.714	8.47	-2.5	4.7	97.8	118	15.2	7.8
365	74	-1.86	34.127	-0.620	7.90	-2.2	4.2	97.9	116	15.1	8.1
365	99	-1.83	34.171	-0.523	7.57	-1.8	3.8	98	120	15.3	9.1
365	119	-1.81	34.208	-0.455	7.08	-1.6	3.5	98.1	115	15.1	9.0
365	138	-1.53	34.258	-0.170	-	-0.3	2.2	98.1	-	-	-
365	158	-0.83	34.400	0.008	5.66	0.1	1.4	98.5	174	19.0	14.9
371	24	-1.80	33.286	-1.580	-	-4.5	8.8	95.7	-	-	-
371	40	-1.80	33.289	-1.413	8.38	-3.6	8.0	95.6	70	11.3	5.2
371	49	-1.84	33.834	-0.892	8.63	-2.7	5.5	97.1	103	14.1	6.5
371	69	-1.84	34.006	-0.743	0.00	-2.4	4.9	97.6	-	-	-
371	83	-1.84	34.063	-0.700	7.65	-2.4	4.7	97.7	101	13.9	8.3
371	99	-1.85	34.115	-0.661	7.59	-2.4	4.5	97.9	104	14.1	8.0
371	119	-1.83	34.160	-0.553	7.73	-2.0	4.0	98	119	15.3	8.8
371	157	-1.19	34.321	-0.160	6.59	-0.5	2.2	98.3	158	18.5	14.1
371	177	-0.59	34.440	0.016	6.73	0	1.3	98.6	260	20.2	15.6

The hydrographic parameters together with the $\delta^{18}O$ measurements of the entire water column from the 1987 *Polarstern* section (section B). The results from the halocline which are listed in the previous table are included again.

sta	depth [m]	Θ [°C]	sal	$\delta^{18}O$ [‰]
269	3	-1.658	34.094	0.252
269	9	-1.664	34.108	0.11
269	20	-1.643	34.154	0.241
269	40	-1.136	34.450	0.14
269	59	-0.454	34.676	0.273
269	79	-0.127	34.739	0.243
269	98	-0.177	34.743	0.19
269	124	-0.195	34.750	0.274
269	147	-0.202	34.758	0.14
269	171	-0.181	34.766	0.245
269	188	-0.144	34.768	0.22
285	31	-1.699	34.202	0.22
285	54	-0.627	34.561	0.25
285	93	0.689	34.781	0.21
285	168	1.458	34.908	0.27
285	287	1.528	34.954	0.25
285	366	1.434	34.962	0.29
285	464	1.281	34.963	0.35
285	622	0.685	34.936	0.29
285	1035	-0.491	34.918	0.26
285	1878	-0.827	34.918	0.29
287	10	-1.750	34.077	0.274
287	31	-1.706	34.180	0.241
287	40	-1.577	34.248	0.218
287	49	-1.217	34.465	0.279
287	59	-0.811	34.573	0.251
287	69	-0.007	34.675	0.261
287	89	0.514	34.751	0.242
287	119	1.186	34.862	0.270
287	167	1.492	34.916	0.286
287	226	1.350	34.922	0.327
287	296	1.521	34.961	0.292
287	474	1.285	34.972	0.299
287	2089	-0.886	34.918	0.252
287	2332	-0.916	34.925	0.280
287	2535	-0.927	34.932	0.261
310	10	-1.822	34.188	0.210
310	29	-1.825	34.217	0.218
310	49	-1.827	34.323	0.193
310	64	-1.793	34.380	0.245
310	80	-1.809	34.398	0.250
310	94	-1.782	34.437	0.236
310	124	-0.183	34.635	0.264
310	138	0.427	34.710	0.298
310	153	0.972	34.781	0.287
310	189	1.793	34.899	0.275
310	247	1.547	34.905	0.216
310	296	1.663	34.939	0.306
310	346	1.577	34.954	0.280
340	10	-1.829	34.076	0.119
340	30	-1.830	34.133	0.099
340	50	-1.837	34.181	0.124
340	80	-1.554	34.351	0.088
340	108	-0.143	34.529	0.129
340	124	0.635	34.673	0.167
340	138	1.110	34.753	0.234
340	152	1.447	34.816	0.240
340	167	1.474	34.827	0.218
340	188	1.696	34.878	0.254
340	246	1.457	34.902	0.247
340	345	1.661	34.939	0.283
358	5	-1.791	–	-0.37
358	15	-1.791	34.028	-0.38
358	20	-1.791	34.044	-0.34
358	44	-1.841	34.199	-0.22
358	69	-1.860	34.232	-0.27

sta	depth [m]	Θ [°C]	sal	$\delta^{18}O$ [‰]
358	89	-1.859	34.235	-0.3
358	109	-1.485	34.324	-0.03
358	124	-1.241	34.383	0.026
358	138	-0.719	34.450	0.048
358	152	0.149	34.566	0.08
358	168	0.823	34.674	0.201
358	188	1.200	–	0.225
358	217	1.615	34.830	0.18
358	246	1.891	34.905	0.22
358	295	1.705	34.906	0.23
358	345	1.721	34.939	0.196
358	395	1.378	34.922	0.22
358	493	0.994	34.918	0.23
358	592	0.803	34.927	0.27
358	691	0.416	34.917	0.26
358	789	0.146	34.912	0.231
358	864	-0.019	34.920	0.21
358	913	-0.120	34.920	0.23
358	989	-0.223	34.922	0.23
358	1085	-0.343	34.922	0.28
358	1231	-0.496	34.921	0.264
358	1379	-0.610	34.922	0.26
358	1577	-0.721	34.922	0.266
358	1773	-0.804	34.922	0.25
358	1919	-0.847	34.922	0.18
358	2066	-0.881	–	0.276
358	2215	-0.906	34.926	0.27
358	2362	-0.923	34.929	0.312
358	2556	-0.940	34.931	0.34
358	2947	-0.958	34.935	0.25
358	3142	-0.958	34.939	0.376
358	3288	-0.955	34.941	0.3
358	3433	-0.949	34.943	0.25
358	3580	-0.947	34.941	0.264
358	3726	-0.947	34.941	0.3
358	3850	-0.947	34.942	0.3
358	3947	-0.948	34.944	0.32
358	3993	-0.948	34.943	0.305
358	2752	-0.951	34.934	0.3

sta	depth [m]	Θ [°C]	sal	$\delta^{18}O$ [‰]
362	20	-1.814	33.868	-0.75
362	40	-1.847	34.112	-0.63
362	59	-1.850	34.168	-0.59
362	74	-1.854	34.181	-0.56
362	89	-1.834	34.206	-0.52
362	104	-1.811	34.216	-0.46
362	132	-1.355	34.301	-0.03
362	147	-1.118	34.351	0.015
362	162	-0.522	34.449	-0.03
362	197	0.841	34.640	0.184
362	217	1.493	34.804	0.23
362	247	1.820	34.885	0.287
362	296	1.716	34.908	0.29
362	395	1.279	34.918	0.28
362	494	0.911	34.917	0.26
364	21	-1.804	33.607	-1.1
364	30	-1.812	33.686	-0.99
364	40	-1.836	33.905	-0.84
364	49	-1.840	33.928	-0.77
364	59	-1.843	33.960	-0.79
364	69	-1.848	34.078	-0.65
364	83	-1.847	34.123	-0.6
364	148	-1.421	34.282	-0.14
364	197	-0.157	34.509	0.038
365	25	-1.807	33.58	-1.07
365	49	-1.839	34.083	-0.71
365	74	-1.855	34.127	-0.62
365	99	-1.829	34.171	-0.52
365	119	-1.814	34.208	-0.46
365	138	-1.530	34.258	-0.17
365	158	-0.825	34.400	0.008
365	198	0.551	34.627	0.13
365	246	1.439	34.824	0.254
365	246	1.439	34.824	0.254
365	297	1.236	34.863	0.21

sta	depth [m]	Θ [°C]	sal	$\delta^{18}O$ [‰]
371	24	-1.803	33.286	-1.58
371	40	-1.803	33.289	-1.41
371	49	-1.841	33.834	-0.89
371	69	-1.842	34.006	-0.74
371	83	-1.841	34.063	-0.70
371	99	-1.854	34.115	-0.66
371	119	-1.834	34.160	-0.55
371	157	-1.189	34.321	-0.16
371	177	-0.592	34.440	0.016
371	272	1.187	34.857	0.25
371	305	0.798	34.836	0.21
371	372	0.726	34.872	0.08
371	1969	-0.817	34.925	0.236
371	2704	-0.938	34.933	0.237
371	2918	-0.950	34.936	0.270

B.2 Table of $\delta^{18}O$ measurements and silicate values from 1991 *Oden* (ARCTIC 91; sections A and C)

The hydrographic parameters are listed together with the $\delta^{18}O$, and silicate measurements [*Anderson and Carlson,* 1991]. All $\delta^{18}O$ measurements were made in the frame of this study at Lamont–Doherty Earth Observatory (L–DEO) in the laboratory of Dr. R. Fairbanks.

sta	depth [m]	Θ [°C]	salinity	$\delta^{18}O$ [‰]	silicate [$\mu mol\, l^{-1}$]
4	5	1.543	32.056	-0.003	1.36
4	30	3.540	34.688	0.115	3.41
4	75	3.549	34.937	0.237	4.91
4	150	3.053	34.978	0.302	5.22
4	300	2.822	35.002	0.297	5.61
4	500	2.130	34.982	0.280	6.07
8	10	-1.676	33.545	-0.409	2.87
8	20	-1.605	33.877	-0.339	2.98
8	40	-1.741	34.210	-0.292	3.16
8	60	-1.804	34.255	-0.296	3.23
8	80	-1.825	34.276	-0.367	3.40
8	100	-1.816	34.305	-0.318	3.34
8	125	-0.704	34.398	-0.080	4.69
8	150	0.474	34.620	0.096	5.44
8	175	1.052	34.737	0.173	5.49
8	250	1.606	34.909	0.217	5.82
9	5	-1.736	33.475	-0.293	2.80
9	15	-1.778	33.684	-0.230	2.80
9	30	-1.762	33.762	-0.190	2.90
9	50	-1.826	34.105	-0.064	3.04
9	75	-1.836	34.140	-0.102	3.19
9	100	-1.564	34.208	-0.031	3.71
9	150	0.754	34.619	0.155	5.21
9	200	1.487	34.819	0.361	5.53
9	300	1.627	34.921	0.364	5.85

sta	depth [m]	Θ [°C]	salinity	$\delta^{18}O$ [‰]	silicate [$\mu mol\, l^{-1}$]
10	10	-1.742	33.276	-1.066	3.19
10	48	-1.801	34.066	-0.610	3.15
10	100	-1.816	34.159	-0.455	3.32
10	176	0.677	34.649	0.180	5.37
10	250	1.575	34.879	0.356	5.74
11	9	-1.752	33.024	-1.529	3.66
11	15	-1.736	33.017	-1.606	3.65
11	24	-1.745	33.135	-1.500	3.76
11	50	-1.784	33.796	-1.180	3.89
11	74	-1.732	34.002	-0.687	4.16
11	100	-1.335	34.228	-0.291	4.81
11	125	-0.641	34.401	-0.048	5.02
11	149	0.164	34.566	0.072	5.42
11	176	0.766	34.699	0.143	5.50
11	200	1.257	34.804	0.266	5.49
11	250	1.328	34.864	0.275	5.70
11	300	1.400	34.906	0.277	5.77
11	399	1.045	34.902	0.237	6.12
11	504	0.886	34.919	0.253	6.32
12	10	-1.740	32.844	-1.886	3.92
12	25	-1.739	32.856	-1.814	3.88
12	75	-1.609	34.049	-0.445	4.78
12	125	-0.505	34.431	-0.074	5.25
12	200	0.953	34.783	0.166	5.57
12	300	1.233	34.902	0.242	5.91
14	10	-1.737	32.810	-1.878	3.83
14	15	-1.732	32.818	-1.980	3.79
14	25	-1.735	32.828	-1.868	3.83
14	29	-1.712	32.860	-1.895	3.78
14	50	-1.760	33.515	-1.559	4.10
14	75	-1.644	34.018	-0.591	4.65
14	100	-1.122	34.287	-0.184	5.00
14	125	-0.632	34.410	-0.059	5.19
14	150	0.055	34.565	0.049	5.48
14	200	0.953	34.773	0.169	5.56
14	250	1.115	34.852	0.180	5.72
14	300	1.232	34.901	0.233	5.88
14	400	0.939	34.909	0.212	6.21
14	500	0.663	34.905	0.213	6.39
14	601	0.361	34.898	0.161	6.54

sta	depth [m]	Θ [°C]	salinity	$\delta^{18}O$ [‰]	silicate [$\mu mol\, l^{-1}$]
16	5	-1.704	32.726	-1.979	4.61
16	25	-1.723	32.747	-1.976	4.61
16	50	-1.792	33.333	-1.908	4.70
16	100	-1.418	34.198	-0.266	5.17
16	150	-0.284	34.498	-0.029	5.35
16	200	-0.597	34.745	0.147	5.50
16	250	0.852	34.836	0.174	5.70
16	300	0.887	34.865	0.227	5.80
16	400	0.711	34.884	0.252	6.17
16	500	0.480	34.883	0.207	6.23
16	699	-0.009	34.885	0.245	6.57
16	792	-0.129	34.890	0.208	6.83
16	900	-0.251	34.895	0.217	7.10
16	1099	-0.403	34.908	0.313	7.69
16	1099	-0.403	34.908	0.321	7.69
16	1499	-0.621	34.921	0.273	9.35
16	1599	-0.655	34.923	0.287	9.80
16	1700	-0.689	34.924	0.266	10.20
16	1801	-0.736	34.924	0.262	10.23
16	2000	-0.811	34.923	0.277	10.42
16	2250	-0.869	34.925	0.291	10.62
16	2502	-0.903	34.928	0.293	10.78
16	2750	-0.927	34.931	0.284	11.10
16	3001	-0.939	34.940	0.376	11.06
16	3001	-0.939	34.940	0.398	11.06
16	3250	-0.951	34.937	0.301	11.11
16	3500	-0.955	34.940	0.284	11.16
16	3702	-0.952	34.940	0.303	11.24
16	3900	-0.948	34.942	0.275	11.27
16	4098	-0.946	34.943	0.361	11.33
16	4352	-0.946	34.945	0.306	11.32
16	4451	-0.945	34.944	0.346	11.30
17	16	-1.745	32.725	-1.895	4.43
17	30	-1.740	32.737	-1.854	4.43
17	58	-1.796	33.315	-1.745	4.83
17	75	-1.694	33.761	-0.719	5.50
17	100	-1.550	34.145	-0.310	5.08
17	150	-0.553	34.446	-0.048	5.08
17	200	0.301	34.709	0.180	5.35
17	250	0.761	34.820	0.172	5.63
17	250	0.848	34.826	0.172	5.35
17	300	0.823	34.849	0.195	5.73
17	400	0.660	34.873	0.187	6.05

sta	depth [m]	Θ [°C]	salinity	$\delta^{18}O$ [‰]	silicate [$\mu mol\, l^{-1}$]
18	10	-1.739	32.645	-1.968	4.62
18	35	-1.725	33.030	-1.943	4.54
18	76	-1.746	33.619	-1.199	5.00
18	101	-1.593	34.091	-0.371	5.30
18	125	-1.255	34.267	-0.175	5.19
18	200	0.177	34.668	0.135	5.49
18	301	0.920	34.863	0.225	5.72
18	500	0.456	34.880	0.253	6.22
21	10	-1.733	32.476	-2.368	7.27
21	44	-1.739	33.120	-1.899	7.80
21	50	-1.703	33.343	-1.433	8.09
21	75	-1.628	33.962	-0.529	5.86
21	95	-1.478	34.215	-0.270	4.92
21	100	-1.383	34.249	-0.264	4.88
21	125	-0.934	34.404	-0.115	5.00
21	201	0.414	34.743	0.127	5.51
21	251	0.750	34.823	0.205	5.69
21	300	0.836	34.853	0.199	5.77
23	10	-1.708	31.924	-2.508	9.10
23	25	-1.709	31.919	-2.465	9.08
23	35	-1.684	32.282	-2.401	8.60
23	47	-1.617	33.043	-1.485	14.75
23	75	-1.587	34.048	-0.414	6.12
23	92	-1.445	34.215	-0.215	5.73
23	125	-1.009	34.396	-0.049	5.52
23	151	-0.595	34.509	0.011	5.53
23	201	0.314	34.733	0.203	5.69
23	250	0.671	34.820	0.200	5.83
23	300	0.792	34.857	0.215	5.78
23	320	0.791	34.864	0.245	5.83
23	400	0.667	34.881	0.287	6.13
23	449	0.547	34.883	0.254	6.11
23	497	0.394	34.882	0.243	6.33

sta	depth [m]	Θ [°C]	salinity	$\delta^{18}O$ [‰]	silicate [$\mu mol\, l^{-1}$]
26	10	-1.714	31.679	-2.545	10.30
26	15	-1.723	31.695	-2.541	10.28
26	35	-1.722	31.720	-2.529	10.25
26	50	-1.745	32.632	-2.201	9.25
26	68	-1.670	33.184	-1.510	12.82
26	80	-1.574	33.609	-0.839	12.53
26	100	-1.534	34.059	-0.453	7.61
26	121	-1.318	34.225	-0.277	6.83
26	150	-0.710	34.424	-0.128	6.93
26	200	-0.009	34.653	0.076	7.12
26	250	0.400	34.803	0.194	6.72
26	300	0.480	34.835	0.168	6.45
26	400	0.484	34.869	0.254	7.06
26	500	0.396	34.876	0.209	6.96
26	602	0.198	34.879	0.223	6.97
26	699	0.045	34.885	0.216	7.07
26	800	-0.072	34.890	0.216	7.22
26	900	-0.158	34.898	0.245	7.47
26	998	-0.223	34.906	0.259	7.74
26	1098	-0.282	34.913	0.256	8.14
26	1098	-0.282	34.913	0.273	8.14
26	1300	-0.379	34.933	0.235	9.19
26	1499	-0.438	34.937	0.248	10.41
26	1700	-0.479	34.946	0.250	11.36
26	1898	-0.502	34.949	0.272	12.03
26	2099	-0.513	34.952	0.269	12.40
26	2299	-0.520	34.954	0.218	12.65
26	2496	-0.525	34.954	0.257	12.67
26	2701	-0.531	34.955	0.303	12.52
26	2900	-0.535	34.955	0.246	12.38
26	3098	-0.541	34.954	0.278	12.28
26	3098	-0.541	34.954	0.283	12.28
26	3300	-0.544	34.954	0.281	12.13
26	3498	-0.545	34.954	0.273	12.07
26	3699	-0.545	34.954	0.324	12.07
26	3849	-0.545	34.956	0.289	12.07
26	3990	-0.545	34.955	0.315	12.11
31	10	-1.710	31.678	-2.937	13.00
31	24	-1.712	31.686	-2.935	12.98
31	69	-1.647	33.059	-1.639	13.18
31	90	-1.626	33.881	-0.641	6.68
31	124	-1.321	34.250	-0.284	5.56
31	250	0.699	34.816	0.218	5.63
31	330	0.826	34.862	0.255	5.84

sta	depth [m]	Θ [°C]	salinity	$\delta^{18}O$ [‰]	silicate [$\mu mol\, l^{-1}$]
33	9	-1.735	32.081	-2.644	10.45
33	25	-1.766	32.652	-2.530	6.44
33	50	-1.785	33.210	-2.261	5.69
33	70	-1.780	33.414	-1.825	5.87
33	90	-1.692	33.887	-0.782	5.85
33	130	-1.202	34.279	-0.205	5.68
33	150	-0.770	34.409	-0.058	5.73
33	200	0.193	34.674	0.137	5.79
33	250	0.694	34.815	0.204	5.69
33	300	0.759	34.837	0.201	5.84
33	500	0.464	34.881	0.227	6.23
33	701	-0.033	34.881	0.225	6.59
33	899	-0.285	34.891	0.212	7.08
33	1100	-0.415	34.901	0.245	7.70
33	1349	-0.537	34.915	0.248	8.91
33	1599	-0.642	34.922	0.231	10.04
33	1801	-0.719	34.923	0.270	10.53
33	2199	-0.853	34.924	0.226	10.85
33	2400	-0.887	34.926	0.274	11.03
33	2650	-0.915	34.928	0.243	11.16
33	2900	-0.930	34.931	0.266	11.21
33	3098	-0.941	34.937	0.274	11.24
33	3298	-0.948	34.936	0.242	11.29
33	3700	-0.954	34.940	0.302	11.32
33	3999	-0.947	34.943	0.298	11.45
33	4148	-0.946	34.943	0.267	11.46
33	4382	-0.946	34.943	0.300	11.41
43	16	-1.722	31.664	-2.872	13.84
43	25	-1.727	31.740	-2.853	13.82
43	36	-1.722	31.791	-2.814	13.94
43	50	-1.470	32.476	-1.531	28.60
43	62	-1.485	33.325	-1.105	24.39
43	75	-1.510	33.821	-0.644	14.26
43	101	-1.341	34.166	-0.311	9.85
43	125	-0.899	34.362	-0.173	9.03
43	160	-0.320	34.566	0.003	9.24
43	200	0.089	34.694	0.125	9.61
43	240	0.362	34.793	0.196	9.18
43	330	0.431	34.848	0.199	8.90

sta	depth [m]	Θ [°C]	salinity	$\delta^{18}O$ [‰]	silicate [$\mu mol\, l^{-1}$]
46	17	-1.764	32.322	-2.615	8.96
46	20	-1.774	32.355	-2.642	8.84
46	36	-1.735	33.182	-2.081	7.22
46	56	-1.790	34.187	-0.588	6.87
46	76	-1.670	33.881	-0.884	7.69
46	76	-1.670	33.881	-0.916	7.69
46	101	-1.481	34.165	-0.383	6.61
46	126	-1.015	34.351	-0.131	6.25
46	151	-0.613	34.482	-0.046	6.35
46	251	0.608	34.816	0.209	6.32
46	351	0.511	34.854	0.196	7.15
48	10	-1.795	32.971	-2.216	5.06
48	25	-1.798	32.973	-2.219	5.05
48	35	-1.799	33.009	-2.138	5.03
48	60	-1.752	33.821	-1.109	5.10
48	75	-1.718	33.975	-0.356	5.12
48	100	-1.331	34.238	-0.258	5.69
48	150	-0.346	34.511	-0.028	6.02
48	190	0.638	34.705	0.139	5.92
48	259	0.705	34.824	0.181	6.01
48	320	0.889	34.875	0.227	6.13
49	25	-1.804	33.022	-2.072	4.84
49	45	-1.779	33.741	-1.383	5.10
49	65	-1.721	33.994	-0.803	5.27
49	80	-1.586	34.103	-0.581	5.55
49	105	-1.356	34.253	-0.307	5.39
49	160	-0.235	34.511	0.022	5.95
49	200	0.693	34.708	0.113	6.00
49	255	1.343	34.867	0.203	6.02
49	320	1.273	34.904	0.216	6.20
51	27	-1.816	33.311	-1.677	5.79
51	37	-1.784	33.720	-1.440	5.65
51	42	-1.792	33.769	-1.429	5.40
51	57	-1.826	33.905	-1.278	4.88
51	77	-1.816	34.010	-1.097	4.71
51	112	-1.614	34.143	-0.552	5.06
51	167	0.362	34.583	0.088	5.81
51	202	1.090	34.739	0.161	5.89
51	252	1.386	34.869	0.203	5.95
51	282	1.173	34.862	0.204	6.00
51	332	1.232	34.902	0.242	6.13

sta	depth [m]	Θ [°C]	salinity	$\delta^{18}O$ [‰]	silicate [$\mu mol\, l^{-1}$]
55	16	-1.814	33.569	-1.126	4.59
55	25	-1.754	33.616	-1.103	4.70
55	40	-1.609	33.763	-0.936	4.66
55	56	-1.338	34.055	-0.611	4.79
55	74	-1.068	34.164	-0.491	4.92
55	94	-0.860	34.261	-0.376	5.15
55	109	-0.299	34.390	-0.183	5.33
55	133	0.279	34.524	-0.072	5.52
55	149	0.661	34.630	0.066	5.70
55	175	1.257	34.752	0.110	5.71
55	201	1.498	34.815	0.183	5.76
55	250	1.721	34.895	0.193	5.82
55	325	1.499	34.911	0.219	5.98
58	16	-1.825	33.608	-0.629	3.50
58	26	-1.804	33.794	-0.615	3.55
58	42	-1.544	34.230	-0.550	4.17
58	50	-1.600	34.237	-0.533	4.06
58	74	-1.690	34.311	-0.384	3.68
58	120	-0.414	34.463	-0.191	4.78
58	176	2.477	34.890	0.238	5.26
58	190	2.537	34.909	0.220	5.32
58	242	2.670	34.965	0.274	5.51
61	10	1.347	33.383	0.031	0.65
61	26	3.054	34.145	0.166	1.34
61	49	4.291	34.586	0.233	2.68
61	70	4.222	34.763	0.270	3.96
61	102	4.050	34.875	0.262	4.95
61	140	4.076	34.875	0.247	4.99
61	172	3.959	34.921	0.292	5.60
61	188	3.989	34.956	0.265	5.69

B.3 Table of $\delta^{18}O$ measurements from 1985 *Meteor* (M71, sta. 79)

The hydrographic parameters are listed together with the $\delta^{18}O$measurements. All $\delta^{18}O$ measurements were made in the frame of this study at Lamont–Doherty Earth Observatory (L–DEO) in the laboratory of Dr. R. Fairbanks.

sta	depth [m]	Θ [°C]	salinity	$\delta^{18}O$ [‰]
79	5	8.565	35.167	0.305
79	10	8.484	35.131	0.329
79	49	5.856	35.122	0.324
79	99	5.306	35.109	0.359
79	198	4.626	35.116	0.329
79	297	4.387	35.078	0.316
79	394	4.020	35.071	0.345
79	493	3.604	35.050	0.288
79	641	2.155	34.971	0.258
79	789	0.883	34.921	0.254
79	937	-0.031	34.897	0.240
79	1085	-0.357	34.904	0.275
79	1085	-0.357	34.904	0.272
79	1283	-0.594	34.913	0.282
79	1577	-0.808	34.915	0.281
79	1871	-0.923	34.914	0.310
79	2166	-0.993	34.913	0.271
79	2459	-1.033	34.915	0.262
79	2752	-1.049	34.912	0.267
79	2949	-1.052	34.911	0.255
79	2949	-1.052	34.911	0.235
79	3095	-1.053	34.910	0.299
79	3163	-1.054	34.911	0.245
79	3192	-1.053	34.911	0.335
79	3226	-1.053	34.909	0.275

B.4 Table of $\delta^{18}O$ measurements from 1988 *Meteor* (M8, sta. 617)

The hydrographic parameters are listed together with the $\delta^{18}O$measurements. All $\delta^{18}O$ measurements were made in the frame of this study at Lamont–Doherty Earth Observatory (L–DEO) in the laboratory of Dr. R. Fairbanks.

sta	depth [m]	Θ [°C]	salinity	$\delta^{18}O$ [‰]
617	22	-0.711	34.485	0.115
617	37	-0.705	34.485	0.140
617	62	0.579	34.891	0.213
617	111	0.460	34.919	0.227
617	159	-0.080	34.891	0.209
617	209	-0.192	34.895	0.204
617	260	-0.532	34.884	0.203
617	310	-0.537	34.889	0.269
617	359	-	34.894	0.262
617	409	-0.533	34.899	0.252
617	460	-0.640	34.895	0.232
617	508	-0.798	34.888	0.198
617	756	-1.027	34.884	0.230
617	1009	-1.085	34.889	0.254
617	1009	-1.085	34.889	0.246
617	1257	-1.092	34.893	0.251
617	1753	-1.128	34.897	0.245
617	2254	-1.136	34.900	0.211
617	2961	-1.186	34.899	0.245
617	2961	-1.186	34.899	0.281
617	3489	-1.211	34.894	0.249

B.5 Table of $\delta^{18}O$ and salinity measurements from the Laptev Sea (E.S.A.R.E.'92)

The $\delta^{18}O$ and salinity measurements are listed from surface water, ice and snow samples taken in the Laptev Sea during E.S.A.R.E.'92 [*Dethleff et al.*, 1993]. All $\delta^{18}O$ and salinity measurements were made in the frame of this study at Lamont–Doherty Earth Observatory (L–DEO). The $\delta^{18}O$ measurements were performed in the laboratory of Dr. R. Fairbanks and the salinity measurements were made in the laborarory of Dr. T. Takahashi.

sta	latitude [°N]	longitude [°E]	salinity	$\delta^{18}O$ [‰]	sample type
2	71.75	127.15	0.0722	-16.779	ice
2	71.75	127.15	0.1165	-27.973	snow
4	72.50	130.00	2.0909	-14.414	ice
4	72.50	130.00	15.5124	-24.484	snow
5	73.48	129.97	15.5425	-14.230	water
6	73.75	128.25	19.9022	-10.687	water
6	73.75	128.25	1.7691	-20.605	snow
7	74.09	125.02	22.4228	-6.070	snow
8	74.48	129.83	28.4287	-5.864	snow
3	71.81	129.00	0.047	-20.598	water
3	71.81	129.00	0.1738	-16.081	ice
3	71.81	129.00	0.043	-26.362	snow
14	76.99	134.97	31.3460	-1.911	water
17	79.02	140.02	33.8211	-0.979	water
17	79.02	140.02	5.9770	-1.780	ice
17	79.02	140.02	2.7688	-19.022	snow

B.6 Table of $\delta^{18}O$ and salinity measurements from the Barents Sea

The results of $\delta^{18}O$ and salinity measurements are listed from water samples taken in the Barents Sea during an expedition with RV *Dalnie Zelentsy* in summer 1992 [*Nürnberg and Groth,* 1993]. All $\delta^{18}O$ and salinity measurements were made in the frame of this study at Lamont–Doherty Earth Observatory (L–DEO). The $\delta^{18}O$ measurements were performed in the laboratory of Dr. R. Fairbanks and the salinity measurements were made in the laborarory of Dr. T. Takahashi.

sta no.	latitude [°N]	longitude [°E]	depth [m]	water temp. [°C]	salinity	$\delta^{18}O$ [‰]	sampling location	bottom depth [m]
8	77.32	62.28	5	0.50	33.8204	0.178	off Novaya Zemlya	219
9	77.49	61.71	5	2.00	34.1811	0.256	off Novaya Zemlya	335
10	78.06	61.19	5	3.00	32.7971	0.025	off Novaya Zemlya	415
11	78.91	59.00	50	1.00	33.8330	-0.069	off Novaya Zemlya	260
13	79.83	61.48	5	1.25	33.8848	-0.076	off Franz–Josef– Land	145
13	79.83	61.48	50	-1.00	34.3074	-0.097	off Franz–Josef– Land	145
16	81.12	63.53	50	-1.25	33.6559	0.181	Greem Bell Island	275
12	79.88	58.68	5	-0.50	34.0443	-0.082	Wilczek Island	43
15	80.62	58.10	5	1.00	34.1544	-0.018	Chejsa Island	34
15	80.62	58.10	34	-1.00	34.1916	-0.006	Chejsa Island	34
14	80.40	59.63	5	-1.00	34.0603	-0.023	Camp	40
14	80.40	59.63	40	-1.20	34.1565	0.021	Camp	40
5	75.56	56.45	5	4.00	33.8373	-0.122	Nordenskiold Bay	165
5	75.56	56.45	50	3.25	34.2191	-0.272	Nordenskiold Bay	165
3	73.01	51.89	5	6.00	33.8456	-0.098	off Novaya Zemlya	70
3	73.01	51.89	50	4.25	33.9374	-0.182	off Novaya Zemlya	70
2	72.61	51.37	50	6.00	34.3190	0.171	off Novaya Zemlya	85
1	71.58	44.41	50	?	34.7091	0.140	off Novaya Zemlya	85

C Indexes

C.1 List of Tables

C.2 List of Figures

Acknowledgements

I gratefully want to thank everybody who supported me during this study.

Prof. K. O. Münnich for being my doctoral advisor.

Prof. H. G. Dosch for taking the "Koreferat".

Peter Schlosser for conceptualizing the project and for offering the chance to work at the Lamont–Doherty Earth Observatory of Columbia University.

Rick Fairbanks and his group for support and the possibility to perform over a thousand ^{18}O measurements in his laboratory.

The various people and institutions who helped providing the samples: The crews of RV POLARSTERN and ODEN for assistance during sample collection. Brenda Ekwurzel collected the samples during the ARCTIC 91 expedition. Gerhard Bönisch collected the samples during the Ark IV/3 expedition. Heidi Kassens, Dirk Nürnberg and Elke Groth (GEOMAR, Kiel) collected the samples from the Laptev and Barents seas. Salinity data from the Polarstern and Oden cruises were kindly provided by the ODF facility of the Scripps Institution of Oceanography. The silicate samples from the Oden stations were measured by G. Kattner (AWI, Bremerhaven).

The "inhabitants" of the Geochemistry Building at L-DEO for making me feel at home.

Financial support was provided by a stipend through the Landesgraduiertenförderungsgesetz, the Office of Naval Research (grant no. N00014-90-J-1362), and the National Science Foundation (grant no. DPP90-22890).